Louterbach, M., Roddaz, M., Bailleul, J., Antoine, P.-O., Anet, S., Kim, J.-H., van Soelen, E., Parra, F., Gérard, J., Calderon, Y., Gagnaison, C., Sinninghe Damsté, J.S. & Baby, P. (2014). Evidences for a Paleocene marine incursion in southern Amazonia (Madre de Dios Sub-Andean Zone, Peru). Palaeogeography, Palaeoclimatology, Palaeoecology, 414, 451–471

Elsevier Editorial System(tm) for Palaeogeography, Palaeoclimatology, Palaeoecology
Manuscript Draft

Manuscript Number: PALAEO7489R1

Title: Evidences for a Paleocene marine incursion in Southern Amazonia (Madre de Dios Sub-Andean Zone, Peru)

Article Type: Research Paper

Keywords: Paleogene; marine incursion; Amazonian foreland basin; tidal deposits; micro paleontology; vertebrates paleontology; organic geochemistry; Nd-Sr isotopes; Madre de Dios basin; Peru; Andes.

Corresponding Author: Mrs. Mélanie Louterbach,

Corresponding Author's Institution: University of Paul Sabatier

First Author: Mélanie Louterbach

Order of Authors: Mélanie Louterbach; Martin Roddaz; Julien Bailleul; Pierre-Olivier Antoine; Sylvain Adnet; J.H. Kim; E. van Soelen; Francisco Parra; Jean Gérard; Ysabel Calderon; Cyril Gagnaison; Jaap S. Sinninghe Damsté; Patrice Baby

Abstract: This article presents new biostratigraphic dating, facies analysis, organic geochemical data and Nd-Sr isotopic provenance from five outcrops of southern Amazonia (MD-85, MD-177 MD-184, MD-255 and MD-256) to document for the first time the presence of a shallow marine ingression in the Paleocene of southern Amazonia basin. The co-occurrence of a selachian assemblage encompassing Potobatis sp., Ouledia sp., and Pristidae indet. with the ostracod Protobuntonia sp. and the charophytes Peckichara cf. varians meridionalis, Platychara perlata, and Feistiella cf. gildemeisteri suggests a Paleocene age for the studied deposits (most likely Thanetian but potentially Danian). Fifteen facies have been recognized and have been grouped into three facies assemblages. Facies association A corresponds to the sedimentary filling of a tide-influenced meandering channel formed in the fluvial-tidal transition zone. Facies association B is related to more distal tidal-flats, little channelized tidal inlets and saltmarshes deposits. Facies association C corresponds to a stressed shallow marine environment such as a bay or a lagoon. The δ13CTOC value (-23.4 ‰) of MD-184 is enriched in 13C compared to the other samples suggesting the presence of substantial amounts of marine organic matter in MD-184. The δ13CTOC values of samples from other outcrops (-27.3 to -29.8 ‰) indicate a mixed organic matter origin, from terrestrial to brackish environments. The analyzed sediments have similar Nd-Sr isotopic compositions as those of the Cenozoic sediments of the Altiplano (εNd(0) values from -6.2 to -10.7 and 87Sr/86Sr compositions from 0.712024 to 0.719026) indicating a similar volcanic source. This multidisciplinary dataset documents the presence of a tide-dominated estuary sourced by the proto Western Cordillera debouching into a shallow marine bay during Paleocene times. This transgression might be explained by subsidence created in response to the proto-Western Cordillera loading. Similar to Miocene marine incursions affecting the Pebas megawetland, Paleogene marine incursions in the Amazonian foreland basin associated with Andean uplift may have played a role in the Neotropical biodiversity dynamics in favouring biogeographical isolation and promoting allopatric speciation for terrestrial organisms.

Highlights:

The presence of agglutinated benthic foraminifer *Karreriella conversa*, ostracod *Protobuntonia* and charophyte *Peckichara cf. varians meridionalis* suggest a Paleogene age for the studied deposits.

We define three facies associations related to a tide-dominated estuary debouching into a shallow-marine bay or lagoon.

The $\delta_{13}C_{TOC}$ values show a marine influence (-23.4 ‰) or a mixed terrestrial-marine influence (-27.3 to -29.8 ‰)

Nd-Sr isotopic provenance data show an Andean provenance.

Paleocene marine incursion can be related to the subsidence created in response to the proto-Western Cordillera loading.

# Evidences for a Paleocene marine incursion in Southern Amazonia (Madre de Dios Sub-Andean Zone, Peru)

M. Louterbach [1,2,3], M. Roddaz[1], J. Bailleul[2], P.-O. Antoine[4], S. Adnet[3], J.H. Kim[5], E. van Soelen[5], F. Parra[1], J. Gérard[3], Y. Calderon[6] , C. Gagnaison[2], J. S. Sinninghe Damsté[5] and P. Baby[1]

[1] *Géosciences-Environnement Toulouse, Université de Toulouse; UPS (SVT-OMP); LMTG; CNRS; IRD; 14 Avenue Édouard Belin, F-31400 Toulouse, France*

[2] *Bassins-Réservoirs-Ressources, Institut Polytechnique Lasalle Beauvais, Département Géosciences, 19 rue Pierre Waguet, BP 30313, F-60026 Beauvais Cedex, France*

[3] *REPSOL Exploracion S.A., Calle Mendez Alavaro 44, 28045 Madrid, Spain*

[4] *Institut des Sciences de l'Évolution (ISE-M, UMR - CNRS 5554), c.c. 64, Université Montpellier 2, Place Eugène Bataillon, F-34095 Montpellier Cedex 05, France*

[5] *Royal Netherlands Institute for Sea Research (NIOZ), Department of Marine Organic Biogeochemistry, Den Burg (Texel), The Netherlands*

[6] *PERUPETRO S.A., Luis Aldana 320 - San Borja, Lima, Peru*

ABSTRACT

This article presents new biostratigraphic dating, facies analysis, organic geochemical data and Nd-Sr isotopic provenance from five outcrops of southern Amazonia (MD-85, MD-177 MD-184, MD-255 and MD-256) to document for the first time the presence of a shallow marine ingression in the Paleocene of southern Amazonia basin. The co-occurrence of a selachian assemblage encompassing *Potobatis* sp., *Ouledia* sp., and Pristidae indet. with the ostracod *Protobuntonia* sp. and the charophytes *Peckichara* cf. *varians meridionalis*, *Platychara perlata*, and *Feistiella* cf. *gildemeisteri* suggests a Paleocene age for the studied deposits (most likely Thanetian but potentially Danian). Fifteen facies have been recognized and have been grouped into three facies assemblages. Facies association A corresponds to the sedimentary filling of a tide-influenced meandering channel formed in the fluvial-tidal transition zone. Facies association B is related to more distal tidal-flats, little channelized tidal inlets and saltmarshes deposits. Facies association C corresponds to a stressed shallow marine environment such as a bay or a lagoon. The $\delta^{13}C_{TOC}$ value (-23.4 ‰) of MD-184 is enriched in $^{13}C$ compared to the other samples suggesting the presence of substantial amounts of marine organic matter in MD-184. The $\delta^{13}C_{TOC}$ values of samples from other outcrops (-27.3 to -29.8 ‰) indicate a mixed organic matter origin, from terrestrial to brackish environments. The analyzed sediments have similar Nd-Sr isotopic compositions as those of the Cenozoic sediments of the Altiplano ($\varepsilon$Nd(0) values from –6.2 to -10.7 and $^{87}Sr/^{86}Sr$ compositions from 0.712024 to 0.719026) indicating a similar volcanic source. This multidisciplinary dataset documents the presence of a tide-dominated estuary sourced by the proto Western Cordillera debouching into a shallow marine bay during Paleocene times. This transgression might be explained by subsidence created in response to the proto-Western Cordillera loading. Similar to Miocene marine incursions affecting the Pebas megawetland, Paleogene marine incursions in the Amazonian foreland basin associated with Andean uplift may have played a role in the

Neotropical biodiversity dynamics in favouring biogeographical isolation and promoting allopatric speciation for terrestrial organisms.

*Keywords*: Paleogene; marine incursion; Amazonian foreland basin; tidal deposits; micro paleontology; vertebrates paleontology; organic geochemistry; Nd-Sr isotopes; Madre de Dios basin; Peru; Andes.

## 1. Introduction

The Amazon basin is the world's largest Cenozoic fluvial basin with an actual drainage area of $5.8\times10^6$ km2 and a depositional area of approximately 2.5 to $3\times10^6$ km2. The Amazon rainforest, with an area of about $5.6\times10^6$ km2, is the largest rainforest ecosystem, representing nearly 50% of the total tropical rainforest area on Earth. The Amazon rainforest plays a significant role in global climate, the carbon cycle and biodiversity and is the most species-rich terrestrial ecosystem in the world. However, the timing of the origin and evolutionary causes of this diversity are still highly debated. A recent synthesis by Hoorn et al. (2010) has highlighted the complex links between Andean mountain building, climate variability and biodiversity development throughout Cenozoic times in the Amazonian basin. In particular the occurrence of inland seaway is important not only in promoting biogeographical isolation and allopatric speciation but also in controlling the precipitation rates in the Amazon basin (Jeffery et al., 2012). Consequently, determining the number, timing and duration of Cenozoic marine incursions recorded in Amazonian basin is fundamental not only for reconstructing paleo-Amazonian landscapes and ecosystems through time but also for understanding the close relationships between Andean mountain building and the Cenozoic climate and biotic evolution of South America.

Several marine incursions have already been described in the Cenozoic sedimentary record of the Amazonian foreland basins (Roddaz et al., 2010). For instance, the existence and persistence of the early to middle Miocene Pebas megawetland system in northern Amazonia is thought to have promoted the high biodiversity of the Amazon rainforest (for a review, see (Hoorn et al., 2010) and references therein). However, the extent of this Pebas system and the number of marine ingressions that have occurred is still under debate (Campbell et al., 2006; Hovikoski et al., 2007; Hoorn et al., 2010) mainly because of poor stratigraphic dating and the lack of regional data integration. In comparison, few studies document Paleogene marine

incursions in the Amazonian basin. For instance, there is some evidence of a marine ingression during Eocene to Oligocene times in Colombia (Santos et al., 2008), Ecuador (Christophoul et al., 2002) and northern Peru (Hermoza et al., 2005b), but no data exist for earlier marine incursions.

In this study, new biostratigraphical, sedimentological and geochemical data are presented to highlight a Paleocene marine ingression in southern Peru, Madre de Dios basin. A new paleo-depositional model for these coastal deposits is also proposed. Finally, the paleogeography and paleo-extension of this shallow marine ingression are discussed.

## 2. Geological background

### *2.1. Paleocene sedimentary record in the Amazonian foreland basins*

In nearly all the Central Andean sedimentary basins, late Eocene to early Oligocene times are marked by a widespread sedimentary hiatus (Mpodozis and Allmendinger, 1993; Marocco et al., 1995) corresponding to a major tectonic phase primarily called Incaic 1 phase (Noble et al., 1990; Jaillard, 1996; Hermoza, 2004). However, there are some localities in northern and Central Andean foreland basins where Paleocene strata have been preserved and can be described (Fig. 1 and Fig. 2).

In central Colombia, the Cuervos formation is late Paleocene in age (Jaramillo and Dilcher, 2000; 2001) and its sedimentary rocks correspond to mudstones deposited in a distal alluvial to coastal plain environment, in a foredeep position (Cooper et al., 1995; Parra et al., 2009). In the Putumayo basin of southern Colombia, the Rumiyaco Formation is barren of fossils and then remains poorly constrained but it is assumed that it is early Paleocene in age. The Rumiyaco Formation unconformably overlays the Cretaceous series and builts up a sedimentary wedge onlapping onto older strata and disappearing toward the east of the basin. The formation is characterized by possibly marine-related to mostly continental fine-grained deposits in the western part of the Putumayo basin and evolves eastward into continental sandstones (Bejarano, 1991; Casero, 1997; Córdoba et al., 1997; Londoño et al., 2012). In the Ecuadorian Oriente basin, Paleocene strata dated by charophytes (Faucher and Savoyat, 1973) are represented by the deposits of the fluvial Tena Formation. Various studies demonstrated that sediments from Tena Formation are derived from the Eastern Cordillera of Ecuador (Ruiz et al., 2004, 2007; Martin-Gombojav and Winkler, 2008).

**Comentario [L,M1]:** I added Cooper's reference for the Cuervos Fm-.

**Comentario [L,M2]:** Additional references

In Peru, Paleocene strata are very scarce and are only identified in the eastern border of the Altiplano (Vilquechico Group and Lower Muñani Formation), in the Cusco-Sicuani

105 area (Puquin Formation) or in the present-day foreland basin (Yahuarango or Huayabamba
106 Formations) (Sigé et al., 2004; Gelfo and Sigé, 2011). These strata generally consist of
107 reddish fine-grained continental deposits and are defined as the Red Beds Formation (Naeser
108 et al., 1991; Jaillard, 1993a; Hermoza et al., 2005b). The Lower Muñani Formation is dated
109 between 55.9 and 53.4 Ma by mammalian biostratigraphy and by magnetostratigraphy (Cande
110 and Kent, 1992; Sigé et al., 2004). The Yahuarango (Huallaga and Marañon basins) and
111 Huayabamba (Madre de Dios and Beni basins) formations are poorly constrained. Only a few
112 charophytes have been documented and provide a Paleocene age (Gutierrez, 1982) for these
113 fluvial deposits (Fig. 2).

114 In Bolivia, Paleocene strata are virtually absent in the Amazonian foreland basin
115 (Roddaz et al., 2010) (Fig. 2). Paleocene deposits documented in the Eastern Cordillera of
116 southern Bolivia correspond to the mostly continental Santa Lucía and Cayara Formations,
117 Danian and Thanetian in age, respectively (Marshall et al., 1997; DeCelles and Horton, 2003).
118 However, a typically marine stingray (*Potobatis semperei*) was recently recognized within a
119 marly horizon at the top of the Danian Santa Lucía Formation (Cappetta and Gayet, 2013).

120 *2.2. Stratigraphy and structure of the Madre de Dios basin*

121 The Madre de Dios basin is part of the southern Amazonian foreland basins system
122 (Roddaz et al., 2005). The Madre de Dios foreland basin is located northeastward to the
123 Eastern Cordillera (EC) of southern Peru and can be subdivided into the Sub-Andean Zone
124 (SAZ) and the Madre de Dios plain tectonomorphic units (Fig. 1-B) (Gil, 2001; Hermoza,
125 2004). The SAZ is characterized by both sedimentary filling and active deformation. In the
126 SAZ, propagation of deformation towards the Madre de Dios plain is controlled by the
127 development of deep duplexes, whose shortening is accommodated in surface by imbricates
128 and by the Sub-Andean thrust front. The Sub-Andean thrust front corresponds to the eastern

129 border of the SAZ and is responsible for transportation of a piggy-back basin, which outcrops
130 as a large syncline called Salvación syncline in the study area (Fig. 1-B). The deformed and
131 still active SAZ only corresponds to the internal (western) part of Madre de Dios foreland
132 basin. The external (eastern) part of the basin is situated east to the Sub-Andean thrust front
133 and corresponds to the non-deformed part of the system, the Madre de Dios plain. In this
134 study, we will only focus on outcropping strata from the Salvación syncline, in the SAZ of
135 Madre de Dios basin.

136 Upper Cretaceous to Cenozoic strata in Salvación piggy-back basin consist of +/- 4500
137 m of an alternance of marine, tide-influenced and fluvial deposits (Gil, 2001; Hermoza,
138 2004). Because of the very scarce outcrops, fauna and palynomorph material available in the
139 studied area, the general chronostratigraphy of this succession is quite difficult to assess and
140 many interrogations subsist for the Cretaceous-Paleogene interval (Gil, 2001; Hermoza,
141 2004), while Miocene deposits are much better constrained in terms of biochronology and
142 chronostratigraphy (Marivaux et al., 2012; Antoine et al., 2013; Antoine et al., Submitted).
143 Paleogene strata in the Salvación series and more broadly in the Madre de Dos basin are
144 supposed to correspond to the fluvial Huayabamba or the Red beds Formation.

## 3. Methodology

In the Madre de Dios basin, Paleogene deposits crop out along the Alto Madre de Dios River between the Pongo de Coñeq Canyon and the Pantiacolla anticline, which correspond to the verticalized flanks of the Salvación Syncline (Fig. 1-B). This paper focuses on five selected exposures in cutbanks along the Alto Madre de Dios River. The section includes MD-177, MD-255, MD-256, MD-85 and MD-184 outcrops (Fig. 1-B and Fig. 1-C). Their precise locations are given in the online Supplementary Table A. The five concerned localities yield similar micro- and macrofossils (foraminifers, charophytes, molluscs, ostracods, as well as chondrichthyan and actinopterygian fishes), which allows us to consider them as being time equivalent (Table 1 and Fig. 3). Fifteen sedimentary facies are characterized on the basis of their lithologies, their physical and biogenic sedimentary structures, their palynological and paleontological content, and their geometry (Table 2). For limestone layers of MD-184, standard microfacies descriptions have also been realized. Each of these fifteen facies is interpreted in terms of depositional processes and related depositional environment. On the basis of these interpretations and with regards to the geometrical relationships between the facies, three facies associations are proposed (Table 2).

In order to determine the nature of the organic matter (terrestrial versus marine), we analyzed four samples for $\delta^{13}C_{TOC}$ content (Table 3) at the NIOZ Institute, Netherlands. The $\delta^{13}C_{TOC}$ of higher plants that use the Calvin-Benson cycle of carbon fixation (i.e. so-called $C_3$ plants) ranges from -29.3 to -25.5 ‰, with an average value of about -27 ‰ (e.g. Tyson, 1995). The typical marine $\delta^{13}C$ $C_{TOC}$ values are in the range of -18 to -22 ‰ (e.g. Meyers, 1997). Additional geochemical rock-eval analysis (for sample MD 184) has also been carried out by Repsol Exploration S.A.

Four selected samples of mudstones from outcrops MD-177, MD-85, MD-184 and MD-255 were measured at the University of Toulouse for their Nd-Sr isotopic compositions, providing sedimentary provenance information (Table 4). Aliquots containing about 1000 ng of Sr and Nd were loaded onto the ion-exchange columns. Sr and Nd were separated using the Sr-SPEC, TRU-SPEC and LN-SPEC resins (Eichrom®). Nd-Sr isotopic ratios were measured using a Finnigan Mat 261 thermal ionization mass spectrom in dynamic mode following Viers et al. (2008). The measured $^{143}Nd/^{144}Nd$ ratios are presented as the fractional deviation in parts per $10^4$ (units) from $^{143}Nd/^{144}Nd$ in a Chondritic Uniform Reservoir (CHUR) as measured at the present-day:

$$\varepsilon Nd(0) = [(^{143}Nd/^{144}Nd)_S/I_{CHUR}(0)\_1]*10^4$$

where $(^{143}Nd/^{144}Nd)S$ is the present-day ratio measured in the sample, and $I_{CHUR}(0)$ is the $^{143}Nd/^{144}Nd$ in the CHUR reference reservoir at the present ($I_{CHUR}(0) = 0.512638$ (Jacobsen and Wasserburg, 1980).

## 4. Results

### *4.1. New biostratigraphical and paleoenvironmental constraints from fossil assemblage*

#### *4.1.1. Biostratigraphy*

Comentario [L,M3]: This paragraph has been deeply modified.

The fossil content of stratigraphic interest recovered in the studied sections is detailed in the Table 1 and Fig. 3. The concerned material includes vertebrates (chondrichtyans and actinopterygians), ostracods, benthonic foraminifers, and charophytes. Being only recognized at genus, family level, or above, the molluscs found in MD-177, MD-184, and MD-85 are of no use in terms of biostratigraphy (Table 1). Accordingly, MD-177 and MD-184 yielded unidentified Charophyta and Ostracoda.

The dominant taxon among vertebrate remains in the concerned deposits is the batoid *Ouledia* sp. (MD-177; MD-184; MD-85; see Table 1 and Fig. 3 for biostratigraphical results details and Fig. 4 C-D, I-J for an illustration of the key stratigraphic markers). This fossil genus of butterfly rays (gymnurids) is well-known in tropical coastal deposits from Africa and Asia, ranging from the Thanetian up to the Priabonian (Cappetta, 2012). In MD-184, *Ouledia* is found in association with a pristid sawfish. Pristids are a cosmopolitan family restricted to Cenozoic marine and estuarine localities at world scale (i.e., Danian and onward; Cappetta, 2012). In MD-85, *Ouledia* sp. (mainly represented by worn teeth) co-occurs with *Potobatis* sp. (Fig. 4 G-H), a dasyatoid stingray so far endemic to Danian marine levels from the top of the El Molino Fm., Bolivia (Cappetta and Gayet, 2013). However, in MD-85, the prismatic teeth referred to as *Potobatis* sp. are eroded and might have been reworked, which would concur to consider the Danian epoch as a floor age for MD-85. The vertebrate assemblages also include dozens of teeth of an unidentified pycnodontid bony fish (MD-177, MD-184; Fig. 4 E-F), distinct from but potentially allied to ?*Ocloedus toncoensis* (Maastrichtian-Danian of South America; Gonella et al., 2012). Pycnodontids are well represented in

Mesozoic and early Paleogene localities, before the family gets extinct during the middle Eocene (Gayet et al., 1993; Poyato-Ariza and Wenz, 2002).

Microfossils of high biostratigraphical interest were recovered in MD-255 and MD-85. The agglutinated benthonic foraminifer *Karreriella conversa* (Eggerellidae), found in MD-255, has an Upper Cretaceous-Lutetian range (Fig. 2; Gradstein et al., 1988; Valchev, 2007). The best constrained locality is MD-85, with a diversified charophyte flora (17 specimens of *Peckichara* cf. *varians meridionalis*; 10 specimens of *Platychara perlata*?; 15 specimens of *Feistiella* cf. *gildemeisteri*), the ostracod *Protobuntonia* sp., and benthonic foraminifers (*Reophax* sp., *Bathysiphon* sp., and *Rhabdammina* sp.). The ostracod *Protobuntonia* ranges from the Coniacian up to the Thanetian epoch (Morsi et al., 2011); the fragile and delicate valves referred to this taxon in MD-85 are complete (i.e., not likely to be transported or reworked). The charophyte *Platychara perlata* has a Danian last occurrence in Peru (Sigé et al., 2004). The charophyte *Peckichara* cf. *varians meridionalis* is restricted to the Maastrichtian-Thanetian interval (e.g. Musacchio, 1990; Aubry et al., 2005). The charophyte *Feistiella* cf. *gildemeisteri*, previously recorded in the Paleocene Yahuarango Formation from Huallaga area, in northern Peru (Hermoza et al., 2005b; Roddaz et al., 2010) and at Laguna Umayo, southern Peru (Jaillard, 1993a), ranges from the Maastrichtian up to the Thanetian or the earliest Ypresian (Sigé et al., 2004; Gelfo et al., 2009; Gelfo and Sigé, 2011; Woodburne et al., 2014).

Once combined, all these biostratigraphical data preclude any referral i) to Mesozoic times (*Potobatis*, Pristidae, and *Ouledia* have a Paleocene First Appearance Datum [FAD]) or ii) to a post-Paleocene interval (*Protobuntonia*; *Platychara perlata*; *Peckichara* cf. *varians meridionalis*). In other words, they strongly concur to indicate a Paleocene age for the deposits described in the northern part of the Madre de Dios Basin (MD-85, MD-177, MD-184, and MD-255 localities; Table 1 and Fig. 3). Yet, based on the biostratigraphical markers

recognized in the concerned sections, the age of the studied marine incursion cannot be further refined definitely. However, this marine incursion is more likely to coincide with Danian or Thanetian times (Hypotheses 1 and 2, respectively; Fig. 3). The Hypothesis 1 (Danian) favors the known range of *Potobatis* (then not reworked at MD-85) and of *Platychara perlata*. This would in turn imply a Danian first occurrence for *Ouledia*, 3-8 million years before its known FAD (Fig. 3). The Hypothesis 2 (Thanetian) is constrained by the conspicuous presence of *Ouledia* in three localities. In that case, *Potobatis* teeth might be reworked in MD-85 and/or the stratigraphical range (as for the charophyte *Platychara perlata* , same locality) is to be extended up to the Thanetian epoch (Fig. 3).

We tend to favor the Hypothesis 2, due to the occurrence of hundreds of fresh specimens referred to as *Ouledia* sp. found in MD-85, MD-177, and MD-184. Furthermore, it cannot be discarded that the two prismatic teeth of *Potobatis* and the 10 oogonia of *Platychara perlata* were reworked from Danian deposits eroded upstream by the time of deposition of MD-85.

*4.1.2. Paleoenvironments*

Thus far, late Cretaceous and Paleocene selachian faunas from Andean and sub-Andean basins consist only of batoids (i.e. no shark is recorded), further known to be highly endemic (de Mowbray and Visser, 1984; Gayet et al., 1993; Cappetta and Gayet, 2013). Together with the complete absence of associated sharks, the co-occurrence of *Ouledia* (MD-177; MD-184; MD-85), *Potobatis* (MD-85), two unidentified dasyatoids (MD-177), and a pristid (MD-184) point to shallow waters in a proximal marine or estuarine environment for the Paleocene deposits described in this study (Cappetta, 2012; Cappetta and Gayet, 2013). The ichthyofauna also includes a high number of pycnodontiform bony fish remains (Pycnodontidae indet.; MD-177; MD-184; MD-85, see Fig. 3 and Fig. 4), some of them being found in partial anatomical connection (i.e., no transport). This extinct group is only recorded

in marine deposits (shallow water seas; Gayet et al., 1993). However, a freshwater influence is supported by the presence of numerous isolated teeth of characiform bony fishes (MD-177; MD-184; MD-85). Today, characiforms are strictly restricted to freshwaters (Gayet et al., 1993). Serrasalmine characiform teeth with a plesiomorphic pattern (*Colossoma*-like) were in particular recognized in MD-184.

The agglutinated foraminifer assemblage, including *Karreriella conversa* (MD-255), *Reophax*, *Bathysiphon*, and *Rhabdammina* (MD-85), points to a shallow marine inner platform, under unstable environmental conditions, with frequent detrital/terrigenous influxes. Such a continental influence is further attested by the presence of numerous charophyte oogonia (likely to be transported during river flooding episodes) and riverine to brackish molluscs (e.g., *Corbicula* and *Aylacostoma*). No open sea indicator, such as dinoflagellates or planktonic foraminifers, has been recorded throughout the sections.

To sum up, the macro- and microfossil assemblages (vertebrates, molluscs, ostracods, foraminifers, and charophytes) as documented in MD-177, MD-184, MD-255, and MD-85 (Table 1 and Fig. 3) point to an initial idea of the depositional environment: a shallow marine inner platform, under unstable environmental conditions, with frequent detrital/terrigenous influxes from a river estuary or delta.

### *4.2. Depositional environments from sedimentary analysis*

In this section, the facies associations are described and interpreted. Diagnostic criteria of the facies are summarized in Table 2.

#### *4.2.1. Facies association A: the Fluvial-tidal transition zone*

Facies association A is made up of four facies: A1, A2, A3, and A4. These four facies have only been described at the location of outcrop MD-255 (Fig. 1-C). Outcrop MD-255 displays two channel-shape stacked bodies showing concave-up basal surfaces. The lateral

extension of these sedimentary bodies is close to 150 m long and their thickness reaches 4 to 5 m (Fig. 5-A and Fig. 5-B). Facies A1, A2 and A3 have been recognized within the channelized bodies, whereas facies A4 has been observed above and laterally to the channels (Fig. 5).

Facies A1 (total thickness of 20 to 120 cm) has been observed at the base of the channel-shape bodies. It generally starts with an accumulation of millimetric to centimetric mud clasts scattered in fine- to medium-grained sandstone, forming a few cm-thick microconglomeratic matrix-supported mud breccias, erosive at its base. Mud clasts disappear upwards and the facies evolves into fine- to medium-grained sandstones. These sandstones are massive or are organized into tangential cross-bedding forming 30 cm thick tangential co-sets (Fig. 6-A). Some reactivation surfaces can be observed. Both tangential sets and co-sets can be highlighted by thin mud drapes and generally present the same dip direction. However, some foresets can dip in the opposite direction. Facies A1 ends with an undulate rippled surface with heights of 1 to 2.5 cm and wavelengths of 15 to 20 cm, showing ichnofabrics *Arenicolites* and possible *Dactiloides* (Fig. 6-B and Fig. 6-C). Facies A1 corresponds to the coarsest deposits described in the area.

Facies A2 (total thickness of 1 to 1.20 m) consists of slightly oblique heterolithic strata (Fig. 6-F) overlying Facies A1 after a sharp transition (Fig. 5-B). Massive fine-grained sandstones or flaser bedding with asymmetrical climbing ripples highlighted by frequent mud drapes (15 to 30 cm thick) (Fig. 6-E) alternates with wavy bedding or planar muddy lamination in fine-grained sandstones (10 to 20 cm) (Fig. 6-G). The distribution of the thin planar mud drapes observed within the fine-grained sandstones of the wavy bedding often displays a rhythmic pattern, with intervals of inframillimetric sandstone beds evolving gradually to millimetric and then centimetric thicker sandy beds suggesting coarsening-up

303 cycles (Fig. 6-G and Fig. 6-F). Mud accumulation can be 1 mm to 1 cm thick. Horizontal and
304 to a lesser extent vertical undetermined burrows are occasionally present.

305 Facies A3 also corresponds to slightly oblique heterolitic strata (total thickness > 60
306 cm). In comparison with Facies A2, Facies A3 is coarser as it is made up of thicker sandy
307 beds (20 to 40 cm thick) intercalated with thin muddy to silty beds (2 to 5 cm thick). Fine-
308 grained sandstones present tangential cross-bedding with planar laminations at their base
309 representing their bottomset (Fig. 6-D). Rare asymmetrical ripples in the opposite direction
310 can also be observed at the top of the tangential laminations. These sansdstones are also
311 heterolithic as almost all the sandy tangential and planar laminae are highlited by thin mud
312 drapes. Regular chanching thicknesses of millimetric to centimetric sandy layers and
313 inframillimetric to millimetric muddy layers suggests a rhythmic pattern (Fig. 6-D). Facies A1
314 and A3 are both made up of tangential cross-bedding in fine-grained sandstones, but
315 differences with Facies A1 result in: 1) the scale of the structures (Facies A1 is made up of
316 larger-scale cross-bedding compared to Facies A3), 2) the general geometry of the bodies
317 (Facies A1 corresponds to the laterally filling of a channelized body whereas Facies A2
318 corresponds to more tabular deposits) and 3) the texture and internal organization of the
319 sediments (more finer texture and more heterolithic and rhythmic patterns for Facies A1).

320 Strata from both facies A2 and A3 present an oblique pattern, prograding from the
321 south-eastern channel margin towards the north-western margin of the channel (Fig. 5-A and
322 Fig. 5-B).

323 Facies A4 corresponds to siltstone layers (2 m thick) intercalated with fine-grained
324 sandstone layers (10 cm thick). These sandstones present a sharp contact with the underlying
325 siltstones and show climbing-ripples structures. Siltstones evolve upwards into mudstones (>2

m thick), where root traces develop at the top of the section. Rare benthic foraminifer *Karreriella conversa* can be preserved in this facies.

Interpretation:

Stacked channels geometries as observed at MD-255 are common in fluvial and tidal settings. In both cases channels are erosive at their base and can be composed of fining- and thinning-up strata evolving gradually upwards into shaly strata. These shales can correspond to either fluvial floodplain or tidal flat deposits depending on the depositional environment.

The massive or cross-bedded fine- to medium-grained sandstones with basal mud clasts above erosional surfaces (Facies A1) could represent purely fluvial channel filling with bottom reworking lag deposits (Facies Gt and Gh from Miall, 1996). However the presence of ichnofabric *Arenicolites* (and possible *Dactiloides*?) observed at the top of this facies (Fig. 6-C) and the presence of the benthic foraminifer *Karriella conversa* (Facies A4) suggest deposition in, respectively, tide-influenced environment (deltaic or estuarine) and deposition in shallow marine platform with continental influx (see Table 1). Facies Association A is therefore related to both tidal and fluvial environments.

Reactivation surfaces as observed within the cross-bedded sandstones of facies A1 can be caused by tidal current reversals (Klein, 1970; de Mowbray and Visser, 1984) even if these surfaces could also be produced by river-discharge variations and erosion of brink by arrival of a new bedform in fluvial settings (Dalrymple, 1984). The occurrence of rare bidirectional trough cross-bedding (Fig. 6-A) suggests a depositional area receiving opposite-direction currents, dominated either by flood or ebb currents. The prograding pattern displayed by the tangential cross-bedded sandstones suggests lateral accretion processes. Mud clasts have been deposited at the base of the channels by gravity processes. They are common in channel bottom deposits in many tide-dominated or influenced environments because of the erosion

by high-energy currents of thin muddy layers forming slack water drapes, or because of the erosion by lateral accretion of muddy tidal-flat and salt-marsh deposits (Dalrymple and Choi, 2007). In conclusion, we interpret Facies A1 as dune deposits formed during the early-stage of a tide-influenced channel settlement controlled by both fluvial and tidal processes.

Facies A2 and A3 overly the basal filling of the channelized bodies and constitute small-scale Inclined Heterolithic Stratification (IHS). These IHS developed by lateral accretion within the channels (Fig. 5-A and Fig. 5-B). Although IHS may be observed in fluvial environments (e.g., Jackson, 1981; Page et al., 2003), they are most common in tide-influenced settings (Dalrymple et al., 2003). In addition, Facies A2 and A3 often display rhythmic patterns and heterolithic textures. Interlamination of mud and fine-grained sands results from suspension and weak traction current and may occur in fluvial overbank deposits (lithofacies Fl, Miall, 1996). However, alternation of sand and mud laminae within millimetric wavy and flaser beddings (Facies A2 and A3) is more frequent in tidal depositional environment. Concerning Facies A2 and A3, the abundance of wavy and flaser bedding, mud drapes and rhytmicity rather suggests tidal influence on deposition (Nio and Yang, 1991). Recurrent thickness fluctuations observed within the cross-bedded sandstones in the successive sandy beds of Facies A3 (Fig. 6-D) may be interpreted as the result of neap-spring influence (Eriksson et al., 1998; Eriksson and Simpson, 2004; Mazumder and Arima, 2005). Similar rhythmicity has also been found within facies A2 (Fig. 6-F and Fig. 6-G). The presence of few thin mud drapes observed within these sandstones may therefore represent deposition during tidal slack-water periods. Facies A2 corresponds to lower hydrodynamic conditions than Facies A3 (coarser sandstones). However, they both constitute IHS, and are interpreted to have been deposited by lateral accretion in a channelized body. Therefore, facies A2 and A3 are both interpreted as tide-influenced point-bar deposits in a meandering

**Comentario [L,M4]:** Neap-spring cycles are related to lunar cycles

channel. Because Facies A3 is situated above Facies A2 (Fig. 5), Facies A3 should be related to a higher energy recovery during the channel deposition history.

Facies A4 corresponds to the uppermost- and finest strata deposited at the top of the channels succession. This silty facies could firstly be interpreted as channel abandonment, fluvial floodplain or tidal-flat deposits. The presence of *Karreriella conversa* indicates deposition in a coastal, brackish water environment (Valchev, 2007) and supports a tidal flat interpretation for facies A4. According to Dalrymple and Choi (2007), the pedogenic structures described in the mudstones at the top of facies A4 could be associated to a period of emersion of a tidal mud flat .

To conclude, Facies association A corresponds to a moderate-energy channel filling history. According to the IHS geometry resulting from lateral accretion processes, this channel is interpreted to be related to a meandering system. Because of the proximity of pedogenetic features and because of the preponderance of fine-grained texture in the facies association, this meandering system could be purely fluvial. However, the evidences of tidal- or marine-related environment (benthic foraminifer, *Arenicolites*) and the evidences of tidal-processes (rhythmic patterns, IHS, mud drapes) finally suggest a mixed fluvial-tidal environment. Facies association A is interpreted to correspond to the sedimentary infilling and abandonment of tide-influenced meandering channels migrating laterally in surrounding tidal-flats and floodplain.

#### *4.2.2. Facies association B: Tide-dominated environment*

Facies association B consists of 5 facies: B1, B2, B3, B4 and B5. They all have been found in MD-256 (Fig. 7) and partially in MD-85 (Fig. 9) and are summarized in Table 2.

Facies B1 corresponds to the infill of isolated channelized sedimentary bodies (~60 to 150 m width and ~1 to 1.50 m in thickness) and has been observed at both MD-256 and MD-

85 localities. No stacking or amalgamated pattern has been noticed. The base of this facies corresponds to a channel-shaped surface. This surface is highlighted by elongated millimetric to centimetric mud clasts forming a breccia of few centimetres-thick and evolving upwards into massive medium- to fine- or very fine-grained sandstone. Internal sigmoid cross-beddings (45 cm in height) are often present in the basal part of these sandstones. Fine-grained sandstones may also display high-angle climbing ripples at their base evolving upwards into low-angle climbing ripples (Fig. 8-A). At the top of the deposits, climbing ripples cross-stratification changes upward into more flattened trough cross-stratification (see channel sedimentary structures within the channel of outcrop MD-85, Fig. 8). Reworked charophyte oogonia, stingray teeth (MD-85), and benthic foraminifer (MD-256) are observed in this facies (Table 1).

Facies B2 (total thickness of ~20 m) consists of reddish mudstones. Root traces and gypsum or anhydrite nodules can develop at the top of the facies (Fig. 8-B). This facies has been observed at the top of the sedimentary section and presents a sharp contact with the underlying Facies B3 (Fig. 7). It is also laterally associated with Facies B1.

Facies B3 and B4 are closely related and often alternate in the section described (Fig. 7). In this case, the contact between the two facies is sharp. Facies B3 (total thickness of 0.50 to 4 m) consists of bioturbated and burrowed reddish mudstones to rare siltstones. Occasional lenticular bedding can occur within the mudstones. Facies B4 (total thickness of 1 to 5 m) corresponds to highly burrowed heterolithic deposits showing regular alternations of very fine to fine-grained sandstones with muddy or silty layers displaying planar horizontal, wavy bedding and lenticular bedding (sets of 10 cm thick) (Fig. 8-C, Fig. 8-D and Fig. 8-E). Burrows are horizontal or vertical but no specific ichnofabric can be determined (Fig. 8-4D). Colour is dark grey to violet. The sedimentary structures in sandstones are highlighted by thin (2 to 3 mm thick) laminae of mud and silty drapes. Thin sand layers can occasionally be

intercalated by mud drapes, thus forming mud couplets. Opposite current dips have been observed in this facies. At the top of sandy strata, fluid escape structures can be observed (Fig. 8-E). Facies B5 (total thickness of ~20 cm) is generally observed above facies B4, after a sharp or progressive contact (Fig. 7). It is made up of clean fine-grained sandstone often ending with a wave-rippled surface (ripples are 1 to 1.5 cm in height with wavelength of 6.5 to 8.5 cm) (Fig. 8-F).

Interpretation:

Facies B1 corresponds to channel infill deposits. Climbing-ripple cross-stratification is a common feature in a wide range of depositional environments in which suspension exceeds the rate of traction transport (Jopling and Walker, 1968; Allen, 1970; Ashley et al., 1982). However, sigmoidal cross-bedding associated with the presence of brackish-water fossils (benthic foraminifer, see Table 1) suggests deposition within a tide-influenced environment. Climbing ripples from tidal environments are different from non-tidal climbing ripples by having common mud drapes and finer-grained texture (Choi, 2010). In a tidal environment, they can be characteristic of tidal inlet infillings in the fluvial-tidal transition zone of estuaries (Dalrymple et al., 1992; Tessier, 1996; Hovikoski et al., 2008). Flood dominated Climbing Ripples Facies (CRF) can also be associated with tidal channel levees found in the inner/straight channel zone of the fluvial-estuarine transition (cf. Mont St Michel estuary; Tessier, 1996). In case of ebb-dominated context, CRF are found in chute channels and chute bars in the meandering zone of the fluvial-estuarine transition (Tessier, 1996). In comparison with Facies A1, Facies B1 is finer-grained and is related to decreasing flow processes (climbing ripples). Geometrically, Facies B1 only concerns isolated channels whereas Facies A1 is related to stacked and thick channels overlain by laterally migrating strata (IHS deposits; Facies A2 and A3, Fig. 5). Channels from Association A represent higher energy channels in comparison with those from Facies Association B (Facies B1). We interpret Facies

448 B1 as tidal inlet deposits. Facies B2 is generally structureless but contains paleosoil horizons
449 and gypsum nodules in a very fine shaly matrix. As it is laterally associated with facies B1, it
450 has been interpreted as salt marshes in a supratidal environment. Facies B3, characterized by
451 muddy deposits with scarce lenticular bedding, could correspond to mud flat deposits in an
452 intertidal environment. Facies B4 is characterized by highly burrowed heterolithic deposits
453 with double mud drapes, wavy and lenticular beddings that are typical sedimentary structures
454 of tide-influenced environments (Nio and Yang, 1991; Dalrymple et al., 1992; Dalrymple and
455 Choi, 2007). We consequently interpret facies B4 as mixed muddy/sandy flat deposits.

456 To conclude, Facies association B is constituted by all the surrounding flats influenced
457 by tidal processes, from the subtidal area (tidal inlet (Facies B1), mixed tidal flats with double
458 mud drapes (Facies B4 and B5) to the intertidal/surpatidal environments (mud flats and
459 saltmarshes, respectively Facies B2 and B3).

460 *4.2.3. Facies association C: Bay and shallow marine environments*

461 Facies association C is composed of six facies: C1, C2, C3, C4, C5 and C6. All the
462 facies have sheet-like geometries, and have been described at outcrops MD-85 (Fig. 9), MD-
463 177 and MD-184 (Fig. 10, section 1 and 2, respectively).

464 Facies C1 (total thickness of 50 cm to >2 m) corresponds to blue-violet-reddish marls
465 to carbonated siltstones with centimetric thick fine-grained sandy layers and occasional
466 centimetric thick carbonaceous layers (Fig. 11-A). Ripples and climbing ripples are present
467 within the sandy layers. Facies C1 contains benthic foraminifer (*Bathysiphon*, Fig. 11-B),
468 Mollusca (Bivalvia: Corbicula and Polymesoda; Gastropoda: Cerithioidea, Pachychilidae,
469 and? *Aylacostoma*), Ostracoda, Chondrichthyes (Myliobatiformes: *Ouledia* sp., Pristidae, and
470 Dasyatoidea), Osteichthyes (Pycnodontiformes: *Coelodus*; Characiformes: Serrasalminae and
471 indet.) (see Table 1). Facies C2 (total of thickness 80 cm to 1 m) is always closely related to

facies C1 and the contact (basal and top) between the two facies is progressive. Facies C2 is similar to facies C1 but contains common sandy and gypsum nodules, root traces and bioturbation. Facies C3 (total thickness of 15 to 50 cm) corresponds to millimetric to centimetric sandy nodules scattered into a violet muddy to silty matrix, forming a matrix-supported breccias. This facies contains numerous organic fragments such as fish vertebrae and ostracods. Facies C4 corresponds to an alternation of marl (5 to 10 cm) and thin limestone strata (2 to 5 cm). Carbonate nodules are frequent within the marls. Limestones commonly present well-developed desiccation crack surfaces at the top of the strata as well as burrows and root traces. Small oyster shells (2 to 4 cm in length) are visible within the limestone strata. Microfacies analysis of thin sections allowed the recognition of oysters (little size species), fish vertebrae fragments, annelid burrows, numerous ostracods and/or phylopods, and undifferentiated gastropods (Fig. 12-A, Fig. 12-B, Fig. 12-C and Fig. 12-D). Only very few ostracods and phylopods present a complete carapace with paired valves but they all present a smooth surface. According to Dunham's classification (Dunham, 1962), the observed limestones can be classified as wackstone to packstone. The matrix is generally micritic or microsparitic. Peloidal micrite (Fig. 12-A and Fig. 12-B) could constitute secondary cementation better than primary matrix. Secondary sparite grains are common, and can form drusic or bird-eyes cements (Fig. 12-B and Fig. 12-D). Facies C5 (strata presenting thickness of 25 to 80 cm) also corresponds to limestone deposits showing desiccation cracks at the top (Fig. 11-C and Fig. 11-D). These strata present undulated base and top. Thin-section shows stromatolith filaments entangled with ostracod carapaces and annelid burrows (Fig. 12-E and Fig. 12-F). The matrix is micritic to microsparitic. Facies C6 correspond to limestone strata (10 to 25cm thick) with abundant small-size oysters (2 to 4 cm in length). Thin-section reveals numerous oysters with lamellar and multilayered structures, annelids burrows, blue (?) algae filaments, fish coprolith and some ostracodes (Fig. 12-G, Fig. 12-H, Fig. 12-I and Fig.

12-J). Root traces are also present. The matrix is made up of micrite or small microsparite crystals. Some bivalve's shells are rounded by a micrite envelope (Fig. 12-G). This facies is separated from the other because of its greatest oysters content.

Interpretation

The ichtyofauna from Facies C1 and C3 is characteristic of a shallow marine environment, with variations from a strong freshwater influence in a more proximal environment to a confined and steady proximal marine environment of normal salinity (as attested by the wide array of obligate marine taxa, such as chondrichthyans and pycnodontiform actinopterygians (Cappetta, 2012). Absence of high energy sedimentary structure in facies C1 suggests deposition in a protected shallow marine environment. Pedogenic structures of Facies C2 are related to episodic emersions of these shallow-marine deposits (originally Facies C1). Facies C3 is interpreted to have been deposited by an episode of higher energy in this shallow marine environment, maybe related to bank collapsing. Facies C4, C5 and C6 correspond to limestones deposited in a subaquatic environment submitted to frequent subaerial exposures as attested by the dessication cracks and root traces and burrows found at the top of the beds The presence of little-sized oysters (characteristic of a stressed environment), smooth-carapaces ostracodes and annelids are consistent with a shallow marine environment (Armstrong and Brasier, 2005) whereas micrite envelopes rounding bivalve's bioclasts indicate an intertidal context. Evidences of frequent subaerial exposures indicate a short-lived and frequently changing depositional environment, from intertidal to lacustrine. Stromatholitic carbonates of Facies C5 are related to a confined and stressed intertidal environment (Wattinne, 2004), whereas the *Ostrea* limestones of Facies C6 are in agreement with a deeper confined marine environment (Enay, 1990) intertidal to upper infralitoral. Because of the presence of some fresh water fossils and the occurrence of frequent emersion,

the depositional setting should be quite close to the coast. To conclude, we interpret facies association C to represent deposition in a bay/lagoon or stressed shallow marine-environment.

### *4.3. Organic Geochemistry*

The TOC contents of the samples were in general very low, ranging from 0.03 to 0.06 wt. % (Table 3). Therefore, care should be taken to interpret the organic geochemical data. Nonetheless, the reproducibility of TOC contents and $\delta^{13}C_{TOC}$ was better than 0.02 wt. % and 0.3 ‰, respectively. The $\delta^{13}C_{TOC}$ values varied from -23.4 to -29.8 ‰ (Table 3).

The $\delta^{13}C_{TOC}$ of higher plants that use the Calvin-Benson cycle of carbon fixation (i.e. so-called $C_3$ plants) ranges from -29.3 to -25.5 ‰, with an average value of about -27 ‰ (e.g. Tyson, 1995). The typical marine $\delta^{13}C_{TOC}$ values are in the range of -18 to -22 ‰ (e.g. Meyers, 1997). The $\delta^{13}C_{TOC}$ values (-27.3 to -29.8 ‰) of MD-177, MD-85, and MD-255 are hence typical of $C_3$ plant-derivated organic matter. In contrast, the $\delta^{13}C_{TOC}$ value (-23.4 ‰) of MD-184 is enriched in $^{13}C$ compared to the other samples, closer to typical marine $\delta^{13}C_{TOC}$ values. This suggests the presence of substantial amounts of aquatic organic matter in MD-184. Notably, it has been shown that the presence of a fresh-water algae *Pediastrum*, which is very common in lagoonal settings, can cause substantially enriched d13CTOC values, up to 2 ‰ (e.g. Steurbaut et al., 2003). Consequently, our organic geochemical results suggest that organic matter in MD-184 might be dominantly derived from aquatic (marine or lagoonal) environments. This interpretation is supported by additional rock-eval analysis results obtained for MD-184, indicating Type II kerogen, which originates from mixtures of zooplankton, phytoplankton, and bacterial debris in marine sediments (Peters and Cassa, 1994). The three other samples (from outcrops MD-85, MD-255, and MD-177) indicate a possible mixed organic matter origin, from terrestrial to brackish environments, but are more characteristic of terrestrial environment

**Comentario [L,M5]:** Additional reference related to algae Pediastrum.

**Comentario [L,M6]:** Additional Rock Eval data for MD 184

**Comentario [L,M7]:** Slightly modified sentence

### *4.4. Nd-Sr isotopic composition*

The Nd-Sr isotopic compositions of the Thanetian sedimentary rocks are shown in Table 4. Overall, the sediments have quite variable εNd(0) values (ranging from -6.2 to -10.7) with a comparatively narrow range of $^{87}Sr/^{86}Sr$ compositions (0.712024 to 0.719026) (Table 4). The four samples analyzed for their Nd-Sr isotopic compositions have been reported in the $^{87}Sr/^{86}Sr$ versus εNd(0) diagram (Fig. 13). The isotopic results are compared with several other relevant source fields: Mesozoic and Neogene volcanic rocks (Rogers and Hawkesworth, 1989; Kay et al., 1994). Quaternary Ecuadorian lavas (Barragan et al., 1998). Cenozoic sedimentary rocks from the Depression, Altiplano, Oriental Cordillera and Subandean zone of Chili and Bolivia (Pinto, 2003); modern suspended sediments from the Solimoes and Madeira rivers (Viers et al., 2008); Neogene deposits from the Amazonian foreland basin of Bolivia, Ecuador and Peru (Roddaz et al., 2005a), and the sand of the Peruvian White Sand (WS) Formation cratonic in origin (Roddaz et al., 2005a). Nd-Sr isotopic compositions of sediments deposited by an Andean drainage define plot within a mélange hyperbole as observed by Basu et al. (1990), Roddaz et al. (2005a) and Roddaz et al. (2012) for Neogene sediments of the Amazonian foreland basins, with one end member being the primitive volcanic arc and the other the upper continental crust of the Brazilian shield. The four analyzed Paleocene samples plot within the field of the Cenozoic Altiplano sediments, indicating a similar Andean provenance. When compared with Neogene Subandean zone sediments, they plot closer to the volcanic arc end member, indicating a greater contribution of the volcanic arc rocks end member for the Paleocene sedimentary rocks relative to Neogene SAZ sediments.

## 5. Depositional environment synthesis

Our biostratigraphical results, sedimentary facies interpretations and organic geochemistry analysis indicate the presence of a tide-influenced shallow marine paleoenvironment during the Paleocene in the northern Madre de Dios Basin. Facies association A corresponds to the sedimentary filling of a tide-influenced meandering channel deposited in the fluvial-tidal transition zone. Facies association B corresponds to tidal flats deposits, tidal inlets and also characterizes a tide-influenced environment but with more distal facies than facies association A. Facies association C, interpreted as deposited in a bay/lagoon or stressed shallow marine-environment, is the most distal facies association. The facies of this association do not show any evidence of tidal nor oscillatory currents.

The transition between the land and the sea in tide-dominated coastal environments is among the most complex on Earth, because of the interaction of numerous physical, chemical and biological processes (Dalrymple and Choi, 2007). Existing depositional models are therefore preliminary because the number of case studies of many of the subenvironments is rather small (Dalrymple and Choi, 2007). However, our dataset makes the possibility to distinguish between tide-dominated delta and tide-dominated estuary. First, from a geological point of view, estuaries are transgressive whereas deltas are regressive (Dalrymple et al., 1992). The tide-dominated Paleocene deposits studied in this paper overly continental deposits of the Yahuarango formation. This stratigraphic succession therefore suggests that the tide-dominated Paleocene deposits are transgressive and related to an estuary. The presence of a Paleocene tide-dominated estuary is further attested by the occurrence of a well expressed tide-influenced meandering zone. According to several works (Dalrymple et al., 1992; Dalrymple and Choi, 2007), only the fluvio-estuarine transition zone in a tide-dominated estuary could explain the occurrence of both opposite currents and meandering channels in a tide-influenced environment. Facies association A could be an illustration of this fluvial-tidal

environment, as it shows evidences of meandering channels influenced by both fluvial and tidal currents (Fig. 14). According to this interpretation, Facies association B could be interpreted as deposited in the outer part of this tide-dominated estuary, where tidal inlets are still present and can laterally be connected to muddy and mixed tidal-flat deposits (Fig. 14). Finally, as Facies association C does not show any evidences of tidal currents, we suggest deposition in a shallow confined marine environment (Fig. 14).

## 6. Paleogeographic and tectonic implications

Comentario [L,M8]: Deeply modified

The data presented in this study document for the first time the existence of Paleocene tide-dominated estuary debouching into a shallow marine bay in the western Amazonian foreland basin. We favor a Thanetian age for this marine incursion but a Danian age cannot be discarded. Most of Paleocene sedimentary rocks of other parts of the Andean/Amazonian foreland basin were mainly deposited in a distal fluvial environment (see Fig. 2 and references therein). The presence of estuarine deposits overlying continental deposits indicates a marine transgression during the Paleocene. This transgression is caused by an increase in accommodation space which in turn depends on the interplay between sediment supply and base level changes (see Catuneanu, 2004 and references therein). In a retroarc foreland basin setting, numerous mechanisms can be envisaged to account for an increase in accommodation space including eustasy, matle processes, foreland related tectonics (i.e. loading/unloading cycles of (i.e. loading/unloading cycles of Catuneanu et al., 1997) and decrease in sediment supply. The Danian and Thanetian periods are characterized by a drop in global sea-level (Fig. 3) (Haq et al., 1987; Hardenbol et al., 1998; Vandenberghe et al., 2012). Consequently the recorded transgression (Danian or Thanetian in age) is not related at first order to a rise in global sea-level. Dynamic loading may be induced by subduction beneath the retroarc foreland basin. Subduction generates long wavelength subsidence (Mitrovica et al., 1989; Catuneanu et al., 1997; Pysklywec and Mitrovica, 2000; Catuneanu, 2004) capable of maintaining the four depozones of the foreland basin system below the base level (Catuneanu et al., 1997; Catuneanu, 2004) and thus of producing accommodation at the basin scale. In fact, we have no idea of the depositional environment of other depozones (wedgetop, proximal foredeep and backbulge) adjacent to our study area so that it is difficult to exclude subsidence dynamic as a possible mechanism. However, the presence of a Paleocene flexural forebulge in the southern Bolivia foreland basin caused by loading of the Western Cordillera

623 (DeCelles and Horton, 2003) suggests that Andean tectonic loading was a first-order control
624 on tectonic subsidence in Paleocene times. This is in agreement with our Nd-Sr isotopic
625 provenance data that show an Andean provenance and hence the presence of an Andean relief
626 in Paleocene times. Short-lived marine ingressions controlled by tectonic loading have also
627 been documented in the Upper Cretaceous Western Canada foreland system (Catuneanu et al.,
628 1999). Shallow marine incursions provoked by Andean tectonic loading have already been
629 documented in the Amazonian foreland basin system (Roddaz et al., 2010) and in the Bolivian
630 retro-arc foreland system (Hernandez et al., 2005). Based on the relatively little thickness of
631 the marine deposits documented in the Madre de Dios basin (40 to 50 m thick outcropping
632 section), we propose that Paleocene marine strata probably correspond to a single high-
633 frequency cycle as defined by Catuneanu (2004). Based on the fact that these higher-
634 frequency cycles are mainly controlled by tectonism in the adjacent belt (Catuneanu, 2004),
635 and based on the relatively low sea-level stage during Paleocene period, we suggest that the
636 marine incursion documented in southern Peru was mainly caused by Andean tectonic loading
637 although additional mantle driven subsidence cannot be excluded.

638 The entrance of this Paleocene marine ingression (Atlantic Ocean, Pacific Ocean or
639 Caribbean Sea) remains to be elucidated. Very few Paleocene marine or coastal deposits are
640 documented in the Andean/Amazonian foreland basins. Paleocene formations of Ecuador and
641 elsewhere in Peru show no evidences of marine or coastal deposits (Fig. 2). In the Bolivian
642 Altiplano and the Eastern Cordillera there is no evidence of any marine influence attested so
643 far except during Danian times in Potosi, Bolivia (El Molino Formation; e.g. Cappetta and
644 Gayet, 2013). Hence the Paleocene paleogeogaphical map proposed here is tentative (Fig. 15-
645 A). In conjunction with the absence of shallow marine deposits in North-western South
646 America, our data might suggest a southern connection with the Atlantic Ocean (Bolivia-
647 Argentina). In any case, more detailed sedimentological works are needed to decipher the

locus of this Paleocene marine entrance. The Paleocene marine transgression documented here predates a well-known Eocene transgression occurring in the Colombian, Ecuadorian and northern Peruvian Amazonian foreland basins and recorded by the Lower Carbonera, Orteguaza and Pozo Formations (Christophoul et al., 2002; Hermoza et al., 2005b; Roddaz et al., 2010). According to these authors, this Eocene marine incursion would come from both the Guyaquil Gulf and the Caribbean Sea (Fig. 15-B). Data from Colombia suggest that a late Eocene transgression flooded south-western Colombia, coming from the south through the Ecuadorian coast (Osorio et al., 2002; Santos et al., 2008). The presence of marine deposits in the Eastern Cordillera and the Central-Eastern Llanos Foothills is more difficult to explain and authors propose a possible corridor through the proto-Lower Magdalena Valley that connected the Caribbean Sea and the Central Llanos Foothills (Santos et al., 2008). In Ecuador and northern Peru, the Eocene shallow marine transgression is recorded by the deposits of Orteguaza and Pozo formation (Fig. 2) as the result of the Western Cordillera loading (Roddaz et al., 2010). The southern limit of this marine incursion is not well-constrained but no Eocene deposits have been recognized in the southern Peruvian and Bolivian Amazonian basin (Fig. 2).

The nature of the Andean source (Eastern or Western Cordillera) for the sediments deposited within the Paleocene estuary also remains unclear. Thermochronological evidences suggest that the first exhumation and/or deformation pulse in the eastern part of the Altiplano or in the Eastern Cordillera of Central Andes occurred in the late Eocene (Kontak et al., 1990; Barnes et al., 2006). Jaillard et al. (1993b) interpreted the absence of strata close to the K-Pg boundary in the Cusco basins as the consequence of an uplift of a proto-eastern cordillera occurring as early as the early to late Paleocene. However, provenance data suggest that the Paleocene estuarine sediments studied here are characterized by a contribution from a volcanic arc source. According to Mamani et al. (2010), the only active volcanic arc during

673 the Paleocene was the Toquepala volcanic arc (91-45 Ma) located in the present-day
674 Coastal/Western Cordillera. This suggests the absence of any significant proto-eastern
675 cordillera relief capable of acting as a barrier to sediments originating from the Western
676 Cordillera Arc. In conclusion, our data suggest that the Paleocene marine incursion could be
677 related to proto western Cordillera loading. This orogenic loading can be related to a drastic
678 change in convergence direction of the subduction from NE to ENE (Soler and Bonhomme,
679 1990) that might have provoked the major late Paleocene tectonic event formerly called Incaic
680 1 tectonic event (Noble et al., 1990; Sempere et al., 1997).

681 According to the data presented in this study and to literature review, at least two
682 marine incursions occurred in the Amazonian foreland basin in early Paleogene times
683 (Paleocene and Eocene, respectively). Both shallow marine incursions are mainly induced by
684 Andean tectonic loading but they did not affect similar areas in the Amazonian foreland
685 basins. Many studies (see Hoorn et al., 2010) have emphasized the role played by the
686 Miocene long-lived Pebas megawetland system in preventing in situ speciation and floristic
687 and plants dispersal between the Andes and Amazonia for at least 6 Ma (Antonelli et al.,
688 2009) and favoring evolutionary transition from marine to freshwater habitats of Neotropical
689 fishes (Lundberg et al., 1998; Lovejoy et al., 2006; 2009). Recurrent Paleogene marine
690 incursions in the Amazonian foreland basin associated with Andean uplift could have
691 provoked biogeographical isolation and promoted allopatric speciation for terrestrial
692 organisms.

## 7. Conclusions

Based on a multidisciplinary approach, this paper documents for the first time the presence of a tide-dominated shallow marine paleoenvironment during the Paleocene interval (Danian or Thanetian) in the Amazonian basin. In details, based on sedimentary facies analysis, organic geochemistry and fossil assemblages, three facies associations related to a tide-dominated estuary debouching into a shallow-marine bay or lagoon have been defined. Facies association A corresponds to the sedimentary filling of a tide-influenced meandering channel formed in the fluvial-tidal transition zone. Facies association B is related to more distal tidal-flats, little channelized tidal inlets and saltmarshes deposits. Facies association C corresponds to a stressed shallow marine environment such as a bay or a lagoon.

The presence of these transgressive estuarine deposits overlying older continental facies is best explained by flexural tectonic subsidence in response to Andean tectonic loading. This is in agreement with the Nd-Sr isotopic provenance data that show an Andean provenance and hence the presence of an Andean relief during Danian or Thanetian times. The volcanic contribution recorded in the Nd-Sr isotopic compositions can be related to the Toquepala volcanic arc (91 to 45 Ma) located in the present-day Coastal/Western Cordillera. This suggests the absence of any significant proto-Eastern Cordillera relief that would have stopped the drainage and the sedimentary influxes from this Western Andean volcanic relief towards the Amazonian basin during Danian or Thanetian times. Consequently the data suggest that the Danian or Thanetian marine incursion can be related to the subsidence created in response to the proto-Western Cordillera loading. We suggest this Paleocene transgression may come from the south and may be related to the Parana Sea. Finally, similar to Miocene marine incursions affecting the Pebas megawetland, Paleogene marine incursions in the Amazonian foreland basin associated with Andean uplift may have played a role in the

717 dynamics of Neotropical paleobiodiversity in favoring biogeographical isolation and
718 promoting allopatric speciation for terrestrial organisms.

## 8. Acknowledgements

We thank Denise Dorhout for analytical support at NIOZ. We are much indebted to Frank P. Wesselingh for mollusk taxonomic identification. The research leading to these results has received funding from the IRD (Institut de Recherche pour le Développement), the Institut Carnot (France) and the European Research Council under the European Union's Seventh Framework Program (FP7/2007-2013) / ERC grant agreement n° [226600].

**Fig. 1**: A/ White stars display Amazonian foreland basins location (northern Andes and part of Central Andes). B) Simplified geological and structural map of the study area. Red squares display the location of the outcrops used for this study. PCC= Pongo de Coñeq Canyon. C) Zoom of Pantiacolla Anticline area, and location of the outcrops.

**Fig. 2**: Stratigraphic correlation chart for Paleogene strata between Amazonian foreland basins from Colombia to northern Bolivia. Shallow marine deposits are coloured in blue. Important biostratigraphical or geochronological references are displayed by white squares. EC= Eastern Cordillera.

**Fig. 3**: Stratigraphical range of biostratigraphical markers in Paleocene localities from the Upper Madre de Dios SAZ, Southeastern Peru. T/R = Transgressive/ Regressive cycles, according to Vandenberghe et al. (2012). Based on data from Gradstein et al. (1988), Musacchio (1990); Gayet et al. (1993); Jaillard (1993a); Sigé et al. (2004); Gelfo et al. (2009); Gelfo and Sigé (2011); Morsi et al. (2011); Cappetta (2012); Gonella et al. (2012); Cappetta and Gayet (2013); Woodburne et al. (2014)

**Fig. 4**: Isolated teeth of marine-brackish fishes recovered from Paleocene MD-184 (A-F) and MD-85 (G-J) localities of the Upper Madre de Dios Sub-Andean Zone, Southeastern Peru. A-B: Pristidae gen. and sp. indet. (MD-184) oral tooth, A. lingual view, B. intermediate view. C-D: *Ouledia* sp (MD-184) oral tooth, C. lingual view, D. lateral view. E-F: Pycnodontidae indet. (MD-184) palatine tooth, E. occlusal view, F. lateral view, G-H: *Potobatis* sp. (MD-85) fragmentary oral tooth, G. occlusal view, H. lingual view of crown (root lacking). I-J: *Ouledia* sp. (MD-85) worn oral tooth, I. lingual view, J. lateral view. Scale bar = 0.5mm.

**Comentario [L,M9]:** New Figure

**Fig. 5**: Outcrop MD-255. A) General outcrop view along the river cutbank. B) Zoom from A. Interpreted photograph of two stacked channels. C/Sedimentary section with Facies code (see Table 2 for details).

749 **Fig. 6**: Facies Photographs for Facies Association A (FA-A). A) Facies A1, showing fine-
750 grained sandtstone with tangential cross-bedding and sets prograding in the same direction.
751 Note that bidirectionality has been observed in this facies. B) Photograph of the rippled-
752 surface of Facies A1. Square indicates the location of photograph C. C) Ichnofabrics from
753 Facies A1 top surface: *Arenicolites* and possible Dactiloides (tubular trace). D) Facies A3.
754 Tangential cross-bedding with planar laminations at their base. Rare asymmetrical ripples in
755 the opposite direction can also be observed at the top of the tangential laminations, suggesting
756 bidirectionality. Regular changes in thickness suggest cyclycity, possibly Neap and Spring
757 cycles. E) Photograph of climbing-rippled cross-stratification of Facies A2, from the zoom
758 section displayed on F). F) View of the heterolithic and cyclic deposits of Facies A2. Black
759 squares indicate the location of photographs E) and G). G) Photograph of Facies A2, with
760 massive fine-grained sandstones or flaser bedding alternating with wavy- or planar muddy
761 lamination.

762 **Fig. 7:** Sedimentary section from outcrop MD-256.

763 **Fig. 8**: Facies photographs of Facies Association B (FA-B). A) Fine-grained sandstone with
764 climbing ripples. B) Root traces and gypsum or anhydrite nodules developing at the top of the
765 reddish mudstones of Facies B2. C) Facies B4. Highly burrowed heterolithic deposits
766 showing regular alternations of very fine to fine-grained sandstones with muddy or silty
767 layers displaying planar horizontal and wavy bedding. D) Horizontal and vertical burrows in
768 Facies B4. E) Fluid-escape structure within deposits of Facies B4. F) Facies B5 with rippled-
769 surface.

770 **Fig. 9**: Outcrop MD-85 near Pantiacolla antincline. A) General view of the outcrop. Black
771 rectangle precise the location of photograph B. B) Enlarged view from A with the location of

772 the sedimentary section 1 described. C) Sedimentary section 2 and Facies code. Note that 100
773 m separates the two sedimentary sections.

774 **Fig. 10**: Sedimentary sections from outcrop MD-177 (Sedimentary section 1) and MD-184
775 (Sedimentary section 2).

776 **Fig. 11**: Photographs from outcrop MD-184. A) Outcrop view of alternating Facies C1 and
777 C2. Note undulated marls/carbonated layers. B) Benthic foraminifer *Bathysiphon* sp. found in
778 facies C1. C) Outcrop view of carbonated layers from Facies C4. D) Dessication cracks at the
779 top of a carbonated layer in Facies C5. Note little-sized oyster visible on that surface.

780 **Fig. 12**: Thin sections photographs from Facies C4, C5 and C6, sampled at MD-184. The
781 number of each thin-section is indicated by "TS-n°". They are located on the sedimentary
782 section 2 of Fig. 10. A), B), C) and D) correspond to thin-sections of alternated marls ans
783 limestones strata from Facies C4. E) and F) correspond to the stromatolithic Limestones of
784 Facies C5. G), H), I) and J) correspond to the Oyster limestones of Facies C6. Fi=Fish
785 vertebra, Mi= Micritic pellets, Dru= Drusic cement, Ga= Gasteropod, Ph= Phylopod, Oy=
786 Oyster, An= Annelid, Str= Stromatolith filaments.

787 **Fig. 13**: 87Sr/86Sr versus εNd(0) diagram. Yellow triangles correspond to the Paleocene
788 samples analyzed in this study. Note that they all plot within the melange hyperbole,
789 indicating an Andean provenance. See text for details.

790 **Fig. 14**: Interpretative diagram for Paleocene Times. Andean relief is active yet and produces
791 sedimentary supply for the fluvial and then estuary system debouching in a shallow interior
792 sea. Black rectangles correspond to the interpretative depositional contexts location of each
793 outcrop: MD-255 corresponds to the fluvio-estuarine meandering transition zone in the
794 proximal estuarine system; MD-256 corresponds to the inner (?) part of the estuary; MD-85
795 corresponds to the outer part of the estuary system and MD-184/177 corresponds to the most

distal environment, also located around the outer part of the estuary system but more connected to a bay or calm confined shallow marine basin.

**Fig. 15**: Paleogeographical reconstructions for Paleogene times. A) Paleogeographic reconstruction of Paleocene Times. The shallow marine sea described in this paper in the Amazonian foreland basin does not present clear connection with existing oceans. B) Paleogeographic reconstruction for Eocene times, related to Pozo shallow marine incursion. See text for details.

**Table 1**: Distribution and relative abundance of fossil content of biostratigraphical interest in Paleocene localities from the Upper Madre de Dios Sub-Andean Zone, Southeastern Peru Ost= Ostracoda; (r)= potentially reworked; (+)= close ally. Relative abundance is denoted by the number of "+" (ranging from + up to +++).

**Comentario [L,M10]:** New Table

**Table 2**: Descriptions and interpretations of sedimentary facies. FA= Facies Association.

**Table 3**: Organic geochemistry results.

**Table 4**: Nd-Sr isotopic compositions for provenance analysis.

**Supplementary Table A**: Outcrops location.

## References


Adnet, S., Gismondi, R.S., Antoine, P.-O., 2014. Comparisons of dental morphology in river stingrays (Chondrichthyes: Potamotrygonidae) with new fossils from the middle Eocene of Peruvian Amazonia rekindle debate on their evolution. Naturwissenschaften 101, 33-45.

Allen, J.R.L., 1970. A quantitative model of climbing ripples and their cross-laminated deposits. Sedimentology 14, 5-26.

Antoine, P.-O., Marivaux, L., Croft, D.A., Billet, G., Ganerød, M., Jaramillo, C., Martin, T., Orliac, M.J., Tejada, J., Altamirano, A.J., 2012. Middle Eocene rodents from Peruvian Amazonia reveal the pattern and timing of caviomorph origins and biogeography. Proceedings of the Royal Society B: Biological Sciences 279, 1319-1326.

Antoine, P.O., Billet, G., Salas-Gismondi, R., Tejada Lara, J., Baby, P., Brusset, S., Espurt, N., Submitted. A new *Carodnia* Simpson, 1935 (Mammalia, Xenungulata) from the early Eocene of Northwestern Peru and a phylogeny of xenungulates at species level. Journal of Mammalian Evolution.

Antoine, P.O., Roddaz, M., Brichau, S., Tejada-Lara, J., Salas-Gismondi, R., Altamirano, A., Louterbach, M., Lambs, L., Otto, T., Brusset, S., 2013. Middle Miocene vertebrates from the Amazonian Madre de Dios Subandean Zone, Peru. Journal of South American Earth Sciences 42, 91-102.

Antonelli, A., Nylander, J.A.A., Persson, C., Sanmartin, I., 2009. Tracing the impact of the Andean uplift on Neotropical plant evolution. PNAS.

Armstrong, H.A., Brasier, M.D., 2005. Microfossil., in: Hart, M. (Ed.), Geological Magazine, 2nd ed. Blackwell Publishing, Malden, Oxford, Carlton.

Ashley, G.M., Southard, J.B., Boothroyd, J.C., 1982. Deposition of climbing-ripple beds: a flume simulation. Sedimentology 29, 67-79.

Aubry, M.-P., Thiry, M., Dupuis, C., Berggren, W., 2005. The Sparnacian deposits of the Paris Basin: A lithostratigraphic classification. Stratigraphy 2, 65-100.

Barnes, J.B., Ehlers, T.A., McQuarrie, N., O'Sullivan, P.B., Pelletier, J.D., 2006. Eocene to recent variations in erosion across the central Andean fold-thrust belt, northern Bolivia: Implications for plateau evolution. Earth and Planetary Science Letters 248, 118-133.

Barragan, R., Geist, D., Hall, M., Larson, P., Kurz, M., 1998. Subduction controls on the compositions of lavas from the Ecuadorian Andes. Earth and Planetary Science Letters 154, 153-166.

Basu, A.R., Sharma, M., Decelles, P.G., 1990. Nd, Sr-Isotopic provenance and trace-element geochemistry of Amazonian foreland basin fluvial sands, Bolivia and Peru. Implications for ensialic Andean orogeny. Earth and Planetary Science Letters 100, 1-17.

Bejarano, A., 1991. Caracterizacion y Evaluacion de Parametros de Registros de Pozos en la Cuenca del Putumayo.

Campbell, K.E., David, C., Romero-pittman, L., 2006. The Pan-Amazonian Ucayali Peneplain, late Neogene sedimentation in Amazonia, and the birth of the modern Amazon River system. Palaeogeography, Palaeoclimatology, Palaeoecology 239, 166-219.

Cande, S.C., Kent, D.V., 1992. A new geomagnetic polarity time scale for the Late Cretaceous and Cenozoic. Journal of Geophysical Research: Solid Earth 97, 13917-13951.

Cappetta, H., 2012. Chondrichthyes (Mesozoic and Cenozoic Elasmobranchii: teeth), in: Schultze, H.-P. (Ed.), Handbook of Paleoichthyology, Munich (Pfeil).

Cappetta, H., Gayet, M., 2013. A new elasmobranch genus (Myliobatiformes, Dasyatoidea) from the Danian of Potosí (Bolivia). Neues Jahrbuch für Geologie und Paläontologie-Abhandlungen 269, 285-290.

Casero, P., 1997. Multidisplinary Correlative Evidences for Polyphase Geological Evolution of the Foot-Hills of the Cordillera Oriental (Colombia).

Catuneanu, O., 2004. Retroarc foreland systems—evolution through time. Journal of African Earth Sciences 38, 225-242.
Catuneanu, O., Beaumont, C., Waschbusch, P., 1997. Interplay of static loads and subduction dynamics in foreland basins: Reciprocal stratigraphies and the “missing” peripheral bulge. Geology 25, 1087-1090.
Catuneanu, O., Sweet, A.R., Miall, A.D., 1999. Concept and styles of reciprocal stratigraphies: Western Canada foreland system. Terra Nova-Oxford 11, 1-8.
Cooper, M., Addison, F., Alvarez, R., Coral, M., Graham, R.H., Hayward, A., Howe, S., Martinez, J., Naar, J., Peñas, R., 1995. Basin development and tectonic history of the Llanos Basin, Eastern Cordillera, and middle Magdalena Valley, Colombia. AAPG bulletin 79, 1421-1442.
Córdoba, F., Buchelli, F., Moros, J., Calderón, W., Guerrero, C., Kairuz, E., Magoon, L., 1997. Proyecto evaluación regional Cuenca del Putumayo—Definición de los sistemas petrolíferos. ECOPETROL, Bogotá.
Choi, K., 2010. Rhythmic Climbing-Ripple Cross-Lamination in Inclined Heterolithic Stratification (IHS) of a Macrotidal Estuarine Channel, Gomso Bay, West Coast of Korea. Journal of Sedimentary Research 80, 550-561.
Christophoul, F., Baby, P., Dávila, C., 2002. Stratigraphic responses to a major tectonic event in a foreland basin: the Ecuadorian Oriente Basin from Eocene to Oligocene times. Tectonophysics 345, 281-298.
Dalrymple, R.W., 1984. Runoff microdeltas; a potential emergence indicator in cross-bedded sandstones. Journal of Sedimentary Research 54, 825-830.
Dalrymple, R.W., Baker, E.K., Harris, P.T., Hughes, M.G., 2003. Sedimentology and stratigraphy of a tide-dominated, foreland-basin delta (Fly River, Papua New Guinea), in: Sidi, F.H., Nummedal, D., Imbert, P., Darman, H., and Posamentier, H.W. (Ed.), Tropical Deltas of Southeast Asia—Sedimentology, Stratigraphy, and Petroleum Geology. SEPM, Special Publication, pp. 147-173.
Dalrymple, R.W., Choi, K., 2007. Morphologic and facies trends through the fluvial–marine transition in tide-dominated depositional systems: A schematic framework for environmental and sequence-stratigraphic interpretation. Earth-Science Reviews 81, 135-174.
Dalrymple, R.W., Zaitlin, B.A., Boyd, R., 1992. Estuarine facies models: conceptual basis and stratigraphic implications. Journal of Sedimentary Research 62, 1130-1146.
de Mowbray, T., Visser, M.J., 1984. Reactivation surfaces in subtidal channel deposits, Oosterschelde, Southwest Netherlands. Journal of Sedimentary Research 54, 811-824.
DeCelles, P.G., Horton, B.K., 2003. Early to middle Tertiary foreland basin development and the history of Andean crustal shortening in Bolivia. Geological Society of America Bulletin 115, 58-77.
Dunham, R.J., 1962. Classification of carbonate rocks according to depositional texture, in: W. E. Ham, e. (Ed.), Classifications of carbonate rocks - a symposium, pp. 108–121.
Enay, R., 1990. Paléontologie des invertébrés, Paris.
Eriksson, K.A., Simpson, E.L., 2004. Precambrian tidalites: recognition and significance., in: Eriksson, P.G., Altermann,W., Nelson, D., Mueller, W., Cateneau, O., Strand, K. (Ed.), Tempos and Events in Precambrian Time. Developments in Precambrian Geology. Elsevier, Amsterdam, pp. 631– 642.
Eriksson, P.G., Condie, K.C., Tirsgaard, H., Mueller, W.U., Altermann, W., Miall, A.D., Aspler, L.B., Catuneanu, O., Chiarenzelli, J.R., 1998. Precambrian clastic sedimentation systems. Sedimentary Geology 120, 5-53.
Faucher, B., Savoyat, E., 1973. Esquisse géologique des Andes de l'Equateur. Revue de géographie physique et de géologie dynamique 15, 115-142.

Gayet, M., Sempre, T., Cappetta, H., Jaillard, E., Lévy, A., 1993. La présence de fossiles marins dans le Crétacé terminal des Andes centrales et ses conséquences paléogéographiques. Palaeogeography, Palaeoclimatology, Palaeoecology 102, 283-319.
Gelfo, J.N., Goin, F.J., Woodburne, M.O., Muizon, C.D., 2009. Biochronological relationships of the earliest South American Paleogene mammalian faunas. Paleontology 52, 251-269.
Gelfo, J.N., Sigé, B., 2011. A new didolodontid mammal from the late Paleocene-earliest Eocene of Laguna Umayo, Peru. Acta Palaeontologica Polonica 56, 665-678.
Gérard, J.R.F., Bromley, R.G., 2008. Ichnofabrics in Clastic sediments: Application to sedimentological and core studies. A practical guide by Jean R.F. Gérard and Richard G. Bromley. Jean R.F. Gérard, Madrid.
Gil, W.F., 2001. Evolution latérale de la déformation d'un front orogénique: exemples des bassins subandins entre 0° et 16°S. University Paul Sabatier, Toulouse.
Gonella, C.A.C., Griffin, M., Cione, A., Cavalli, S.G., Aceñolaza, F.G., 2012. Paleontología de la Formación Yacoraite (Maastrichtiano-Daniano) en el ámbito de la Subcuenca de Tres Cruces, Cordillera Oriental de la provincia de Jujuy, Argentina.
Gradstein, F., Kaminski, M., Berggren, W., 1988. Cenozoic foraminiferal biostratigraphy of the Central North Sea. Abh. Geol. Bundesanstalt 41, 97-108.
Gutierrez, M., 1982. Evaluacion potencial petrolifero cuencas Huallaga, Ucayali y Madre de Dios. Zonacion bioestratigrafica del intervalo Cretacico superior-Tertiario inferior. Petroperu, Internal Report, Lima, p. 29.
Haq, B.U., Hardenbol, J., Vail, P.R., 1987. Chronology of fluctuating sea levels since the Triassic. Science 235, 1156–1167.
Hardenbol, J., Thierry, J., Farley, M.B., Jacquin, T., De Graciansky, P.C., VailP.R., 1998. Mesozoic–Cenozoic sequence chronostratigraphy of european basins. 60SEPM Special Publication, Tulsa, 1–786.
Hermoza, W., 2004. Dynamique tectono-sedimentaire et restauration sequentielle du retro-bassin d'avant-pays des Andes Centrales. Univeristé Paul Sabatier, Toulouse, p. 196.
Hermoza, W., Brusset, S., Baby, P., Gil, W., Roddaz, M., Guerrero, N., Bolaños, R., 2005b. The Huallaga foreland basin evolution: Thrust propagation in a deltaic environment, northern Peruvian Andes. Journal of South American Earth Sciences 19, 21-34.
Hernandez, R.M., Jordan, T.E., Farjat, A.D., Echavarria, L., Idleman, B.D., Reynolds, J.H., 2005. Age, distribution, tectonics, and eustatic controls of the Paranense and Caribbean marine transgressions in southern Bolivia and Argentina. Journal of South American Earth Sciences 19, 495-512.
Hoorn, C., Wesselingh, F.P., ter Steege, H., Bermudez, M.a., Mora, a., Sevink, J., Sanmartín, I., Sanchez-Meseguer, a., Anderson, C.L., Figueiredo, J.P., Jaramillo, C., Riff, D., Negri, F.R., Hooghiemstra, H., Lundberg, J., Stadler, T., Särkinen, T., Antonelli, A., 2010. Amazonia through time: Andean uplift, climate change, landscape evolution, and biodiversity. Science (New York, N.Y.) 330, 927-931.
Hovikoski, J., Gingras, M., Räsänen, M., Rebata, L.A., Guerrero, J., Ranzi, A., Melo, J., Romero, L., del Prado, H.N., Jaimes, F., 2007. The nature of Miocene Amazonian epicontinental embayment: High-frequency shifts of the low-gradient coastline. Geological Society of America Bulletin 119, 1506-1520.
Hovikoski, J., Räsänen, M., Gingras, M., Ranzi, A., Melo, J., 2008. Tidal and seasonal controls in the formation of Late Miocene inclined heterolithic stratification deposits, western Amazonian foreland basin. Sedimentology 55, 499-530.
Jackson, R.G., 1981. Sedimentology of muddy fine-grained channel deposits in meandering streams of the American Middle West. Journal of Sedimentary Research 51, 1169-1192.
Jacobsen, S.B., Wasserburg, G.J., 1980. Sm-Nd isotopic evolution of chondrites. Earth and Planetary Science Letters 50, 139-155.

Jaillard, E., 1993a. The Senonian to Palaeocene tectonic evolution of the Peruvian margin and its relationships with geodynamics. Bulletin de la Société Géologique de France 164, 819-830.
Jaillard, E., 1996. Cretaceous to early Paleogene tectonic evolution of the northern Central Andes (0–18°S) and its relations to geodynamics. Tectonophysics 259, 41-53.
Jaillard, E., Carlotto, V., Cardenas, J., Chavez, R., Gil, W., 1993b. La "Nappe des Couches Rouges" de Cuzco (Sud du Pérou): mise en évidence stratigraphique, interprétations tectoniques et paléogéographiques. C. R. Acad. Sci. Paris 36, 379-386.
Jaramillo, C.A., Dilcher, D.L., 2000. Microfloral diversity patterns of the late Paleocene–Eocene interval in Colombia, northern South America. Geology 28, 815-818.
Jaramillo, C.A., Dilcher, D.L., 2001. Middle Paleogene palynology of Central Colombia, South America: A study of pollen and spores from tropical latitudes. Palaeontographica Abteilung B 258, 87-213.
Jeffery, M.L., Poulsen, C.J., Ehlers, T.A., 2012. Impacts of Cenozoic global cooling, surface uplift, and an inland seaway on South American paleoclimate and precipitation δ18O. Geological Society of America Bulletin 124, 335-351.
Jopling, A.V., Walker, R.G., 1968. Morphology and origin of ripple-drift cross-lamination, with examples from the Pleistocene of Massachusetts. Journal of Sedimentary Research 38, 971-984.
Kay, S.M., Coira, B., Viramonte, J., 1994. Young mafic back arc volcainc-rocks s indicators of continental lithospheric delamination beneath the Argentine Puna plateau, Central Andes J. Geophys. Res.-Solid Earth 99, 24323-24339.
Klein, G.d., 1970. Depositional and dispersal dynamics of intertidal sand bars. Journal of Sedimentary Research 40, 1095-1127.
Kontak, D.J., Farrar, E., Clark, A.H., Archibald, D.A., 1990. Eocene tectono-thermal rejuvenation of an upper Paleozoic-lower Mesozoic terrane in the Cordillera de Carabaya, Puno, southeastern Peru, revealed by K-Ar and 40Ar/39Ar dating. Journal of South American Earth Sciences 3, 231-246.
Londoño, J., Lorenzo, J.M., Ramirez, V., 2012. Lithospheric flexure and related base-level stratigraphic cycles in continental foreland basins: An example from the Putumayo Basin, Northern Andes, in: Gao., D. (Ed.), Tectonics and sedimentation: Implications for petroleum systems. AAPG Memoir pp. 357-375.
Lovejoy, N.R., Albert, J.S., Crampton, W.G.R., 2006. Miocene marine incursions and marine/freshwater transitions: Evidence from Neotropical fishes. Journal of South American Earth Sciences 21, 5-13.
Lovejoy, N.R., Willis, S.C., Albert, J.S., 2009. Molecular signatures of Neogene biogeographical events in the Amazon fish fauna, Amazonia: Landscape and Species Evolution. Wiley-Blackwell Publishing Ltd., pp. 405-417.
Lundberg, J.G., Marshall, L.G., Guerrero, J., 1998. The Stage of Neotropical Fish Diversification: A History of Tropical South American Rivers, in: Malabarba, L.R., R.E. Reis, R.P. Vari, Z.M. Lucena and C.A.S Lucena (Ed.), Phylogeny and Classification of Neotropical Fishes. Edipucrs, Porto Alegre, p. 603.
Mamani, M., Worner, G., Sempere, T., 2010. Geochemical variations in igneous rocks of the Central Andean orocline (13 degrees S to 18 degrees S): Tracing crustal thickening and magma generation through time and space. Geological Society of America Bulletin 122, 162-182.
Marivaux, L., Salas-Gismondi, R., Tejada, J., Billet, G., Louterbach, M., Vink, J., Bailleul, J., Roddaz, M., Antoine, P.O., 2012. A platyrrhine talus from the early Miocene of Peru (Amazonian Madre de Dios Sub-Andean Zone). J. Hum. Evol. 63, 696-703.

1008 Marocco, R., Baudino, R., A., L., 1995. The intermontane Neogene continental basins of the
1009 Central Andes of Ecuador and Peru: Sedimentologic, tectonic and geodynamic implications,
1010 in: A.J. Tankard, R.S., H.J. Welsink (Ed.), Petroleum Basins of South America. Am. Assoc.
1011 Pet. Geol. Mem., pp. 597–613.
1012 Marshall, L.G., Sempere, T., Butler, R.F., 1997. Chronostratigraphy of the mammal-bearing
1013 Paleocene of South America. Journal of South American Earth Sciences 10, 49-70.
1014 Martin-Gombojav, N., Winkler, W., 2008. Recycling of proterozoic crust in the andean
1015 amazon foreland of Ecuador: Implications for orogenic development of the Northern Andes.
1016 Terra Nova 20, 22-31.
1017 Mazumder, R., Arima, M., 2005. Tidal rhythmites and their implications. Earth-Science
1018 Reviews 69, 79-95.
1019 Meyers, P.A., 1997. Organic geochemical proxies of paleoceanographic, paleolimnologic, and
1020 paleoclimatic processes. Organic Geochemistry 27, 213-250.
1021 Miall, A.D., 1996. The geology of fluvial deposits: sedimentary facies, basin analysis and
1022 petroleum geology. Springer-Verlag Inc Berlin.
1023 Mitrovica, J., Beaumont, C., Jarvis, G., 1989. Tilting of continental interiors by the dynamical
1024 effects of subduction. Tectonics 8, 1079-1094.
1025 Morsi, A.-M.M., Speijer, R.P., Stassen, P., Steurbaut, E., 2011. Shallow marine ostracode
1026 turnover in response to environmental change during the Paleocene–Eocene thermal
1027 maximum in northwest Tunisia. Journal of African Earth Sciences 59, 243-268.
1028 Mpodozis, C., Allmendinger, R.W., 1993. Extensional tectonics, Cretaceous Andes, northern
1029 Chile (27°S). Geological Society of America Bulletin 105, 1462-1477.
1030 Musacchio, E.A., 1990. Non-marine Cretaceous ostracods from Argentina and their
1031 palaeobiogeographical relationships, Ostracoda and global events. Springer, pp. 557-569.
1032 Naeser, C.W., Crochet, J., Jaillard, E., Laubacher, G., Mourier, T., Sige, B., 1991. Tertiary
1033 fission-track ages from the Bagua syncline (northern Peru): Stratigraphic and tectonic
1034 implications. Journal of South American Earth Sciences 4, 61-71.
1035 Nio, S.D., Yang, C.S., 1991. Diagnostic attributes of clastic tidal deposits: a review, in: Smith,
1036 D.G., Reinson, G.E., Zeitlin, B.A. and R.A. Rahmani (Ed.), Clastic Tidal Sedimentology.
1037 Canadian Society of Petroleum Geologists, pp. 3-28.
1038 Noble, D.C., McKee, E.H., Mourier, T., Mégard, F., 1990. Cenozoic stratigraphy, magmatic
1039 activity, compressive deformation, and uplift in Northern Peru. Geological Society of
1040 America Bulletin 102, p. 1105-1113.
1041 Osorio, C., Michoux, D., Tellez, G., 2002. Stratigraphy of the Tertiary sequences — Upper
1042 Magdalena and the Putumayo basins, a different point of view for hydrocarbon exploration.
1043 Memorias de la Segunda Convención técnica de la Asociación Colombiana de Geólogos y
1044 Geofísicos del Petróleo, Bogotá, Colombia 10.
1045 Page, K.J., Nanson, G.C., Frazier, P.S., 2003. Floodplain Formation and Sediment
1046 Stratigraphy Resulting from Oblique Accretion on the Murrumbidgee River, Australia. Journal
1047 of Sedimentary Research 73, 5-14.
1048 Parra, M., Mora, A., Jaramillo, C., Strecker, M.R., Sobel, E.R., Quiroz, L., Rueda, M., Torres,
1049 V., 2009. Orogenic wedge advance in the northern Andes: Evidence from the Oligocene-
1050 Miocene sedimentary record of the Medina Basin, Eastern Cordillera, Colombia. Geological
1051 Society Of America Bulletin.
1052 Peters, K.E., Cassa, M.R., 1994. Applied source rock geochemistry. Memoirs of the american
1053 Association of Petroleum Geologists, 93-93.
1054 Pinto, L., 2003. Traçage de l'érosion Cénozoïque des Andes Centrales à l'aide dela
1055 minéralogie et de la géochmie des sédiments (Nord du Chili et Nord-Ouest de la Bolivie).
1056 Université Paul Sabatier, Toulouse.

Poyato-Ariza, F.J., Wenz, S., 2002. A new insight into pycnodontiform fishes. Geodiversitas 24, 139-248.
Pysklywec, R., Mitrovica, J., 2000. Mantle flow mechanisms of epeirogeny and their possible role in the evolution of the Western Canada Sedimentary Basin. Canadian Journal of Earth Sciences 37, 1535-1548.
Roddaz, M., Christophoul, F., Zambrano, J.D.B., Soula, J.C., Baby, P., 2012. Provenance of late Oligocene to quaternary sediments of the Ecuadorian Amazonian foreland basin as inferred from major and trace element geochemistry and Nd-Sr isotopic composition. Journal of South American Earth Sciences 37, 136-153.
Roddaz, M., Hermoza, W., Mora, A., Baby, P., Parra, M., Christophoul, F., Brusset, S., Espurt, N., 2010. Cenozoic sedimentary evolution of the Amazonian foreland basin system, in: Blackwell (Ed.), Amazonia, Landscape and Species Evolution, pp. 61-88.
Roddaz, M., Viers, J., Brusset, S., Baby, P., Hérail, G., 2005a. Sediment provenances and drainage evolution of the Neogene Amazonian foreland basin. Earth and Planetary Science Letters 239, 57-78.
Rogers, G., Hawkesworth, C.J., 1989. A geochemical traverse across the North Chilean Andes: evidence for crust generation from the mantle wedge. Earth and Planetary Science Letters 91, 271-285.
Ruiz, G.M.H., Seward, D., Winkler, W., 2004. Detrital thermochronology - A new perspective on hinterland tectonics, an example from the Andean Amazon Basin, Ecuador. Basin Research 16, 413-430.
Ruiz, G.M.H., Seward, D., Winkler, W., 2007. Evolution of the Amazon Basin in Ecuador with Special Reference to Hinterland Tectonics: Data from Zircon Fission-Track and Heavy Mineral Analysis pp. 907-934.
Santos, C., Jaramillo, C., Bayona, G., Rueda, M., Torres, V., 2008. Late Eocene marine incursion in north-western South America. Palaeogeography, Palaeoclimatology, Palaeoecology 264, 140-146.
Sempere, T., Butler, R.F., Richards, D.R., Marshall, L.G., Sharp, W., Swisher, C.C., 1997. Stratigraphy and chronology of upper Cretaceous lower Paleogene strata in Bolivia and northwest Argentina. Geological Society of America Bulletin 109, 709-727.
Sigé, B., Sempere, T., Butler, Robert F., Marshall, Larry G., Crochet, J.-Y., 2004. Age and stratigraphic reassessment of the fossil-bearing Laguna Umayo red mudstone unit, SE Peru, from regional stratigraphy, fossil record, and paleomagnetism. Geobios 37, 771-794.
Soler, P., Bonhomme, M.G., 1990. Relation of magmatic activìty to plate dynamics In central Peru from Late Cretaceous to present, in: Kay, S.M., and Rapela, C. W., eds (Ed.), Plutonism from Antarctica to Alaska: Boulder, Colorado. Geological Society of America Special Paper.
Steurbaut, E., Magioncalda, R., Dupuis, C., Van Simaeys, S., Roche, E., Roche, M., 2003. Palynology, paleoenvironments, and organic carbon isotope evolution in lagoonal Paleocene-Eocene boundary settings in North Belgium. Special papers of the Geological Society of America, 291-318.
Tessier, B., 1996. River-Ocean Interaction Zone: a Facies Model with climbing Ripple Bedding, in: Romania, N.I.o.M.G.a.G.-e.o. (Ed.), GEO-ECO-MARINA 2.Workshop on "Fluvial-Marine Interactions", Malnas, Romania.
Tyson, R.V., 1995. Sedimentary organic matter: organic facies and palynofacies. Springer.
Valchev, B., 2007. Representatives of Family Eggerellidae Cushman, 1937 from the Palaeocene of the Coastal Part of East Stara Planina. Review of the Bulgarian Geological Society 68, 36-40.
Vandenberghe, N., Hilgen, F., Speijer, R., 2012. The paleogene period. The geologic time scale 2012, 855-921.

Viers, J., Roddaz, M., Filizola, N., Guyot, J.L., Sondag, F., Brunet, P., Zouiten, C., Boucayrand, C., Martin, F., Boaventura, G.R., 2008. Seasonal and provenance controls on Nd-Sr isotopic compositions of Amazon rivers suspended sediments and implications for Nd and Sr fluxes exported to the Atlantic Ocean. Earth and Planetary Science Letters 274, 511-523.

Wattinne, A., 2004. Évolution d'un environnement carbonate lacustre à bioconstructions, en limagne bourbonnaise (Oligo-Miocène, Massif Central, France), Thèse du Muséum National d'Histoire Naturelle, Paris, p. 195.

Woodburne, M.O., Goin, F.J., Bond, M., Carlini, A.A., Gelfo, J.N., López, G.M., Iglesias, A., Zimicz, A.N., 2014. Paleogene land mammal faunas of South America; a response to global climatic changes and indigenous floral diversity. Journal of Mammalian Evolution 21, 1-73.

# Evidences for a Paleocene marine incursion in Southern Amazonia (Madre de Dios Sub-Andean Zone, Peru)

M. Louterbach [1,2,3], M. Roddaz[1], J. Bailleul[2], P.-O. Antoine[4], S. Adnet[3], J.H. Kim[5], E. van Soelen[5], F. Parra[1], J. Gérard[3], Y. Calderon[6] , C. Gagnaison[2], J. S. Sinninghe Damsté[5] and P. Baby[1]

[1] *Géosciences-Environnement Toulouse, Université de Toulouse; UPS (SVT-OMP); LMTG; CNRS; IRD; 14 Avenue Édouard Belin, F-31400 Toulouse, France*

[2] *Bassins-Réservoirs-Ressources, Institut Polytechnique Lasalle Beauvais, Département Géosciences, 19 rue Pierre Waguet, BP 30313, F-60026 Beauvais Cedex, France*

[3] *REPSOL Exploracion S.A., Calle Mendez Alavaro 44, 28045 Madrid, Spain*

[4] *Institut des Sciences de l'Évolution (ISE-M, UMR - CNRS 5554), c.c. 64, Université Montpellier 2, Place Eugène Bataillon, F-34095 Montpellier Cedex 05, France*

[5] *Royal Netherlands Institute for Sea Research (NIOZ), Department of Marine Organic Biogeochemistry, Den Burg (Texel), The Netherlands*

[6] *PERUPETRO S.A., Luis Aldana 320 - San Borja, Lima, Peru*

ABSTRACT

This article presents new biostratigraphic dating, facies analysis, organic geochemical data and Nd-Sr isotopic provenance from five outcrops of southern Amazonia (MD-85, MD-177 MD-184, MD-255 and MD-256) to document for the first time the presence of a shallow marine ingression in the Paleocene of southern Amazonia basin. The co-occurrence of a selachian assemblage encompassing *Potobatis* sp., *Ouledia* sp., and Pristidae indet. with the ostracod *Protobuntonia* sp. and the charophytes *Peckichara* cf. *varians meridionalis*, *Platychara perlata*, and *Feistiella* cf. *gildemeisteri* suggests a Paleocene age for the studied deposits (most likely Thanetian but potentially Danian). Fifteen facies have been recognized and have been grouped into three facies assemblages. Facies association A corresponds to the sedimentary filling of a tide-influenced meandering channel formed in the fluvial-tidal transition zone. Facies association B is related to more distal tidal-flats, little channelized tidal inlets and saltmarshes deposits. Facies association C corresponds to a stressed shallow marine environment such as a bay or a lagoon. The $\delta^{13}C_{TOC}$ value (-23.4 ‰) of MD-184 is enriched in $^{13}C$ compared to the other samples suggesting the presence of substantial amounts of marine organic matter in MD-184. The $\delta^{13}C_{TOC}$ values of samples from other outcrops (-27.3 to -29.8 ‰) indicate a mixed organic matter origin, from terrestrial to brackish environments. The analyzed sediments have similar Nd-Sr isotopic compositions as those of the Cenozoic sediments of the Altiplano (εNd(0) values from –6.2 to -10.7 and $^{87}Sr/^{86}Sr$ compositions from 0.712024 to 0.719026) indicating a similar volcanic source. This multidisciplinary dataset documents the presence of a tide-dominated estuary sourced by the proto Western Cordillera debouching into a shallow marine bay during Paleocene times. This transgression might be explained by subsidence created in response to the proto-Western Cordillera loading. Similar to Miocene marine incursions affecting the Pebas megawetland, Paleogene marine incursions in the Amazonian foreland basin associated with Andean uplift may have played a role in the

Neotropical biodiversity dynamics in favouring biogeographical isolation and promoting allopatric speciation for terrestrial organisms.

*Keywords*: Paleogene; marine incursion; Amazonian foreland basin; tidal deposits; micro paleontology; vertebrates paleontology; organic geochemistry; Nd-Sr isotopes; Madre de Dios basin; Peru; Andes.

## 1. Introduction

The Amazon basin is the world's largest Cenozoic fluvial basin with an actual drainage area of $5.8\times10^6$ km2 and a depositional area of approximately 2.5 to $3\times10^6$ km2. The Amazon rainforest, with an area of about $5.6\times10^6$ km2, is the largest rainforest ecosystem, representing nearly 50% of the total tropical rainforest area on Earth. The Amazon rainforest plays a significant role in global climate, the carbon cycle and biodiversity and is the most species-rich terrestrial ecosystem in the world. However, the timing of the origin and evolutionary causes of this diversity are still highly debated. A recent synthesis by Hoorn et al. (2010) has highlighted the complex links between Andean mountain building, climate variability and biodiversity development throughout Cenozoic times in the Amazonian basin. In particular the occurrence of inland seaway is important not only in promoting biogeographical isolation and allopatric speciation but also in controlling the precipitation rates in the Amazon basin (Jeffery et al., 2012). Consequently, determining the number, timing and duration of Cenozoic marine incursions recorded in Amazonian basin is fundamental not only for reconstructing paleo-Amazonian landscapes and ecosystems through time but also for understanding the close relationships between Andean mountain building and the Cenozoic climate and biotic evolution of South America.

Several marine incursions have already been described in the Cenozoic sedimentary record of the Amazonian foreland basins (Roddaz et al., 2010). For instance, the existence and persistence of the early to middle Miocene Pebas megawetland system in northern Amazonia is thought to have promoted the high biodiversity of the Amazon rainforest (for a review, see (Hoorn et al., 2010) and references therein). However, the extent of this Pebas system and the number of marine ingressions that have occurred is still under debate (Campbell et al., 2006; Hovikoski et al., 2007; Hoorn et al., 2010) mainly because of poor stratigraphic dating and the lack of regional data integration. In comparison, few studies document Paleogene marine

incursions in the Amazonian basin. For instance, there is some evidence of a marine ingression during Eocene to Oligocene times in Colombia (Santos et al., 2008), Ecuador (Christophoul et al., 2002) and northern Peru (Hermoza et al., 2005b), but no data exist for earlier marine incursions.

In this study, new biostratigraphical, sedimentological and geochemical data are presented to highlight a Paleocene marine ingression in southern Peru, Madre de Dios basin. A new paleo-depositional model for these coastal deposits is also proposed. Finally, the paleogeography and paleo-extension of this shallow marine ingression are discussed.

## 2. Geological background

### *2.1. Paleocene sedimentary record in the Amazonian foreland basins*

In nearly all the Central Andean sedimentary basins, late Eocene to early Oligocene times are marked by a widespread sedimentary hiatus (Mpodozis and Allmendinger, 1993; Marocco et al., 1995) corresponding to a major tectonic phase primarily called Incaic 1 phase (Noble et al., 1990; Jaillard, 1996; Hermoza, 2004). However, there are some localities in northern and Central Andean foreland basins where Paleocene strata have been preserved and can be described (Fig. 1 and Fig. 2).

In central Colombia, the Cuervos formation is late Paleocene in age (Jaramillo and Dilcher, 2000; 2001) and its sedimentary rocks correspond to mudstones deposited in a distal alluvial to coastal plain environment, in a foredeep position (Cooper et al., 1995; Parra et al., 2009). In the Putumayo basin of southern Colombia, the Rumiyaco Formation is barren of fossils and then remains poorly constrained but it is assumed that it is early Paleocene in age. The Rumiyaco Formation unconformably overlays the Cretaceous series and builts up a sedimentary wedge onlapping onto older strata and disappearing toward the east of the basin. The formation is characterized by possibly marine-related to mostly continental fine-grained deposits in the western part of the Putumayo basin and evolves eastward into continental sandstones (Bejarano, 1991; Casero, 1997; Córdoba et al., 1997; Londoño et al., 2012). In the Ecuadorian Oriente basin, Paleocene strata dated by charophytes (Faucher and Savoyat, 1973) are represented by the deposits of the fluvial Tena Formation. Various studies demonstrated that sediments from Tena Formation are derived from the Eastern Cordillera of Ecuador (Ruiz et al., 2004, 2007; Martin-Gombojav and Winkler, 2008).

In Peru, Paleocene strata are very scarce and are only identified in the eastern border of the Altiplano (Vilquechico Group and Lower Muñani Formation), in the Cusco-Sicuani

area (Puquin Formation) or in the present-day foreland basin (Yahuarango or Huayabamba Formations) (Sigé et al., 2004; Gelfo and Sigé, 2011). These strata generally consist of reddish fine-grained continental deposits and are defined as the Red Beds Formation (Naeser et al., 1991; Jaillard, 1993a; Hermoza et al., 2005b). The Lower Muñani Formation is dated between 55.9 and 53.4 Ma by mammalian biostratigraphy and by magnetostratigraphy (Cande and Kent, 1992; Sigé et al., 2004). The Yahuarango (Huallaga and Marañon basins) and Huayabamba (Madre de Dios and Beni basins) formations are poorly constrained. Only a few charophytes have been documented and provide a Paleocene age (Gutierrez, 1982) for these fluvial deposits (Fig. 2).

In Bolivia, Paleocene strata are virtually absent in the Amazonian foreland basin (Roddaz et al., 2010) (Fig. 2). Paleocene deposits documented in the Eastern Cordillera of southern Bolivia correspond to the mostly continental Santa Lucía and Cayara Formations, Danian and Thanetian in age, respectively (Marshall et al., 1997; DeCelles and Horton, 2003). However, a typically marine stingray (*Potobatis semperei*) was recently recognized within a marly horizon at the top of the Danian Santa Lucía Formation (Cappetta and Gayet, 2013).

### *2.2. Stratigraphy and structure of the Madre de Dios basin*

The Madre de Dios basin is part of the southern Amazonian foreland basins system (Roddaz et al., 2005). The Madre de Dios foreland basin is located northeastward to the Eastern Cordillera (EC) of southern Peru and can be subdivided into the Sub-Andean Zone (SAZ) and the Madre de Dios plain tectonomorphic units (Fig. 1-B) (Gil, 2001; Hermoza, 2004). The SAZ is characterized by both sedimentary filling and active deformation. In the SAZ, propagation of deformation towards the Madre de Dios plain is controlled by the development of deep duplexes, whose shortening is accommodated in surface by imbricates and by the Sub-Andean thrust front. The Sub-Andean thrust front corresponds to the eastern

129 border of the SAZ and is responsible for transportation of a piggy-back basin, which outcrops
130 as a large syncline called Salvación syncline in the study area (Fig. 1-B). The deformed and
131 still active SAZ only corresponds to the internal (western) part of Madre de Dios foreland
132 basin. The external (eastern) part of the basin is situated east to the Sub-Andean thrust front
133 and corresponds to the non-deformed part of the system, the Madre de Dios plain. In this
134 study, we will only focus on outcropping strata from the Salvación syncline, in the SAZ of
135 Madre de Dios basin.

136 Upper Cretaceous to Cenozoic strata in Salvación piggy-back basin consist of +/- 4500
137 m of an alternance of marine, tide-influenced and fluvial deposits (Gil, 2001; Hermoza,
138 2004). Because of the very scarce outcrops, fauna and palynomorph material available in the
139 studied area, the general chronostratigraphy of this succession is quite difficult to assess and
140 many interrogations subsist for the Cretaceous-Paleogene interval (Gil, 2001; Hermoza,
141 2004), while Miocene deposits are much better constrained in terms of biochronology and
142 chronostratigraphy (Marivaux et al., 2012; Antoine et al., 2013; Antoine et al., Submitted).
143 Paleogene strata in the Salvación series and more broadly in the Madre de Dos basin are
144 supposed to correspond to the fluvial Huayabamba or the Red beds Formation.

## 3. Methodology

In the Madre de Dios basin, Paleogene deposits crop out along the Alto Madre de Dios River between the Pongo de Coñeq Canyon and the Pantiacolla anticline, which correspond to the verticalized flanks of the Salvación Syncline (Fig. 1-B). This paper focuses on five selected exposures in cutbanks along the Alto Madre de Dios River. The section includes MD-177, MD-255, MD-256, MD-85 and MD-184 outcrops (Fig. 1-B and Fig. 1-C). Their precise locations are given in the online Supplementary Table A. The five concerned localities yield similar micro- and macrofossils (foraminifers, charophytes, molluscs, ostracods, as well as chondrichthyan and actinopterygian fishes), which allows us to consider them as being time equivalent (Table 1 and Fig. 3). Fifteen sedimentary facies are characterized on the basis of their lithologies, their physical and biogenic sedimentary structures, their palynological and paleontological content, and their geometry (Table 2). For limestone layers of MD-184, standard microfacies descriptions have also been realized. Each of these fifteen facies is interpreted in terms of depositional processes and related depositional environment. On the basis of these interpretations and with regards to the geometrical relationships between the facies, three facies associations are proposed (Table 2).

In order to determine the nature of the organic matter (terrestrial versus marine), we analyzed four samples for $\delta^{13}C_{TOC}$ content (Table 3) at the NIOZ Institute, Netherlands. The $\delta^{13}C_{TOC}$ of higher plants that use the Calvin-Benson cycle of carbon fixation (i.e. so-called $C_3$ plants) ranges from -29.3 to -25.5 ‰, with an average value of about -27 ‰ (e.g. Tyson, 1995). The typical marine $\delta^{13}C$ $C_{TOC}$ values are in the range of -18 to -22 ‰ (e.g. Meyers, 1997). Additional geochemical rock-eval analysis (for sample MD 184) has also been carried out by Repsol Exploration S.A.

Four selected samples of mudstones from outcrops MD-177, MD-85, MD-184 and MD-255 were measured at the University of Toulouse for their Nd-Sr isotopic compositions, providing sedimentary provenance information (Table 4). Aliquots containing about 1000 ng of Sr and Nd were loaded onto the ion-exchange columns. Sr and Nd were separated using the Sr-SPEC, TRU-SPEC and LN-SPEC resins (Eichrom®). Nd-Sr isotopic ratios were measured using a Finnigan Mat 261 thermal ionization mass spectrom in dynamic mode following Viers et al. (2008). The measured $^{143}Nd/^{144}Nd$ ratios are presented as the fractional deviation in parts per $10^4$ (units) from $^{143}Nd/^{144}Nd$ in a Chondritic Uniform Reservoir (CHUR) as measured at the present-day:

$$\varepsilon Nd(0) = [(^{143}Nd/^{144}Nd)_S/I_{CHUR}(0)\_1]*10^4$$

where $(^{143}Nd/^{144}Nd)S$ is the present-day ratio measured in the sample, and $I_{CHUR}(0)$ is the $^{143}Nd/^{144}Nd$ in the CHUR reference reservoir at the present ($I_{CHUR}(0) = 0.512638$ (Jacobsen and Wasserburg, 1980).

## 4. Results

### *4.1. New biostratigraphical and paleoenvironmental constraints from fossil assemblage*

#### *4.1.1. Biostratigraphy*

The fossil content of stratigraphic interest recovered in the studied sections is detailed in the Table 1 and Fig. 3. The concerned material includes vertebrates (chondrichtyans and actinopterygians), ostracods, benthonic foraminifers, and charophytes. Being only recognized at genus, family level, or above, the molluscs found in MD-177, MD-184, and MD-85 are of no use in terms of biostratigraphy (Table 1). Accordingly, MD-177 and MD-184 yielded unidentified Charophyta and Ostracoda.

The dominant taxon among vertebrate remains in the concerned deposits is the batoid *Ouledia* sp. (MD-177; MD-184; MD-85; see Table 1 and Fig. 3 for biostratigraphical results details and Fig. 4 C-D, I-J for an illustration of the key stratigraphic markers). This fossil genus of butterfly rays (gymnurids) is well-known in tropical coastal deposits from Africa and Asia, ranging from the Thanetian up to the Priabonian (Cappetta, 2012). In MD-184, *Ouledia* is found in association with a pristid sawfish. Pristids are a cosmopolitan family restricted to Cenozoic marine and estuarine localities at world scale (i.e., Danian and onward; Cappetta, 2012). In MD-85, *Ouledia* sp. (mainly represented by worn teeth) co-occurs with *Potobatis* sp. (Fig. 4 G-H), a dasyatoid stingray so far endemic to Danian marine levels from the top of the El Molino Fm., Bolivia (Cappetta and Gayet, 2013). However, in MD-85, the prismatic teeth referred to as *Potobatis* sp. are eroded and might have been reworked, which would concur to consider the Danian epoch as a floor age for MD-85. The vertebrate assemblages also include dozens of teeth of an unidentified pycnodontid bony fish (MD-177, MD-184; Fig. 4 E-F), distinct from but potentially allied to ?*Ocloedus toncoensis* (Maastrichtian-Danian of South America; Gonella et al., 2012). Pycnodontids are well represented in

Mesozoic and early Paleogene localities, before the family gets extinct during the middle Eocene (Gayet et al., 1993; Poyato-Ariza and Wenz, 2002).

Microfossils of high biostratigraphical interest were recovered in MD-255 and MD-85. The agglutinated benthonic foraminifer *Karreriella conversa* (Eggerellidae), found in MD-255, has an Upper Cretaceous-Lutetian range (Fig. 2; Gradstein et al., 1988; Valchev, 2007). The best constrained locality is MD-85, with a diversified charophyte flora (17 specimens of *Peckichara* cf. *varians meridionalis*; 10 specimens of *Platychara perlata*?; 15 specimens of *Feistiella* cf. *gildemeisteri*), the ostracod *Protobuntonia* sp., and benthonic foraminifers (*Reophax* sp., *Bathysiphon* sp., and *Rhabdammina* sp.). The ostracod *Protobuntonia* ranges from the Coniacian up to the Thanetian epoch (Morsi et al., 2011); the fragile and delicate valves referred to this taxon in MD-85 are complete (i.e., not likely to be transported or reworked). The charophyte *Platychara perlata* has a Danian last occurrence in Peru (Sigé et al., 2004). The charophyte *Peckichara* cf. *varians meridionalis* is restricted to the Maastrichtian-Thanetian interval (e.g. Musacchio, 1990; Aubry et al., 2005). The charophyte *Feistiella* cf. *gildemeisteri*, previously recorded in the Paleocene Yahuarango Formation from Huallaga area, in northern Peru (Hermoza et al., 2005b; Roddaz et al., 2010) and at Laguna Umayo, southern Peru (Jaillard, 1993a), ranges from the Maastrichtian up to the Thanetian or the earliest Ypresian (Sigé et al., 2004; Gelfo et al., 2009; Gelfo and Sigé, 2011; Woodburne et al., 2014).

Once combined, all these biostratigraphical data preclude any referral i) to Mesozoic times (*Potobatis*, Pristidae, and *Ouledia* have a Paleocene First Appearance Datum [FAD]) or ii) to a post-Paleocene interval (*Protobuntonia*; *Platychara perlata*; *Peckichara* cf. *varians meridionalis*). In other words, they strongly concur to indicate a Paleocene age for the deposits described in the northern part of the Madre de Dios Basin (MD-85, MD-177, MD-184, and MD-255 localities; Table 1 and Fig. 3). Yet, based on the biostratigraphical markers

recognized in the concerned sections, the age of the studied marine incursion cannot be further refined definitely. However, this marine incursion is more likely to coincide with Danian or Thanetian times (Hypotheses 1 and 2, respectively; Fig. 3). The Hypothesis 1 (Danian) favors the known range of *Potobatis* (then not reworked at MD-85) and of *Platychara perlata*. This would in turn imply a Danian first occurrence for *Ouledia*, 3-8 million years before its known FAD (Fig. 3). The Hypothesis 2 (Thanetian) is constrained by the conspicuous presence of *Ouledia* in three localities. In that case, *Potobatis* teeth might be reworked in MD-85 and/or the stratigraphical range (as for the charophyte *Platychara perlata* , same locality) is to be extended up to the Thanetian epoch (Fig. 3).

We tend to favor the Hypothesis 2, due to the occurrence of hundreds of fresh specimens referred to as *Ouledia* sp. found in MD-85, MD-177, and MD-184. Furthermore, it cannot be discarded that the two prismatic teeth of *Potobatis* and the 10 oogonia of *Platychara perlata* were reworked from Danian deposits eroded upstream by the time of deposition of MD-85.

*4.1.2. Paleoenvironments*

Thus far, late Cretaceous and Paleocene selachian faunas from Andean and sub-Andean basins consist only of batoids (i.e. no shark is recorded), further known to be highly endemic (de Mowbray and Visser, 1984; Gayet et al., 1993; Cappetta and Gayet, 2013). Together with the complete absence of associated sharks, the co-occurrence of *Ouledia* (MD-177; MD-184; MD-85), *Potobatis* (MD-85), two unidentified dasyatoids (MD-177), and a pristid (MD-184) point to shallow waters in a proximal marine or estuarine environment for the Paleocene deposits described in this study (Cappetta, 2012; Cappetta and Gayet, 2013). The ichthyofauna also includes a high number of pycnodontiform bony fish remains (Pycnodontidae indet.; MD-177; MD-184; MD-85, see Fig. 3 and Fig. 4), some of them being found in partial anatomical connection (i.e., no transport). This extinct group is only recorded

in marine deposits (shallow water seas; Gayet et al., 1993). However, a freshwater influence is supported by the presence of numerous isolated teeth of characiform bony fishes (MD-177; MD-184; MD-85). Today, characiforms are strictly restricted to freshwaters (Gayet et al., 1993). Serrasalmine characiform teeth with a plesiomorphic pattern (*Colossoma*-like) were in particular recognized in MD-184.

The agglutinated foraminifer assemblage, including *Karreriella conversa* (MD-255), *Reophax*, *Bathysiphon*, and *Rhabdammina* (MD-85), points to a shallow marine inner platform, under unstable environmental conditions, with frequent detrital/terrigenous influxes. Such a continental influence is further attested by the presence of numerous charophyte oogonia (likely to be transported during river flooding episodes) and riverine to brackish molluscs (e.g., *Corbicula* and *Aylacostoma*). No open sea indicator, such as dinoflagellates or planktonic foraminifers, has been recorded throughout the sections.

To sum up, the macro- and microfossil assemblages (vertebrates, molluscs, ostracods, foraminifers, and charophytes) as documented in MD-177, MD-184, MD-255, and MD-85 (Table 1 and Fig. 3) point to an initial idea of the depositional environment: a shallow marine inner platform, under unstable environmental conditions, with frequent detrital/terrigenous influxes from a river estuary or delta.

### *4.2. Depositional environments from sedimentary analysis*

In this section, the facies associations are described and interpreted. Diagnostic criteria of the facies are summarized in Table 2.

#### *4.2.1. Facies association A: the Fluvial-tidal transition zone*

Facies association A is made up of four facies: A1, A2, A3, and A4. These four facies have only been described at the location of outcrop MD-255 (Fig. 1-C). Outcrop MD-255 displays two channel-shape stacked bodies showing concave-up basal surfaces. The lateral

extension of these sedimentary bodies is close to 150 m long and their thickness reaches 4 to 5 m (Fig. 5-A and Fig. 5-B). Facies A1, A2 and A3 have been recognized within the channelized bodies, whereas facies A4 has been observed above and laterally to the channels (Fig. 5).

Facies A1 (total thickness of 20 to 120 cm) has been observed at the base of the channel-shape bodies. It generally starts with an accumulation of millimetric to centimetric mud clasts scattered in fine- to medium-grained sandstone, forming a few cm-thick microconglomeratic matrix-supported mud breccias, erosive at its base. Mud clasts disappear upwards and the facies evolves into fine- to medium-grained sandstones. These sandstones are massive or are organized into tangential cross-bedding forming 30 cm thick tangential co-sets (Fig. 6-A). Some reactivation surfaces can be observed. Both tangential sets and co-sets can be highlighted by thin mud drapes and generally present the same dip direction. However, some foresets can dip in the opposite direction. Facies A1 ends with an undulate rippled surface with heights of 1 to 2.5 cm and wavelengths of 15 to 20 cm, showing ichnofabrics *Arenicolites* and possible *Dactiloides* (Fig. 6-B and Fig. 6-C). Facies A1 corresponds to the coarsest deposits described in the area.

Facies A2 (total thickness of 1 to 1.20 m) consists of slightly oblique heterolithic strata (Fig. 6-F) overlying Facies A1 after a sharp transition (Fig. 5-B). Massive fine-grained sandstones or flaser bedding with asymmetrical climbing ripples highlighted by frequent mud drapes (15 to 30 cm thick) (Fig. 6-E) alternates with wavy bedding or planar muddy lamination in fine-grained sandstones (10 to 20 cm) (Fig. 6-G). The distribution of the thin planar mud drapes observed within the fine-grained sandstones of the wavy bedding often displays a rhythmic pattern, with intervals of inframillimetric sandstone beds evolving gradually to millimetric and then centimetric thicker sandy beds suggesting coarsening-up

303 cycles (Fig. 6-G and Fig. 6-F). Mud accumulation can be 1 mm to 1 cm thick. Horizontal and
304 to a lesser extent vertical undetermined burrows are occasionally present.

305 Facies A3 also corresponds to slightly oblique heterolitic strata (total thickness > 60
306 cm). In comparison with Facies A2, Facies A3 is coarser as it is made up of thicker sandy
307 beds (20 to 40 cm thick) intercalated with thin muddy to silty beds (2 to 5 cm thick). Fine-
308 grained sandstones present tangential cross-bedding with planar laminations at their base
309 representing their bottomset (Fig. 6-D). Rare asymmetrical ripples in the opposite direction
310 can also be observed at the top of the tangential laminations. These sansdstones are also
311 heterolithic as almost all the sandy tangential and planar laminae are highlited by thin mud
312 drapes. Regular chanching thicknesses of millimetric to centimetric sandy layers and
313 inframillimetric to millimetric muddy layers suggests a rhythmic pattern (Fig. 6-D). Facies A1
314 and A3 are both made up of tangential cross-bedding in fine-grained sandstones, but
315 differences with Facies A1 result in: 1) the scale of the structures (Facies A1 is made up of
316 larger-scale cross-bedding compared to Facies A3), 2) the general geometry of the bodies
317 (Facies A1 corresponds to the laterally filling of a channelized body whereas Facies A2
318 corresponds to more tabular deposits) and 3) the texture and internal organization of the
319 sediments (more finer texture and more heterolithic and rhythmic patterns for Facies A1).

320 Strata from both facies A2 and A3 present an oblique pattern, prograding from the
321 south-eastern channel margin towards the north-western margin of the channel (Fig. 5-A and
322 Fig. 5-B).

323 Facies A4 corresponds to siltstone layers (2 m thick) intercalated with fine-grained
324 sandstone layers (10 cm thick). These sandstones present a sharp contact with the underlying
325 siltstones and show climbing-ripples structures. Siltstones evolve upwards into mudstones (>2

m thick), where root traces develop at the top of the section. Rare benthic foraminifer *Karreriella conversa* can be preserved in this facies.

Interpretation:

Stacked channels geometries as observed at MD-255 are common in fluvial and tidal settings. In both cases channels are erosive at their base and can be composed of fining- and thinning-up strata evolving gradually upwards into shaly strata. These shales can correspond to either fluvial floodplain or tidal flat deposits depending on the depositional environment.

The massive or cross-bedded fine- to medium-grained sandstones with basal mud clasts above erosional surfaces (Facies A1) could represent purely fluvial channel filling with bottom reworking lag deposits (Facies Gt and Gh from Miall, 1996). However the presence of ichnofabric *Arenicolites* (and possible *Dactiloides*?) observed at the top of this facies (Fig. 6-C) and the presence of the benthic foraminifer *Karriella conversa* (Facies A4) suggest deposition in, respectively, tide-influenced environment (deltaic or estuarine) and deposition in shallow marine platform with continental influx (see Table 1). Facies Association A is therefore related to both tidal and fluvial environments.

Reactivation surfaces as observed within the cross-bedded sandstones of facies A1 can be caused by tidal current reversals (Klein, 1970; de Mowbray and Visser, 1984) even if these surfaces could also be produced by river-discharge variations and erosion of brink by arrival of a new bedform in fluvial settings (Dalrymple, 1984). The occurrence of rare bidirectional trough cross-bedding (Fig. 6-A) suggests a depositional area receiving opposite-direction currents, dominated either by flood or ebb currents. The prograding pattern displayed by the tangential cross-bedded sandstones suggests lateral accretion processes. Mud clasts have been deposited at the base of the channels by gravity processes. They are common in channel bottom deposits in many tide-dominated or influenced environments because of the erosion

by high-energy currents of thin muddy layers forming slack water drapes, or because of the erosion by lateral accretion of muddy tidal-flat and salt-marsh deposits (Dalrymple and Choi, 2007). In conclusion, we interpret Facies A1 as dune deposits formed during the early-stage of a tide-influenced channel settlement controlled by both fluvial and tidal processes.

Facies A2 and A3 overly the basal filling of the channelized bodies and constitute small-scale Inclined Heterolithic Stratification (IHS). These IHS developed by lateral accretion within the channels (Fig. 5-A and Fig. 5-B). Although IHS may be observed in fluvial environments (e.g., Jackson, 1981; Page et al., 2003), they are most common in tide-influenced settings (Dalrymple et al., 2003). In addition, Facies A2 and A3 often display rhythmic patterns and heterolithic textures. Interlamination of mud and fine-grained sands results from suspension and weak traction current and may occur in fluvial overbank deposits (lithofacies Fl, Miall, 1996). However, alternation of sand and mud laminae within millimetric wavy and flaser beddings (Facies A2 and A3) is more frequent in tidal depositional environment. Concerning Facies A2 and A3, the abundance of wavy and flaser bedding, mud drapes and rhytmicity rather suggests tidal influence on deposition (Nio and Yang, 1991). Recurrent thickness fluctuations observed within the cross-bedded sandstones in the successive sandy beds of Facies A3 (Fig. 6-D) may be interpreted as the result of neap-spring influence (Eriksson et al., 1998; Eriksson and Simpson, 2004; Mazumder and Arima, 2005). Similar rhythmicity has also been found within facies A2 (Fig. 6-F and Fig. 6-G). The presence of few thin mud drapes observed within these sandstones may therefore represent deposition during tidal slack-water periods. Facies A2 corresponds to lower hydrodynamic conditions than Facies A3 (coarser sandstones). However, they both constitute IHS, and are interpreted to have been deposited by lateral accretion in a channelized body. Therefore, facies A2 and A3 are both interpreted as tide-influenced point-bar deposits in a meandering

channel. Because Facies A3 is situated above Facies A2 (Fig. 5), Facies A3 should be related to a higher energy recovery during the channel deposition history.

Facies A4 corresponds to the uppermost- and finest strata deposited at the top of the channels succession. This silty facies could firstly be interpreted as channel abandonment, fluvial floodplain or tidal-flat deposits. The presence of *Karreriella conversa* indicates deposition in a coastal, brackish water environment (Valchev, 2007) and supports a tidal flat interpretation for facies A4. According to Dalrymple and Choi (2007), the pedogenic structures described in the mudstones at the top of facies A4 could be associated to a period of emersion of a tidal mud flat .

To conclude, Facies association A corresponds to a moderate-energy channel filling history. According to the IHS geometry resulting from lateral accretion processes, this channel is interpreted to be related to a meandering system. Because of the proximity of pedogenetic features and because of the preponderance of fine-grained texture in the facies association, this meandering system could be purely fluvial. However, the evidences of tidal- or marine-related environment (benthic foraminifer, *Arenicolites*) and the evidences of tidal-processes (rhythmic patterns, IHS, mud drapes) finally suggest a mixed fluvial-tidal environment. Facies association A is interpreted to correspond to the sedimentary infilling and abandonment of tide-influenced meandering channels migrating laterally in surrounding tidal-flats and floodplain.

#### *4.2.2. Facies association B: Tide-dominated environment*

Facies association B consists of 5 facies: B1, B2, B3, B4 and B5. They all have been found in MD-256 (Fig. 7) and partially in MD-85 (Fig. 9) and are summarized in Table 2.

Facies B1 corresponds to the infill of isolated channelized sedimentary bodies (~60 to 150 m width and ~1 to 1.50 m in thickness) and has been observed at both MD-256 and MD-

85 localities. No stacking or amalgamated pattern has been noticed. The base of this facies corresponds to a channel-shaped surface. This surface is highlighted by elongated millimetric to centimetric mud clasts forming a breccia of few centimetres-thick and evolving upwards into massive medium- to fine- or very fine-grained sandstone. Internal sigmoid cross-beddings (45 cm in height) are often present in the basal part of these sandstones. Fine-grained sandstones may also display high-angle climbing ripples at their base evolving upwards into low-angle climbing ripples (Fig. 8-A). At the top of the deposits, climbing ripples cross-stratification changes upward into more flattened trough cross-stratification (see channel sedimentary structures within the channel of outcrop MD-85, Fig. 8). Reworked charophyte oogonia, stingray teeth (MD-85), and benthic foraminifer (MD-256) are observed in this facies (Table 1).

Facies B2 (total thickness of ~20 m) consists of reddish mudstones. Root traces and gypsum or anhydrite nodules can develop at the top of the facies (Fig. 8-B). This facies has been observed at the top of the sedimentary section and presents a sharp contact with the underlying Facies B3 (Fig. 7). It is also laterally associated with Facies B1.

Facies B3 and B4 are closely related and often alternate in the section described (Fig. 7). In this case, the contact between the two facies is sharp. Facies B3 (total thickness of 0.50 to 4 m) consists of bioturbated and burrowed reddish mudstones to rare siltstones. Occasional lenticular bedding can occur within the mudstones. Facies B4 (total thickness of 1 to 5 m) corresponds to highly burrowed heterolithic deposits showing regular alternations of very fine to fine-grained sandstones with muddy or silty layers displaying planar horizontal, wavy bedding and lenticular bedding (sets of 10 cm thick) (Fig. 8-C, Fig. 8-D and Fig. 8-E). Burrows are horizontal or vertical but no specific ichnofabric can be determined (Fig. 8-4D). Colour is dark grey to violet. The sedimentary structures in sandstones are highlighted by thin (2 to 3 mm thick) laminae of mud and silty drapes. Thin sand layers can occasionally be

intercalated by mud drapes, thus forming mud couplets. Opposite current dips have been observed in this facies. At the top of sandy strata, fluid escape structures can be observed (Fig. 8-E). Facies B5 (total thickness of ~20 cm) is generally observed above facies B4, after a sharp or progressive contact (Fig. 7). It is made up of clean fine-grained sandstone often ending with a wave-rippled surface (ripples are 1 to 1.5 cm in height with wavelength of 6.5 to 8.5 cm) (Fig. 8-F).

Interpretation:

Facies B1 corresponds to channel infill deposits. Climbing-ripple cross-stratification is a common feature in a wide range of depositional environments in which suspension exceeds the rate of traction transport (Jopling and Walker, 1968; Allen, 1970; Ashley et al., 1982). However, sigmoidal cross-bedding associated with the presence of brackish-water fossils (benthic foraminifer, see Table 1) suggests deposition within a tide-influenced environment. Climbing ripples from tidal environments are different from non-tidal climbing ripples by having common mud drapes and finer-grained texture (Choi, 2010). In a tidal environment, they can be characteristic of tidal inlet infillings in the fluvial-tidal transition zone of estuaries (Dalrymple et al., 1992; Tessier, 1996; Hovikoski et al., 2008). Flood dominated Climbing Ripples Facies (CRF) can also be associated with tidal channel levees found in the inner/straight channel zone of the fluvial-estuarine transition (cf. Mont St Michel estuary; Tessier, 1996). In case of ebb-dominated context, CRF are found in chute channels and chute bars in the meandering zone of the fluvial-estuarine transition (Tessier, 1996). In comparison with Facies A1, Facies B1 is finer-grained and is related to decreasing flow processes (climbing ripples). Geometrically, Facies B1 only concerns isolated channels whereas Facies A1 is related to stacked and thick channels overlain by laterally migrating strata (IHS deposits; Facies A2 and A3, Fig. 5). Channels from Association A represent higher energy channels in comparison with those from Facies Association B (Facies B1). We interpret Facies

B1 as tidal inlet deposits. Facies B2 is generally structureless but contains paleosoil horizons and gypsum nodules in a very fine shaly matrix. As it is laterally associated with facies B1, it has been interpreted as salt marshes in a supratidal environment. Facies B3, characterized by muddy deposits with scarce lenticular bedding, could correspond to mud flat deposits in an intertidal environment. Facies B4 is characterized by highly burrowed heterolithic deposits with double mud drapes, wavy and lenticular beddings that are typical sedimentary structures of tide-influenced environments (Nio and Yang, 1991; Dalrymple et al., 1992; Dalrymple and Choi, 2007). We consequently interpret facies B4 as mixed muddy/sandy flat deposits.

To conclude, Facies association B is constituted by all the surrounding flats influenced by tidal processes, from the subtidal area (tidal inlet (Facies B1), mixed tidal flats with double mud drapes (Facies B4 and B5) to the intertidal/surpatidal environments (mud flats and saltmarshes, respectively Facies B2 and B3).

#### *4.2.3. Facies association C: Bay and shallow marine environments*

Facies association C is composed of six facies: C1, C2, C3, C4, C5 and C6. All the facies have sheet-like geometries, and have been described at outcrops MD-85 (Fig. 9), MD-177 and MD-184 (Fig. 10, section 1 and 2, respectively).

Facies C1 (total thickness of 50 cm to >2 m) corresponds to blue-violet-reddish marls to carbonated siltstones with centimetric thick fine-grained sandy layers and occasional centimetric thick carbonaceous layers (Fig. 11-A). Ripples and climbing ripples are present within the sandy layers. Facies C1 contains benthic foraminifer (*Bathysiphon*, Fig. 11-B), Mollusca (Bivalvia: Corbicula and Polymesoda; Gastropoda: Cerithioidea, Pachychilidae, and? *Aylacostoma*), Ostracoda, Chondrichthyes (Myliobatiformes: *Ouledia* sp., Pristidae, and Dasyatoidea), Osteichthyes (Pycnodontiformes: *Coelodus*; Characiformes: Serrasalminae and indet.) (see Table 1). Facies C2 (total of thickness 80 cm to 1 m) is always closely related to

facies C1 and the contact (basal and top) between the two facies is progressive. Facies C2 is similar to facies C1 but contains common sandy and gypsum nodules, root traces and bioturbation. Facies C3 (total thickness of 15 to 50 cm) corresponds to millimetric to centimetric sandy nodules scattered into a violet muddy to silty matrix, forming a matrix-supported breccias. This facies contains numerous organic fragments such as fish vertebrae and ostracods. Facies C4 corresponds to an alternation of marl (5 to 10 cm) and thin limestone strata (2 to 5 cm). Carbonate nodules are frequent within the marls. Limestones commonly present well-developed desiccation crack surfaces at the top of the strata as well as burrows and root traces. Small oyster shells (2 to 4 cm in length) are visible within the limestone strata. Microfacies analysis of thin sections allowed the recognition of oysters (little size species), fish vertebrae fragments, annelid burrows, numerous ostracods and/or phylopods, and undifferentiated gastropods (Fig. 12-A, Fig. 12-B, Fig. 12-C and Fig. 12-D). Only very few ostracods and phylopods present a complete carapace with paired valves but they all present a smooth surface. According to Dunham's classification (Dunham, 1962), the observed limestones can be classified as wackstone to packstone. The matrix is generally micritic or microsparitic. Peloidal micrite (Fig. 12-A and Fig. 12-B) could constitute secondary cementation better than primary matrix. Secondary sparite grains are common, and can form drusic or bird-eyes cements (Fig. 12-B and Fig. 12-D). Facies C5 (strata presenting thickness of 25 to 80 cm) also corresponds to limestone deposits showing desiccation cracks at the top (Fig. 11-C and Fig. 11-D). These strata present undulated base and top. Thin-section shows stromatolith filaments entangled with ostracod carapaces and annelid burrows (Fig. 12-E and Fig. 12-F). The matrix is micritic to microsparitic. Facies C6 correspond to limestone strata (10 to 25cm thick) with abundant small-size oysters (2 to 4 cm in length). Thin-section reveals numerous oysters with lamellar and multilayered structures, annelids burrows, blue (?) algae filaments, fish coprolith and some ostracodes (Fig. 12-G, Fig. 12-H, Fig. 12-I and Fig.

12-J). Root traces are also present. The matrix is made up of micrite or small microsparite crystals. Some bivalve's shells are rounded by a micrite envelope (Fig. 12-G). This facies is separated from the other because of its greatest oysters content.

Interpretation

The ichtyofauna from Facies C1 and C3 is characteristic of a shallow marine environment, with variations from a strong freshwater influence in a more proximal environment to a confined and steady proximal marine environment of normal salinity (as attested by the wide array of obligate marine taxa, such as chondrichthyans and pycnodontiform actinopterygians (Cappetta, 2012). Absence of high energy sedimentary structure in facies C1 suggests deposition in a protected shallow marine environment. Pedogenic structures of Facies C2 are related to episodic emersions of these shallow-marine deposits (originally Facies C1). Facies C3 is interpreted to have been deposited by an episode of higher energy in this shallow marine environment, maybe related to bank collapsing. Facies C4, C5 and C6 correspond to limestones deposited in a subaquatic environment submitted to frequent subaerial exposures as attested by the dessication cracks and root traces and burrows found at the top of the beds The presence of little-sized oysters (characteristic of a stressed environment), smooth-carapaces ostracodes and annelids are consistent with a shallow marine environment (Armstrong and Brasier, 2005) whereas micrite envelopes rounding bivalve's bioclasts indicate an intertidal context. Evidences of frequent subaerial exposures indicate a short-lived and frequently changing depositional environment, from intertidal to lacustrine. Stromatholitic carbonates of Facies C5 are related to a confined and stressed intertidal environment (Wattinne, 2004), whereas the *Ostrea* limestones of Facies C6 are in agreement with a deeper confined marine environment (Enay, 1990) intertidal to upper infralitoral. Because of the presence of some fresh water fossils and the occurrence of frequent emersion,

the depositional setting should be quite close to the coast. To conclude, we interpret facies association C to represent deposition in a bay/lagoon or stressed shallow marine-environment.

### *4.3. Organic Geochemistry*

The TOC contents of the samples were in general very low, ranging from 0.03 to 0.06 wt. % (Table 3). Therefore, care should be taken to interpret the organic geochemical data. Nonetheless, the reproducibility of TOC contents and $\delta^{13}C_{TOC}$ was better than 0.02 wt. % and 0.3 ‰, respectively. The $\delta^{13}C_{TOC}$ values varied from -23.4 to -29.8 ‰ (Table 3).

The $\delta^{13}C_{TOC}$ of higher plants that use the Calvin-Benson cycle of carbon fixation (i.e. so-called $C_3$ plants) ranges from -29.3 to -25.5 ‰, with an average value of about -27 ‰ (e.g. Tyson, 1995). The typical marine $\delta^{13}C_{TOC}$ values are in the range of -18 to -22 ‰ (e.g. Meyers, 1997). The $\delta^{13}C_{TOC}$ values (-27.3 to -29.8 ‰) of MD-177, MD-85, and MD-255 are hence typical of $C_3$ plant-derivated organic matter. In contrast, the $\delta^{13}C_{TOC}$ value (-23.4 ‰) of MD-184 is enriched in $^{13}C$ compared to the other samples, closer to typical marine $\delta^{13}C_{TOC}$ values. This suggests the presence of substantial amounts of aquatic organic matter in MD-184. Notably, it has been shown that the presence of a fresh-water algae *Pediastrum*, which is very common in lagoonal settings, can cause substantially enriched d13CTOC values, up to 2 ‰ (e.g. Steurbaut et al., 2003). Consequently, our organic geochemical results suggest that organic matter in MD-184 might be dominantly derived from aquatic (marine or lagoonal) environments. This interpretation is supported by additional rock-eval analysis results obtained for MD-184, indicating Type II kerogen, which originates from mixtures of zooplankton, phytoplankton, and bacterial debris in marine sediments (Peters and Cassa, 1994). The three other samples (from outcrops MD-85, MD-255, and MD-177) indicate a possible mixed organic matter origin, from terrestrial to brackish environments, but are more characteristic of terrestrial environment

### *4.4. Nd-Sr isotopic composition*

The Nd-Sr isotopic compositions of the Thanetian sedimentary rocks are shown in Table 4. Overall, the sediments have quite variable εNd(0) values (ranging from -6.2 to -10.7) with a comparatively narrow range of $^{87}Sr/^{86}Sr$ compositions (0.712024 to 0.719026) (Table 4). The four samples analyzed for their Nd-Sr isotopic compositions have been reported in the $^{87}Sr/^{86}Sr$ versus εNd(0) diagram (Fig. 13). The isotopic results are compared with several other relevant source fields: Mesozoic and Neogene volcanic rocks (Rogers and Hawkesworth, 1989; Kay et al., 1994). Quaternary Ecuadorian lavas (Barragan et al., 1998). Cenozoic sedimentary rocks from the Depression, Altiplano, Oriental Cordillera and Subandean zone of Chili and Bolivia (Pinto, 2003); modern suspended sediments from the Solimoes and Madeira rivers (Viers et al., 2008); Neogene deposits from the Amazonian foreland basin of Bolivia, Ecuador and Peru (Roddaz et al., 2005a), and the sand of the Peruvian White Sand (WS) Formation cratonic in origin (Roddaz et al., 2005a). Nd-Sr isotopic compositions of sediments deposited by an Andean drainage define plot within a mélange hyperbole as observed by Basu et al. (1990), Roddaz et al. (2005a) and Roddaz et al. (2012) for Neogene sediments of the Amazonian foreland basins, with one end member being the primitive volcanic arc and the other the upper continental crust of the Brazilian shield. The four analyzed Paleocene samples plot within the field of the Cenozoic Altiplano sediments, indicating a similar Andean provenance. When compared with Neogene Subandean zone sediments, they plot closer to the volcanic arc end member, indicating a greater contribution of the volcanic arc rocks end member for the Paleocene sedimentary rocks relative to Neogene SAZ sediments.

## 5. Depositional environment synthesis

Our biostratigraphical results, sedimentary facies interpretations and organic geochemistry analysis indicate the presence of a tide-influenced shallow marine paleoenvironment during the Paleocene in the northern Madre de Dios Basin. Facies association A corresponds to the sedimentary filling of a tide-influenced meandering channel deposited in the fluvial-tidal transition zone. Facies association B corresponds to tidal flats deposits, tidal inlets and also characterizes a tide-influenced environment but with more distal facies than facies association A. Facies association C, interpreted as deposited in a bay/lagoon or stressed shallow marine-environment, is the most distal facies association. The facies of this association do not show any evidence of tidal nor oscillatory currents.

The transition between the land and the sea in tide-dominated coastal environments is among the most complex on Earth, because of the interaction of numerous physical, chemical and biological processes (Dalrymple and Choi, 2007). Existing depositional models are therefore preliminary because the number of case studies of many of the subenvironments is rather small (Dalrymple and Choi, 2007). However, our dataset makes the possibility to distinguish between tide-dominated delta and tide-dominated estuary. First, from a geological point of view, estuaries are transgressive whereas deltas are regressive (Dalrymple et al., 1992). The tide-dominated Paleocene deposits studied in this paper overly continental deposits of the Yahuarango formation. This stratigraphic succession therefore suggests that the tide-dominated Paleocene deposits are transgressive and related to an estuary. The presence of a Paleocene tide-dominated estuary is further attested by the occurrence of a well expressed tide-influenced meandering zone. According to several works (Dalrymple et al., 1992; Dalrymple and Choi, 2007), only the fluvio-estuarine transition zone in a tide-dominated estuary could explain the occurrence of both opposite currents and meandering channels in a tide-influenced environment. Facies association A could be an illustration of this fluvial-tidal

environment, as it shows evidences of meandering channels influenced by both fluvial and tidal currents (Fig. 14). According to this interpretation, Facies association B could be interpreted as deposited in the outer part of this tide-dominated estuary, where tidal inlets are still present and can laterally be connected to muddy and mixed tidal-flat deposits (Fig. 14). Finally, as Facies association C does not show any evidences of tidal currents, we suggest deposition in a shallow confined marine environment (Fig. 14).

## 6. Paleogeographic and tectonic implications

The data presented in this study document for the first time the existence of Paleocene tide-dominated estuary debouching into a shallow marine bay in the western Amazonian foreland basin. We favor a Thanetian age for this marine incursion but a Danian age cannot be discarded. Most of Paleocene sedimentary rocks of other parts of the Andean/Amazonian foreland basin were mainly deposited in a distal fluvial environment (see Fig. 2 and references therein). The presence of estuarine deposits overlying continental deposits indicates a marine transgression during the Paleocene. This transgression is caused by an increase in accommodation space which in turn depends on the interplay between sediment supply and base level changes (see Catuneanu, 2004 and references therein). In a retroarc foreland basin setting, numerous mechanisms can be envisaged to account for an increase in accommodation space including eustasy, matle processes, foreland related tectonics (i.e. loading/unloading cycles of (i.e. loading/unloading cycles of Catuneanu et al., 1997) and decrease in sediment supply. The Danian and Thanetian periods are characterized by a drop in global sea-level (Fig. 3) (Haq et al., 1987; Hardenbol et al., 1998; Vandenberghe et al., 2012). Consequently the recorded transgression (Danian or Thanetian in age) is not related at first order to a rise in global sea-level. Dynamic loading may be induced by subduction beneath the retroarc foreland basin. Subduction generates long wavelength subsidence (Mitrovica et al., 1989; Catuneanu et al., 1997; Pysklywec and Mitrovica, 2000; Catuneanu, 2004) capable of maintaining the four depozones of the foreland basin system below the base level (Catuneanu et al., 1997; Catuneanu, 2004) and thus of producing accommodation at the basin scale. In fact, we have no idea of the depositional environment of other depozones (wedgetop, proximal foredeep and backbulge) adjacent to our study area so that it is difficult to exclude subsidence dynamic as a possible mechanism. However, the presence of a Paleocene flexural forebulge in the southern Bolivia foreland basin caused by loading of the Western Cordillera

(DeCelles and Horton, 2003) suggests that Andean tectonic loading was a first-order control on tectonic subsidence in Paleocene times. This is in agreement with our Nd-Sr isotopic provenance data that show an Andean provenance and hence the presence of an Andean relief in Paleocene times. Short-lived marine ingressions controlled by tectonic loading have also been documented in the Upper Cretaceous Western Canada foreland system (Catuneanu et al., 1999). Shallow marine incursions provoked by Andean tectonic loading have already been documented in the Amazonian foreland basin system (Roddaz et al., 2010) and in the Bolivian retro-arc foreland system (Hernandez et al., 2005). Based on the relatively little thickness of the marine deposits documented in the Madre de Dios basin (40 to 50 m thick outcropping section), we propose that Paleocene marine strata probably correspond to a single high-frequency cycle as defined by Catuneanu (2004). Based on the fact that these higher-frequency cycles are mainly controlled by tectonism in the adjacent belt (Catuneanu, 2004), and based on the relatively low sea-level stage during Paleocene period, we suggest that the marine incursion documented in southern Peru was mainly caused by Andean tectonic loading although additional mantle driven subsidence cannot be excluded.

The entrance of this Paleocene marine ingression (Atlantic Ocean, Pacific Ocean or Caribbean Sea) remains to be elucidated. Very few Paleocene marine or coastal deposits are documented in the Andean/Amazonian foreland basins. Paleocene formations of Ecuador and elsewhere in Peru show no evidences of marine or coastal deposits (Fig. 2). In the Bolivian Altiplano and the Eastern Cordillera there is no evidence of any marine influence attested so far except during Danian times in Potosi, Bolivia (El Molino Formation; e.g. Cappetta and Gayet, 2013). Hence the Paleocene paleogeogaphical map proposed here is tentative (Fig. 15-A). In conjunction with the absence of shallow marine deposits in North-western South America, our data might suggest a southern connection with the Atlantic Ocean (Bolivia-Argentina). In any case, more detailed sedimentological works are needed to decipher the

locus of this Paleocene marine entrance. The Paleocene marine transgression documented here predates a well-known Eocene transgression occurring in the Colombian, Ecuadorian and northern Peruvian Amazonian foreland basins and recorded by the Lower Carbonera, Orteguaza and Pozo Formations (Christophoul et al., 2002; Hermoza et al., 2005b; Roddaz et al., 2010). According to these authors, this Eocene marine incursion would come from both the Guyaquil Gulf and the Caribbean Sea (Fig. 15-B). Data from Colombia suggest that a late Eocene transgression flooded south-western Colombia, coming from the south through the Ecuadorian coast (Osorio et al., 2002; Santos et al., 2008). The presence of marine deposits in the Eastern Cordillera and the Central-Eastern Llanos Foothills is more difficult to explain and authors propose a possible corridor through the proto-Lower Magdalena Valley that connected the Caribbean Sea and the Central Llanos Foothills (Santos et al., 2008). In Ecuador and northern Peru, the Eocene shallow marine transgression is recorded by the deposits of Orteguaza and Pozo formation (Fig. 2) as the result of the Western Cordillera loading (Roddaz et al., 2010). The southern limit of this marine incursion is not well-constrained but no Eocene deposits have been recognized in the southern Peruvian and Bolivian Amazonian basin (Fig. 2).

The nature of the Andean source (Eastern or Western Cordillera) for the sediments deposited within the Paleocene estuary also remains unclear. Thermochronological evidences suggest that the first exhumation and/or deformation pulse in the eastern part of the Altiplano or in the Eastern Cordillera of Central Andes occurred in the late Eocene (Kontak et al., 1990; Barnes et al., 2006). Jaillard et al. (1993b) interpreted the absence of strata close to the K-Pg boundary in the Cusco basins as the consequence of an uplift of a proto-eastern cordillera occurring as early as the early to late Paleocene. However, provenance data suggest that the Paleocene estuarine sediments studied here are characterized by a contribution from a volcanic arc source. According to Mamani et al. (2010), the only active volcanic arc during

673 the Paleocene was the Toquepala volcanic arc (91-45 Ma) located in the present-day
674 Coastal/Western Cordillera. This suggests the absence of any significant proto-eastern
675 cordillera relief capable of acting as a barrier to sediments originating from the Western
676 Cordillera Arc. In conclusion, our data suggest that the Paleocene marine incursion could be
677 related to proto western Cordillera loading. This orogenic loading can be related to a drastic
678 change in convergence direction of the subduction from NE to ENE (Soler and Bonhomme,
679 1990) that might have provoked the major late Paleocene tectonic event formerly called Incaic
680 1 tectonic event (Noble et al., 1990; Sempere et al., 1997).

681 According to the data presented in this study and to literature review, at least two
682 marine incursions occurred in the Amazonian foreland basin in early Paleogene times
683 (Paleocene and Eocene, respectively). Both shallow marine incursions are mainly induced by
684 Andean tectonic loading but they did not affect similar areas in the Amazonian foreland
685 basins. Many studies (see Hoorn et al., 2010) have emphasized the role played by the
686 Miocene long-lived Pebas megawetland system in preventing in situ speciation and floristic
687 and plants dispersal between the Andes and Amazonia for at least 6 Ma (Antonelli et al.,
688 2009) and favoring evolutionary transition from marine to freshwater habitats of Neotropical
689 fishes (Lundberg et al., 1998; Lovejoy et al., 2006; 2009). Recurrent Paleogene marine
690 incursions in the Amazonian foreland basin associated with Andean uplift could have
691 provoked biogeographical isolation and promoted allopatric speciation for terrestrial
692 organisms.

## 7. Conclusions

Based on a multidisciplinary approach, this paper documents for the first time the presence of a tide-dominated shallow marine paleoenvironment during the Paleocene interval (Danian or Thanetian) in the Amazonian basin. In details, based on sedimentary facies analysis, organic geochemistry and fossil assemblages, three facies associations related to a tide-dominated estuary debouching into a shallow-marine bay or lagoon have been defined. Facies association A corresponds to the sedimentary filling of a tide-influenced meandering channel formed in the fluvial-tidal transition zone. Facies association B is related to more distal tidal-flats, little channelized tidal inlets and saltmarshes deposits. Facies association C corresponds to a stressed shallow marine environment such as a bay or a lagoon.

The presence of these transgressive estuarine deposits overlying older continental facies is best explained by flexural tectonic subsidence in response to Andean tectonic loading. This is in agreement with the Nd-Sr isotopic provenance data that show an Andean provenance and hence the presence of an Andean relief during Danian or Thanetian times. The volcanic contribution recorded in the Nd-Sr isotopic compositions can be related to the Toquepala volcanic arc (91 to 45 Ma) located in the present-day Coastal/Western Cordillera. This suggests the absence of any significant proto-Eastern Cordillera relief that would have stopped the drainage and the sedimentary influxes from this Western Andean volcanic relief towards the Amazonian basin during Danian or Thanetian times. Consequently the data suggest that the Danian or Thanetian marine incursion can be related to the subsidence created in response to the proto-Western Cordillera loading. We suggest this Paleocene transgression may come from the south and may be related to the Parana Sea. Finally, similar to Miocene marine incursions affecting the Pebas megawetland, Paleogene marine incursions in the Amazonian foreland basin associated with Andean uplift may have played a role in the

717 dynamics of Neotropical paleobiodiversity in favoring biogeographical isolation and
718 promoting allopatric speciation for terrestrial organisms.

## 8. Acknowledgements

We thank Denise Dorhout for analytical support at NIOZ. We are much indebted to Frank P. Wesselingh for mollusk taxonomic identification. The research leading to these results has received funding from the IRD (Institut de Recherche pour le Développement), the Institut Carnot (France) and the European Research Council under the European Union's Seventh Framework Program (FP7/2007-2013) / ERC grant agreement n° [226600].

**Fig. 1**: A/ White stars display Amazonian foreland basins location (northern Andes and part of Central Andes). B) Simplified geological and structural map of the study area. Red squares display the location of the outcrops used for this study. PCC= Pongo de Coñeq Canyon. C) Zoom of Pantiacolla Anticline area, and location of the outcrops.

**Fig. 2**: Stratigraphic correlation chart for Paleogene strata between Amazonian foreland basins from Colombia to northern Bolivia. Shallow marine deposits are coloured in blue. Important biostratigraphical or geochronological references are displayed by white squares. EC= Eastern Cordillera.

**Fig. 3**: Stratigraphical range of biostratigraphical markers in Paleocene localities from the Upper Madre de Dios SAZ, Southeastern Peru. T/R = Transgressive/ Regressive cycles, according to Vandenberghe et al. (2012). Based on data from Gradstein et al. (1988), Musacchio (1990); Gayet et al. (1993); Jaillard (1993a); Sigé et al. (2004); Gelfo et al. (2009); Gelfo and Sigé (2011); Morsi et al. (2011); Cappetta (2012); Gonella et al. (2012); Cappetta and Gayet (2013); Woodburne et al. (2014)

**Fig. 4**: Isolated teeth of marine-brackish fishes recovered from Paleocene MD-184 (A-F) and MD-85 (G-J) localities of the Upper Madre de Dios Sub-Andean Zone, Southeastern Peru. A-B: Pristidae gen. and sp. indet. (MD-184) oral tooth, A. lingual view, B. intermediate view. C-D: *Ouledia* sp (MD-184) oral tooth, C. lingual view, D. lateral view. E-F: Pycnodontidae indet. (MD-184) palatine tooth, E. occlusal view, F. lateral view, G-H: *Potobatis* sp. (MD-85) fragmentary oral tooth, G. occlusal view, H. lingual view of crown (root lacking). I-J: *Ouledia* sp. (MD-85) worn oral tooth, I. lingual view, J. lateral view. Scale bar = 0.5mm.

**Fig. 5**: Outcrop MD-255. A) General outcrop view along the river cutbank. B) Zoom from A. Interpreted photograph of two stacked channels. C/Sedimentary section with Facies code (see Table 2 for details).

**Fig. 6**: Facies Photographs for Facies Association A (FA-A). A) Facies A1, showing fine-grained sandtstone with tangential cross-bedding and sets prograding in the same direction. Note that bidirectionality has been observed in this facies. B) Photograph of the rippled-surface of Facies A1. Square indicates the location of photograph C. C) Ichnofabrics from Facies A1 top surface: *Arenicolites* and possible Dactiloides (tubular trace). D) Facies A3. Tangential cross-bedding with planar laminations at their base. Rare asymmetrical ripples in the opposite direction can also be observed at the top of the tangential laminations, suggesting bidirectionality. Regular changes in thickness suggest cyclycity, possibly Neap and Spring cycles. E) Photograph of climbing-rippled cross-stratification of Facies A2, from the zoom section displayed on F). F) View of the heterolithic and cyclic deposits of Facies A2. Black squares indicate the location of photographs E) and G). G) Photograph of Facies A2, with massive fine-grained sandstones or flaser bedding alternating with wavy- or planar muddy lamination.

**Fig. 7:** Sedimentary section from outcrop MD-256.

**Fig. 8**: Facies photographs of Facies Association B (FA-B). A) Fine-grained sandstone with climbing ripples. B) Root traces and gypsum or anhydrite nodules developing at the top of the reddish mudstones of Facies B2. C) Facies B4. Highly burrowed heterolithic deposits showing regular alternations of very fine to fine-grained sandstones with muddy or silty layers displaying planar horizontal and wavy bedding. D) Horizontal and vertical burrows in Facies B4. E) Fluid-escape structure within deposits of Facies B4. F) Facies B5 with rippled-surface.

**Fig. 9**: Outcrop MD-85 near Pantiacolla antincline. A) General view of the outcrop. Black rectangle precise the location of photograph B. B) Enlarged view from A with the location of

772 the sedimentary section 1 described. C) Sedimentary section 2 and Facies code. Note that 100
773 m separates the two sedimentary sections.

774 **Fig. 10**: Sedimentary sections from outcrop MD-177 (Sedimentary section 1) and MD-184
775 (Sedimentary section 2).

776 **Fig. 11**: Photographs from outcrop MD-184. A) Outcrop view of alternating Facies C1 and
777 C2. Note undulated marls/carbonated layers. B) Benthic foraminifer *Bathysiphon* sp. found in
778 facies C1. C) Outcrop view of carbonated layers from Facies C4. D) Dessication cracks at the
779 top of a carbonated layer in Facies C5. Note little-sized oyster visible on that surface.

780 **Fig. 12**: Thin sections photographs from Facies C4, C5 and C6, sampled at MD-184. The
781 number of each thin-section is indicated by "TS-n°". They are located on the sedimentary
782 section 2 of Fig. 10. A), B), C) and D) correspond to thin-sections of alternated marls ans
783 limestones strata from Facies C4. E) and F) correspond to the stromatolithic Limestones of
784 Facies C5. G), H), I) and J) correspond to the Oyster limestones of Facies C6. Fi=Fish
785 vertebra, Mi= Micritic pellets, Dru= Drusic cement, Ga= Gasteropod, Ph= Phylopod, Oy=
786 Oyster, An= Annelid, Str= Stromatolith filaments.

787 **Fig. 13**: 87Sr/86Sr versus εNd(0) diagram. Yellow triangles correspond to the Paleocene
788 samples analyzed in this study. Note that they all plot within the melange hyperbole,
789 indicating an Andean provenance. See text for details.

790 **Fig. 14**: Interpretative diagram for Paleocene Times. Andean relief is active yet and produces
791 sedimentary supply for the fluvial and then estuary system debouching in a shallow interior
792 sea. Black rectangles correspond to the interpretative depositional contexts location of each
793 outcrop: MD-255 corresponds to the fluvio-estuarine meandering transition zone in the
794 proximal estuarine system; MD-256 corresponds to the inner (?) part of the estuary; MD-85
795 corresponds to the outer part of the estuary system and MD-184/177 corresponds to the most

distal environment, also located around the outer part of the estuary system but more connected to a bay or calm confined shallow marine basin.

**Fig. 15**: Paleogeographical reconstructions for Paleogene times. A) Paleogeographic reconstruction of Paleocene Times. The shallow marine sea described in this paper in the Amazonian foreland basin does not present clear connection with existing oceans. B) Paleogeographic reconstruction for Eocene times, related to Pozo shallow marine incursion. See text for details.

**Table 1**: Distribution and relative abundance of fossil content of biostratigraphical interest in Paleocene localities from the Upper Madre de Dios Sub-Andean Zone, Southeastern Peru Ost= Ostracoda; (r)= potentially reworked; (+)= close ally. Relative abundance is denoted by the number of "+" (ranging from + up to +++).

**Table 2**: Descriptions and interpretations of sedimentary facies. FA= Facies Association.

**Table 3**: Organic geochemistry results.

**Table 4**: Nd-Sr isotopic compositions for provenance analysis.

**Supplementary Table A**: Outcrops location.

## References


Adnet, S., Gismondi, R.S., Antoine, P.-O., 2014. Comparisons of dental morphology in river stingrays (Chondrichthyes: Potamotrygonidae) with new fossils from the middle Eocene of Peruvian Amazonia rekindle debate on their evolution. Naturwissenschaften 101, 33-45.

Allen, J.R.L., 1970. A quantitative model of climbing ripples and their cross-laminated deposits. Sedimentology 14, 5-26.

Antoine, P.-O., Marivaux, L., Croft, D.A., Billet, G., Ganerød, M., Jaramillo, C., Martin, T., Orliac, M.J., Tejada, J., Altamirano, A.J., 2012. Middle Eocene rodents from Peruvian Amazonia reveal the pattern and timing of caviomorph origins and biogeography. Proceedings of the Royal Society B: Biological Sciences 279, 1319-1326.

Antoine, P.O., Billet, G., Salas-Gismondi, R., Tejada Lara, J., Baby, P., Brusset, S., Espurt, N., Submitted. A new *Carodnia* Simpson, 1935 (Mammalia, Xenungulata) from the early Eocene of Northwestern Peru and a phylogeny of xenungulates at species level. Journal of Mammalian Evolution.

Antoine, P.O., Roddaz, M., Brichau, S., Tejada-Lara, J., Salas-Gismondi, R., Altamirano, A., Louterbach, M., Lambs, L., Otto, T., Brusset, S., 2013. Middle Miocene vertebrates from the Amazonian Madre de Dios Subandean Zone, Peru. Journal of South American Earth Sciences 42, 91-102.

Antonelli, A., Nylander, J.A.A., Persson, C., Sanmartin, I., 2009. Tracing the impact of the Andean uplift on Neotropical plant evolution. PNAS.

Armstrong, H.A., Brasier, M.D., 2005. Microfossil., in: Hart, M. (Ed.), Geological Magazine, 2nd ed. Blackwell Publishing, Malden, Oxford, Carlton.

Ashley, G.M., Southard, J.B., Boothroyd, J.C., 1982. Deposition of climbing-ripple beds: a flume simulation. Sedimentology 29, 67-79.

Aubry, M.-P., Thiry, M., Dupuis, C., Berggren, W., 2005. The Sparnacian deposits of the Paris Basin: A lithostratigraphic classification. Stratigraphy 2, 65-100.

Barnes, J.B., Ehlers, T.A., McQuarrie, N., O'Sullivan, P.B., Pelletier, J.D., 2006. Eocene to recent variations in erosion across the central Andean fold-thrust belt, northern Bolivia: Implications for plateau evolution. Earth and Planetary Science Letters 248, 118-133.

Barragan, R., Geist, D., Hall, M., Larson, P., Kurz, M., 1998. Subduction controls on the compositions of lavas from the Ecuadorian Andes. Earth and Planetary Science Letters 154, 153-166.

Basu, A.R., Sharma, M., Decelles, P.G., 1990. Nd, Sr-Isotopic provenance and trace-element geochemistry of Amazonian foreland basin fluvial sands, Bolivia and Peru. Implications for ensialic Andean orogeny. Earth and Planetary Science Letters 100, 1-17.

Bejarano, A., 1991. Caracterizacion y Evaluacion de Parametros de Registros de Pozos en la Cuenca del Putumayo.

Campbell, K.E., David, C., Romero-pittman, L., 2006. The Pan-Amazonian Ucayali Peneplain, late Neogene sedimentation in Amazonia, and the birth of the modern Amazon River system. Palaeogeography, Palaeoclimatology, Palaeoecology 239, 166-219.

Cande, S.C., Kent, D.V., 1992. A new geomagnetic polarity time scale for the Late Cretaceous and Cenozoic. Journal of Geophysical Research: Solid Earth 97, 13917-13951.

Cappetta, H., 2012. Chondrichthyes (Mesozoic and Cenozoic Elasmobranchii: teeth), in: Schultze, H.-P. (Ed.), Handbook of Paleoichthyology, Munich (Pfeil).

Cappetta, H., Gayet, M., 2013. A new elasmobranch genus (Myliobatiformes, Dasyatoidea) from the Danian of Potosí (Bolivia). Neues Jahrbuch für Geologie und Paläontologie-Abhandlungen 269, 285-290.

Casero, P., 1997. Multidisplinary Correlative Evidences for Polyphase Geological Evolution of the Foot-Hills of the Cordillera Oriental (Colombia).

Catuneanu, O., 2004. Retroarc foreland systems—evolution through time. Journal of African Earth Sciences 38, 225-242.
Catuneanu, O., Beaumont, C., Waschbusch, P., 1997. Interplay of static loads and subduction dynamics in foreland basins: Reciprocal stratigraphies and the “missing” peripheral bulge. Geology 25, 1087-1090.
Catuneanu, O., Sweet, A.R., Miall, A.D., 1999. Concept and styles of reciprocal stratigraphies: Western Canada foreland system. Terra Nova-Oxford 11, 1-8.
Cooper, M., Addison, F., Alvarez, R., Coral, M., Graham, R.H., Hayward, A., Howe, S., Martinez, J., Naar, J., Peñas, R., 1995. Basin development and tectonic history of the Llanos Basin, Eastern Cordillera, and middle Magdalena Valley, Colombia. AAPG bulletin 79, 1421-1442.
Córdoba, F., Buchelli, F., Moros, J., Calderón, W., Guerrero, C., Kairuz, E., Magoon, L., 1997. Proyecto evaluación regional Cuenca del Putumayo—Definición de los sistemas petrolíferos. ECOPETROL, Bogotá.
Choi, K., 2010. Rhythmic Climbing-Ripple Cross-Lamination in Inclined Heterolithic Stratification (IHS) of a Macrotidal Estuarine Channel, Gomso Bay, West Coast of Korea. Journal of Sedimentary Research 80, 550-561.
Christophoul, F., Baby, P., Dávila, C., 2002. Stratigraphic responses to a major tectonic event in a foreland basin: the Ecuadorian Oriente Basin from Eocene to Oligocene times. Tectonophysics 345, 281-298.
Dalrymple, R.W., 1984. Runoff microdeltas; a potential emergence indicator in cross-bedded sandstones. Journal of Sedimentary Research 54, 825-830.
Dalrymple, R.W., Baker, E.K., Harris, P.T., Hughes, M.G., 2003. Sedimentology and stratigraphy of a tide-dominated, foreland-basin delta (Fly River, Papua New Guinea), in: Sidi, F.H., Nummedal, D., Imbert, P., Darman, H., and Posamentier, H.W. (Ed.), Tropical Deltas of Southeast Asia—Sedimentology, Stratigraphy, and Petroleum Geology. SEPM, Special Publication, pp. 147-173.
Dalrymple, R.W., Choi, K., 2007. Morphologic and facies trends through the fluvial–marine transition in tide-dominated depositional systems: A schematic framework for environmental and sequence-stratigraphic interpretation. Earth-Science Reviews 81, 135-174.
Dalrymple, R.W., Zaitlin, B.A., Boyd, R., 1992. Estuarine facies models: conceptual basis and stratigraphic implications. Journal of Sedimentary Research 62, 1130-1146.
de Mowbray, T., Visser, M.J., 1984. Reactivation surfaces in subtidal channel deposits, Oosterschelde, Southwest Netherlands. Journal of Sedimentary Research 54, 811-824.
DeCelles, P.G., Horton, B.K., 2003. Early to middle Tertiary foreland basin development and the history of Andean crustal shortening in Bolivia. Geological Society of America Bulletin 115, 58-77.
Dunham, R.J., 1962. Classification of carbonate rocks according to depositional texture, in: W. E. Ham, e. (Ed.), Classifications of carbonate rocks - a symposium, pp. 108–121.
Enay, R., 1990. Paléontologie des invertébrés, Paris.
Eriksson, K.A., Simpson, E.L., 2004. Precambrian tidalites: recognition and significance., in: Eriksson, P.G., Altermann,W., Nelson, D., Mueller, W., Cateneau, O., Strand, K. (Ed.), Tempos and Events in Precambrian Time. Developments in Precambrian Geology. Elsevier, Amsterdam, pp. 631– 642.
Eriksson, P.G., Condie, K.C., Tirsgaard, H., Mueller, W.U., Altermann, W., Miall, A.D., Aspler, L.B., Catuneanu, O., Chiarenzelli, J.R., 1998. Precambrian clastic sedimentation systems. Sedimentary Geology 120, 5-53.
Faucher, B., Savoyat, E., 1973. Esquisse géologique des Andes de l'Equateur. Revue de géographie physique et de géologie dynamique 15, 115-142.

Gayet, M., Sempre, T., Cappetta, H., Jaillard, E., Lévy, A., 1993. La présence de fossiles marins dans le Crétacé terminal des Andes centrales et ses conséquences paléogéographiques. Palaeogeography, Palaeoclimatology, Palaeoecology 102, 283-319.
Gelfo, J.N., Goin, F.J., Woodburne, M.O., Muizon, C.D., 2009. Biochronological relationships of the earliest South American Paleogene mammalian faunas. Paleontology 52, 251-269.
Gelfo, J.N., Sigé, B., 2011. A new didolodontid mammal from the late Paleocene-earliest Eocene of Laguna Umayo, Peru. Acta Palaeontologica Polonica 56, 665-678.
Gérard, J.R.F., Bromley, R.G., 2008. Ichnofabrics in Clastic sediments: Application to sedimentological and core studies. A practical guide by Jean R.F. Gérard and Richard G. Bromley. Jean R.F. Gérard, Madrid.
Gil, W.F., 2001. Evolution latérale de la déformation d'un front orogénique: exemples des bassins subandins entre 0° et 16°S. University Paul Sabatier, Toulouse.
Gonella, C.A.C., Griffin, M., Cione, A., Cavalli, S.G., Aceñolaza, F.G., 2012. Paleontología de la Formación Yacoraite (Maastrichtiano-Daniano) en el ámbito de la Subcuenca de Tres Cruces, Cordillera Oriental de la provincia de Jujuy, Argentina.
Gradstein, F., Kaminski, M., Berggren, W., 1988. Cenozoic foraminiferal biostratigraphy of the Central North Sea. Abh. Geol. Bundesanstalt 41, 97-108.
Gutierrez, M., 1982. Evaluacion potencial petrolifero cuencas Huallaga, Ucayali y Madre de Dios. Zonacion bioestratigrafica del intervalo Cretacico superior-Tertiario inferior. Petroperu, Internal Report, Lima, p. 29.
Haq, B.U., Hardenbol, J., Vail, P.R., 1987. Chronology of fluctuating sea levels since the Triassic. Science 235, 1156–1167.
Hardenbol, J., Thierry, J., Farley, M.B., Jacquin, T., De Graciansky, P.C., VailP.R., 1998. Mesozoic–Cenozoic sequence chronostratigraphy of european basins. 60SEPM Special Publication, Tulsa, 1–786.
Hermoza, W., 2004. Dynamique tectono-sedimentaire et restauration sequentielle du retro-bassin d'avant-pays des Andes Centrales. Univeristé Paul Sabatier, Toulouse, p. 196.
Hermoza, W., Brusset, S., Baby, P., Gil, W., Roddaz, M., Guerrero, N., Bolaños, R., 2005b. The Huallaga foreland basin evolution: Thrust propagation in a deltaic environment, northern Peruvian Andes. Journal of South American Earth Sciences 19, 21-34.
Hernandez, R.M., Jordan, T.E., Farjat, A.D., Echavarria, L., Idleman, B.D., Reynolds, J.H., 2005. Age, distribution, tectonics, and eustatic controls of the Paranense and Caribbean marine transgressions in southern Bolivia and Argentina. Journal of South American Earth Sciences 19, 495-512.
Hoorn, C., Wesselingh, F.P., ter Steege, H., Bermudez, M.a., Mora, a., Sevink, J., Sanmartín, I., Sanchez-Meseguer, a., Anderson, C.L., Figueiredo, J.P., Jaramillo, C., Riff, D., Negri, F.R., Hooghiemstra, H., Lundberg, J., Stadler, T., Särkinen, T., Antonelli, A., 2010. Amazonia through time: Andean uplift, climate change, landscape evolution, and biodiversity. Science (New York, N.Y.) 330, 927-931.
Hovikoski, J., Gingras, M., Räsänen, M., Rebata, L.A., Guerrero, J., Ranzi, A., Melo, J., Romero, L., del Prado, H.N., Jaimes, F., 2007. The nature of Miocene Amazonian epicontinental embayment: High-frequency shifts of the low-gradient coastline. Geological Society of America Bulletin 119, 1506-1520.
Hovikoski, J., Räsänen, M., Gingras, M., Ranzi, A., Melo, J., 2008. Tidal and seasonal controls in the formation of Late Miocene inclined heterolithic stratification deposits, western Amazonian foreland basin. Sedimentology 55, 499-530.
Jackson, R.G., 1981. Sedimentology of muddy fine-grained channel deposits in meandering streams of the American Middle West. Journal of Sedimentary Research 51, 1169-1192.
Jacobsen, S.B., Wasserburg, G.J., 1980. Sm-Nd isotopic evolution of chondrites. Earth and Planetary Science Letters 50, 139-155.

Jaillard, E., 1993a. The Senonian to Palaeocene tectonic evolution of the Peruvian margin and its relationships with geodynamics. Bulletin de la Société Géologique de France 164, 819-830.
Jaillard, E., 1996. Cretaceous to early Paleogene tectonic evolution of the northern Central Andes (0–18°S) and its relations to geodynamics. Tectonophysics 259, 41-53.
Jaillard, E., Carlotto, V., Cardenas, J., Chavez, R., Gil, W., 1993b. La "Nappe des Couches Rouges" de Cuzco (Sud du Pérou): mise en évidence stratigraphique, interprétations tectoniques et paléogéographiques. C. R. Acad. Sci. Paris 36, 379-386.
Jaramillo, C.A., Dilcher, D.L., 2000. Microfloral diversity patterns of the late Paleocene–Eocene interval in Colombia, northern South America. Geology 28, 815-818.
Jaramillo, C.A., Dilcher, D.L., 2001. Middle Paleogene palynology of Central Colombia, South America: A study of pollen and spores from tropical latitudes. Palaeontographica Abteilung B 258, 87-213.
Jeffery, M.L., Poulsen, C.J., Ehlers, T.A., 2012. Impacts of Cenozoic global cooling, surface uplift, and an inland seaway on South American paleoclimate and precipitation δ18O. Geological Society of America Bulletin 124, 335-351.
Jopling, A.V., Walker, R.G., 1968. Morphology and origin of ripple-drift cross-lamination, with examples from the Pleistocene of Massachusetts. Journal of Sedimentary Research 38, 971-984.
Kay, S.M., Coira, B., Viramonte, J., 1994. Young mafic back arc volcainc-rocks s indicators of continental lithospheric delamination beneath the Argentine Puna plateau, Central Andes J. Geophys. Res.-Solid Earth 99, 24323-24339.
Klein, G.d., 1970. Depositional and dispersal dynamics of intertidal sand bars. Journal of Sedimentary Research 40, 1095-1127.
Kontak, D.J., Farrar, E., Clark, A.H., Archibald, D.A., 1990. Eocene tectono-thermal rejuvenation of an upper Paleozoic-lower Mesozoic terrane in the Cordillera de Carabaya, Puno, southeastern Peru, revealed by K-Ar and 40Ar/39Ar dating. Journal of South American Earth Sciences 3, 231-246.
Londoño, J., Lorenzo, J.M., Ramirez, V., 2012. Lithospheric flexure and related base-level stratigraphic cycles in continental foreland basins: An example from the Putumayo Basin, Northern Andes, in: Gao., D. (Ed.), Tectonics and sedimentation: Implications for petroleum systems. AAPG Memoir pp. 357-375.
Lovejoy, N.R., Albert, J.S., Crampton, W.G.R., 2006. Miocene marine incursions and marine/freshwater transitions: Evidence from Neotropical fishes. Journal of South American Earth Sciences 21, 5-13.
Lovejoy, N.R., Willis, S.C., Albert, J.S., 2009. Molecular signatures of Neogene biogeographical events in the Amazon fish fauna, Amazonia: Landscape and Species Evolution. Wiley-Blackwell Publishing Ltd., pp. 405-417.
Lundberg, J.G., Marshall, L.G., Guerrero, J., 1998. The Stage of Neotropical Fish Diversification: A History of Tropical South American Rivers, in: Malabarba, L.R., R.E. Reis, R.P. Vari, Z.M. Lucena and C.A.S Lucena (Ed.), Phylogeny and Classification of Neotropical Fishes. Edipucrs, Porto Alegre, p. 603.
Mamani, M., Worner, G., Sempere, T., 2010. Geochemical variations in igneous rocks of the Central Andean orocline (13 degrees S to 18 degrees S): Tracing crustal thickening and magma generation through time and space. Geological Society of America Bulletin 122, 162-182.
Marivaux, L., Salas-Gismondi, R., Tejada, J., Billet, G., Louterbach, M., Vink, J., Bailleul, J., Roddaz, M., Antoine, P.O., 2012. A platyrrhine talus from the early Miocene of Peru (Amazonian Madre de Dios Sub-Andean Zone). J. Hum. Evol. 63, 696-703.

Marocco, R., Baudino, R., A., L., 1995. The intermontane Neogene continental basins of the Central Andes of Ecuador and Peru: Sedimentologic, tectonic and geodynamic implications, in: A.J. Tankard, R.S., H.J. Welsink (Ed.), Petroleum Basins of South America. Am. Assoc. Pet. Geol. Mem., pp. 597–613.
Marshall, L.G., Sempere, T., Butler, R.F., 1997. Chronostratigraphy of the mammal-bearing Paleocene of South America. Journal of South American Earth Sciences 10, 49-70.
Martin-Gombojav, N., Winkler, W., 2008. Recycling of proterozoic crust in the andean amazon foreland of Ecuador: Implications for orogenic development of the Northern Andes. Terra Nova 20, 22-31.
Mazumder, R., Arima, M., 2005. Tidal rhythmites and their implications. Earth-Science Reviews 69, 79-95.
Meyers, P.A., 1997. Organic geochemical proxies of paleoceanographic, paleolimnologic, and paleoclimatic processes. Organic Geochemistry 27, 213-250.
Miall, A.D., 1996. The geology of fluvial deposits: sedimentary facies, basin analysis and petroleum geology. Springer-Verlag Inc Berlin.
Mitrovica, J., Beaumont, C., Jarvis, G., 1989. Tilting of continental interiors by the dynamical effects of subduction. Tectonics 8, 1079-1094.
Morsi, A.-M.M., Speijer, R.P., Stassen, P., Steurbaut, E., 2011. Shallow marine ostracode turnover in response to environmental change during the Paleocene–Eocene thermal maximum in northwest Tunisia. Journal of African Earth Sciences 59, 243-268.
Mpodozis, C., Allmendinger, R.W., 1993. Extensional tectonics, Cretaceous Andes, northern Chile (27°S). Geological Society of America Bulletin 105, 1462-1477.
Musacchio, E.A., 1990. Non-marine Cretaceous ostracods from Argentina and their palaeobiogeographical relationships, Ostracoda and global events. Springer, pp. 557-569.
Naeser, C.W., Crochet, J., Jaillard, E., Laubacher, G., Mourier, T., Sige, B., 1991. Tertiary fission-track ages from the Bagua syncline (northern Peru): Stratigraphic and tectonic implications. Journal of South American Earth Sciences 4, 61-71.
Nio, S.D., Yang, C.S., 1991. Diagnostic attributes of clastic tidal deposits: a review, in: Smith, D.G., Reinson, G.E., Zeitlin, B.A. and R.A. Rahmani (Ed.), Clastic Tidal Sedimentology. Canadian Society of Petroleum Geologists, pp. 3-28.
Noble, D.C., McKee, E.H., Mourier, T., Mégard, F., 1990. Cenozoic stratigraphy, magmatic activity, compressive deformation, and uplift in Northern Peru. Geological Society of America Bulletin 102, p. 1105-1113.
Osorio, C., Michoux, D., Tellez, G., 2002. Stratigraphy of the Tertiary sequences — Upper Magdalena and the Putumayo basins, a different point of view for hydrocarbon exploration. Memorias de la Segunda Convención técnica de la Asociación Colombiana de Geólogos y Geofísicos del Petróleo, Bogotá, Colombia 10.
Page, K.J., Nanson, G.C., Frazier, P.S., 2003. Floodplain Formation and Sediment Stratigraphy Resulting from Oblique Accretion on the Murrumbidgee River, Australia. Journal of Sedimentary Research 73, 5-14.
Parra, M., Mora, A., Jaramillo, C., Strecker, M.R., Sobel, E.R., Quiroz, L., Rueda, M., Torres, V., 2009. Orogenic wedge advance in the northern Andes: Evidence from the Oligocene-Miocene sedimentary record of the Medina Basin, Eastern Cordillera, Colombia. Geological Society Of America Bulletin.
Peters, K.E., Cassa, M.R., 1994. Applied source rock geochemistry. Memoirs of the american Association of Petroleum Geologists, 93-93.
Pinto, L., 2003. Traçage de l'érosion Cénozoïque des Andes Centrales à l'aide dela minéralogie et de la géochmie des sédiments (Nord du Chili et Nord-Ouest de la Bolivie). Université Paul Sabatier, Toulouse.

Poyato-Ariza, F.J., Wenz, S., 2002. A new insight into pycnodontiform fishes. Geodiversitas 24, 139-248.
Pysklywec, R., Mitrovica, J., 2000. Mantle flow mechanisms of epeirogeny and their possible role in the evolution of the Western Canada Sedimentary Basin. Canadian Journal of Earth Sciences 37, 1535-1548.
Roddaz, M., Christophoul, F., Zambrano, J.D.B., Soula, J.C., Baby, P., 2012. Provenance of late Oligocene to quaternary sediments of the Ecuadorian Amazonian foreland basin as inferred from major and trace element geochemistry and Nd-Sr isotopic composition. Journal of South American Earth Sciences 37, 136-153.
Roddaz, M., Hermoza, W., Mora, A., Baby, P., Parra, M., Christophoul, F., Brusset, S., Espurt, N., 2010. Cenozoic sedimentary evolution of the Amazonian foreland basin system, in: Blackwell (Ed.), Amazonia, Landscape and Species Evolution, pp. 61-88.
Roddaz, M., Viers, J., Brusset, S., Baby, P., Hérail, G., 2005a. Sediment provenances and drainage evolution of the Neogene Amazonian foreland basin. Earth and Planetary Science Letters 239, 57-78.
Rogers, G., Hawkesworth, C.J., 1989. A geochemical traverse across the North Chilean Andes: evidence for crust generation from the mantle wedge. Earth and Planetary Science Letters 91, 271-285.
Ruiz, G.M.H., Seward, D., Winkler, W., 2004. Detrital thermochronology - A new perspective on hinterland tectonics, an example from the Andean Amazon Basin, Ecuador. Basin Research 16, 413-430.
Ruiz, G.M.H., Seward, D., Winkler, W., 2007. Evolution of the Amazon Basin in Ecuador with Special Reference to Hinterland Tectonics: Data from Zircon Fission-Track and Heavy Mineral Analysis pp. 907-934.
Santos, C., Jaramillo, C., Bayona, G., Rueda, M., Torres, V., 2008. Late Eocene marine incursion in north-western South America. Palaeogeography, Palaeoclimatology, Palaeoecology 264, 140-146.
Sempere, T., Butler, R.F., Richards, D.R., Marshall, L.G., Sharp, W., Swisher, C.C., 1997. Stratigraphy and chronology of upper Cretaceous lower Paleogene strata in Bolivia and northwest Argentina. Geological Society of America Bulletin 109, 709-727.
Sigé, B., Sempere, T., Butler, Robert F., Marshall, Larry G., Crochet, J.-Y., 2004. Age and stratigraphic reassessment of the fossil-bearing Laguna Umayo red mudstone unit, SE Peru, from regional stratigraphy, fossil record, and paleomagnetism. Geobios 37, 771-794.
Soler, P., Bonhomme, M.G., 1990. Relation of magmatic activìty to plate dynamics In central Peru from Late Cretaceous to present, in: Kay, S.M., and Rapela, C. W., eds (Ed.), Plutonism from Antarctica to Alaska: Boulder, Colorado. Geological Society of America Special Paper.
Steurbaut, E., Magioncalda, R., Dupuis, C., Van Simaeys, S., Roche, E., Roche, M., 2003. Palynology, paleoenvironments, and organic carbon isotope evolution in lagoonal Paleocene-Eocene boundary settings in North Belgium. Special papers of the Geological Society of America, 291-318.
Tessier, B., 1996. River-Ocean Interaction Zone: a Facies Model with climbing Ripple Bedding, in: Romania, N.I.o.M.G.a.G.-e.o. (Ed.), GEO-ECO-MARINA 2.Workshop on "Fluvial-Marine Interactions", Malnas, Romania.
Tyson, R.V., 1995. Sedimentary organic matter: organic facies and palynofacies. Springer.
Valchev, B., 2007. Representatives of Family Eggerellidae Cushman, 1937 from the Palaeocene of the Coastal Part of East Stara Planina. Review of the Bulgarian Geological Society 68, 36-40.
Vandenberghe, N., Hilgen, F., Speijer, R., 2012. The paleogene period. The geologic time scale 2012, 855-921.

Viers, J., Roddaz, M., Filizola, N., Guyot, J.L., Sondag, F., Brunet, P., Zouiten, C., Boucayrand, C., Martin, F., Boaventura, G.R., 2008. Seasonal and provenance controls on Nd-Sr isotopic compositions of Amazon rivers suspended sediments and implications for Nd and Sr fluxes exported to the Atlantic Ocean. Earth and Planetary Science Letters 274, 511-523.

Wattinne, A., 2004. Évolution d'un environnement carbonate lacustre à bioconstructions, en limagne bourbonnaise (Oligo-Miocène, Massif Central, France), Thèse du Muséum National d'Histoire Naturelle, Paris, p. 195.

Woodburne, M.O., Goin, F.J., Bond, M., Carlini, A.A., Gelfo, J.N., López, G.M., Iglesias, A., Zimicz, A.N., 2014. Paleogene land mammal faunas of South America; a response to global climatic changes and indigenous floral diversity. Journal of Mammalian Evolution 21, 1-73.

**Figure 1**

Click here to download high resolution image

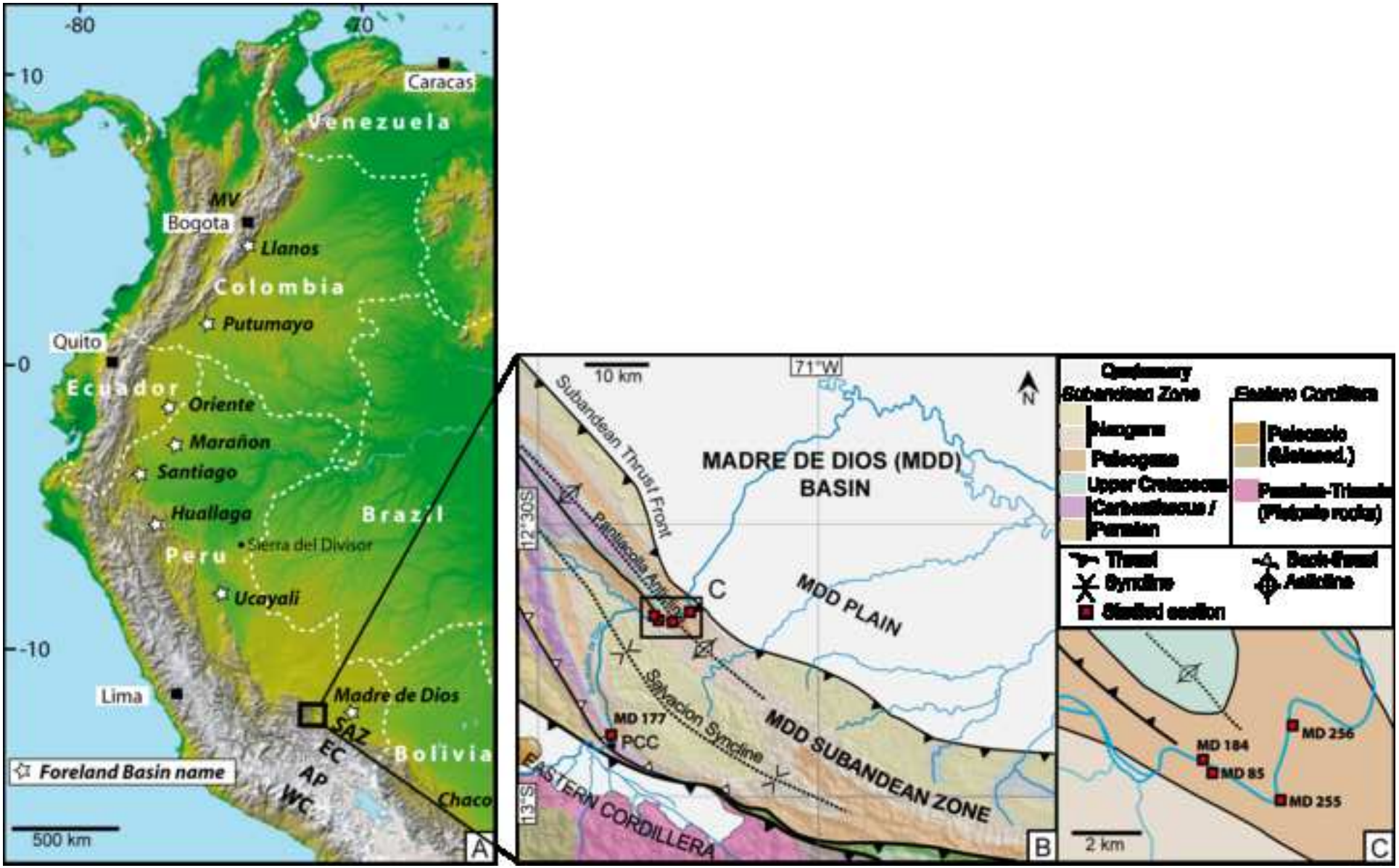

Figure 2

Click here to download high resolution image

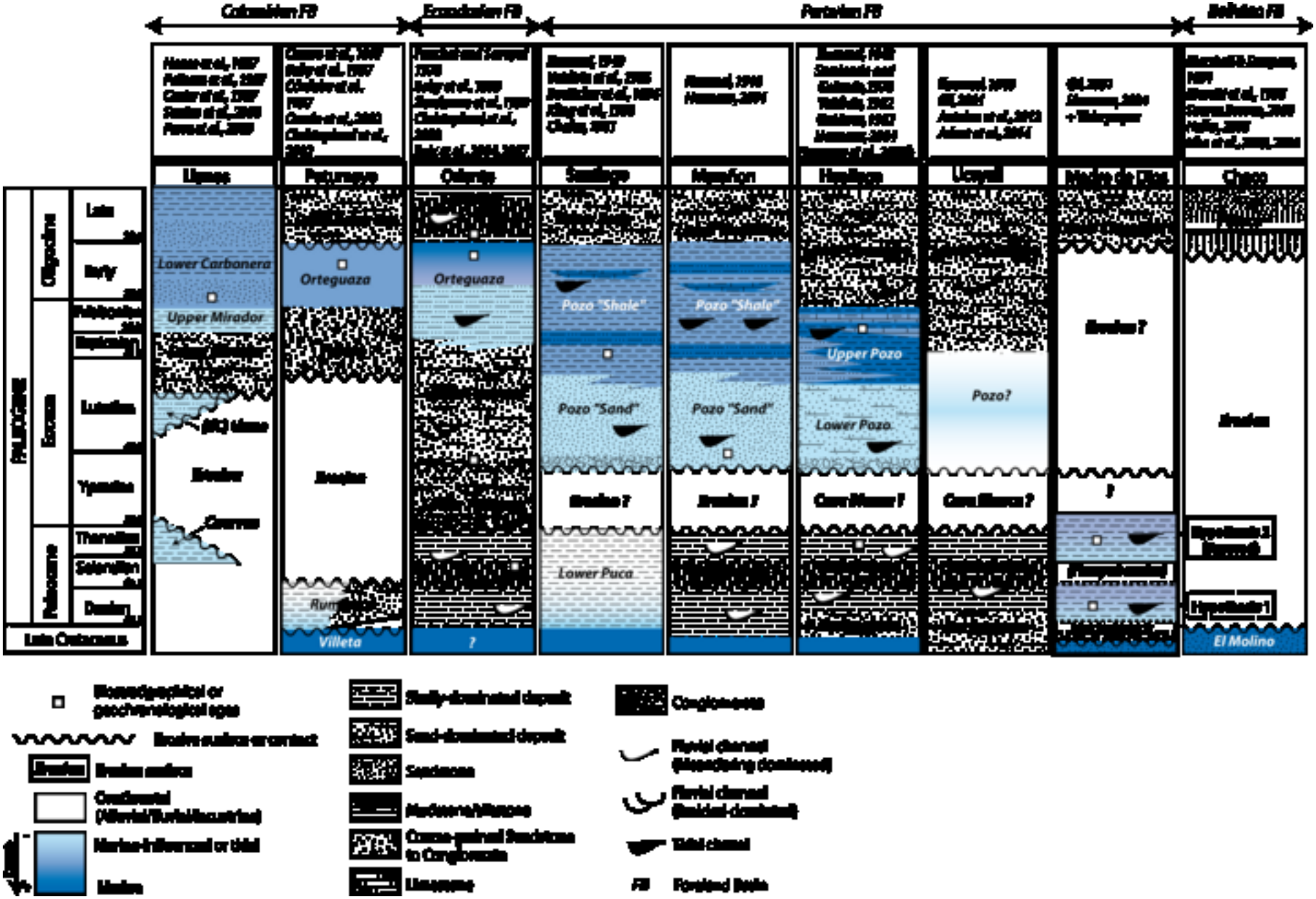

**Figure 3**

Click here to download high resolution image

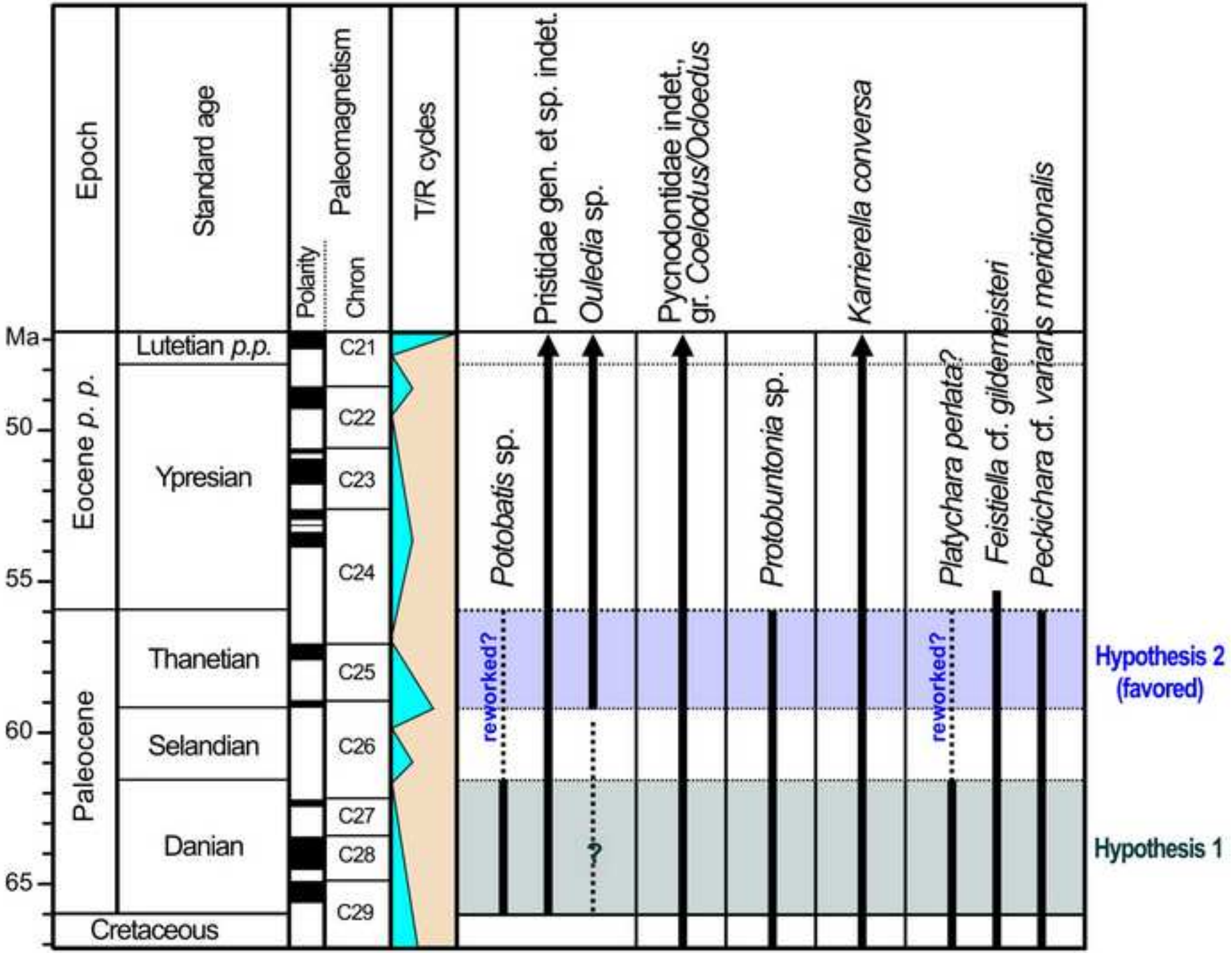

Figure 4

Click here to download high resolution image

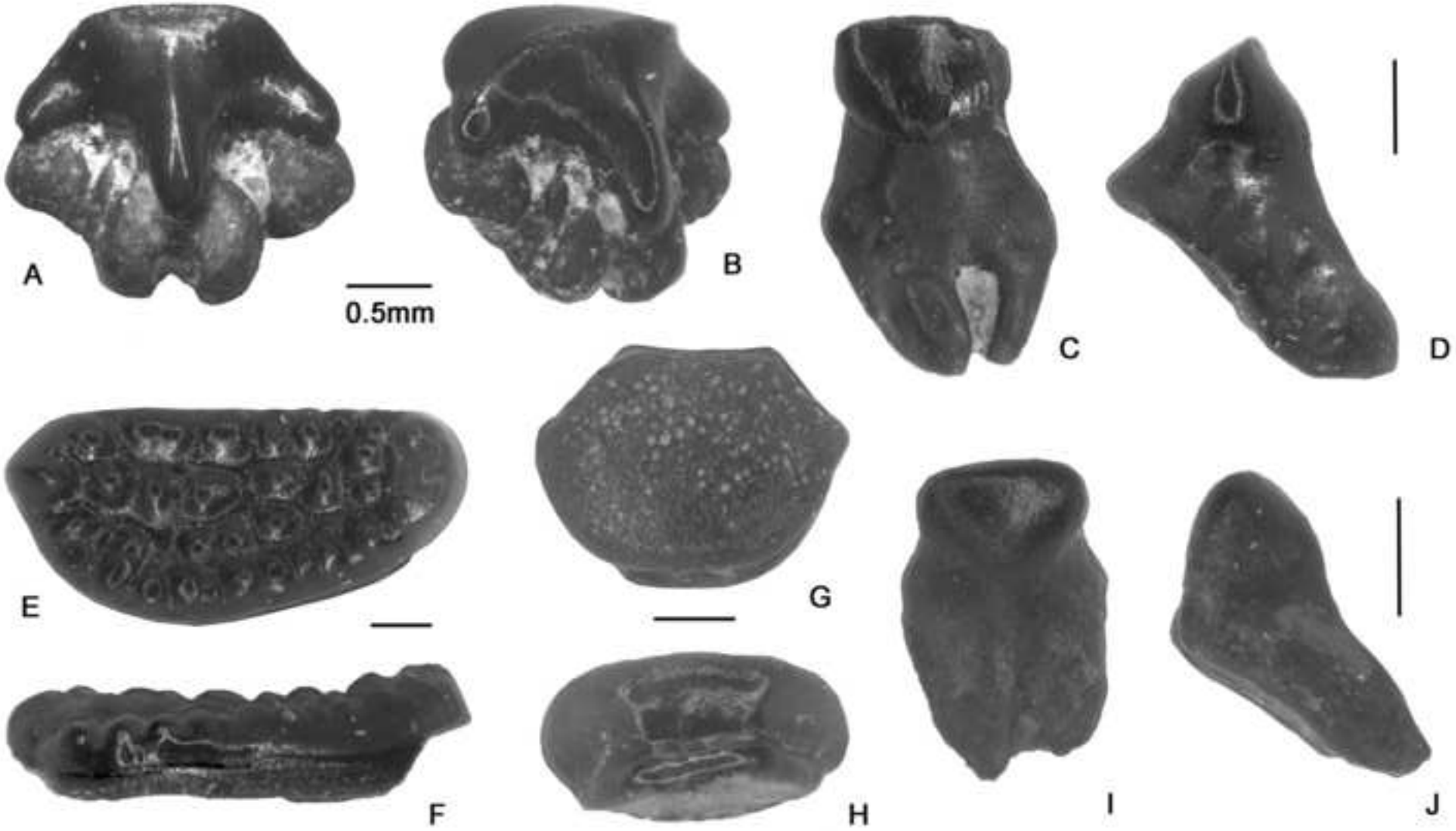

**Figure 5**

Click here to download high resolution image

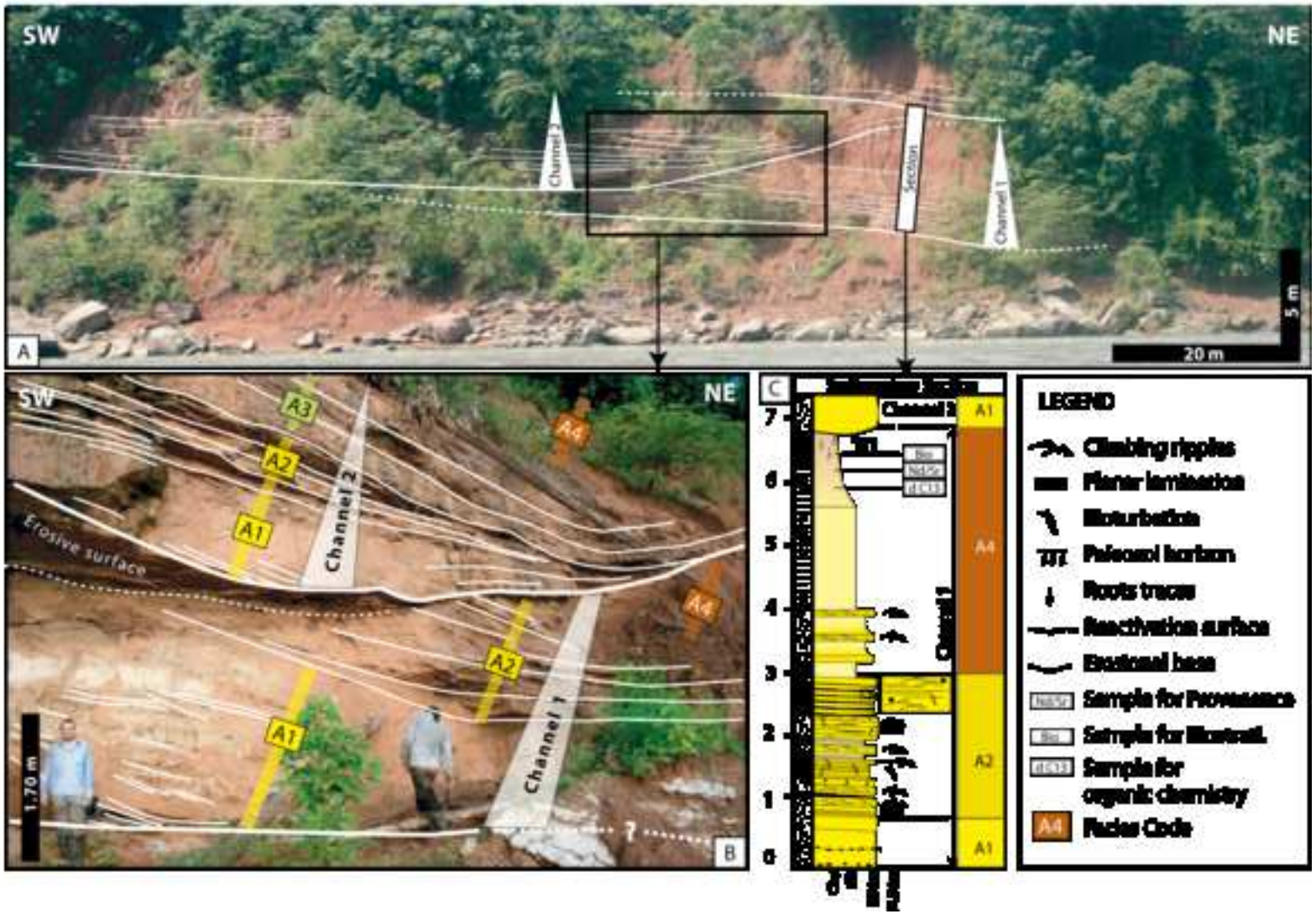

**Figure 6**

Click here to download high resolution image

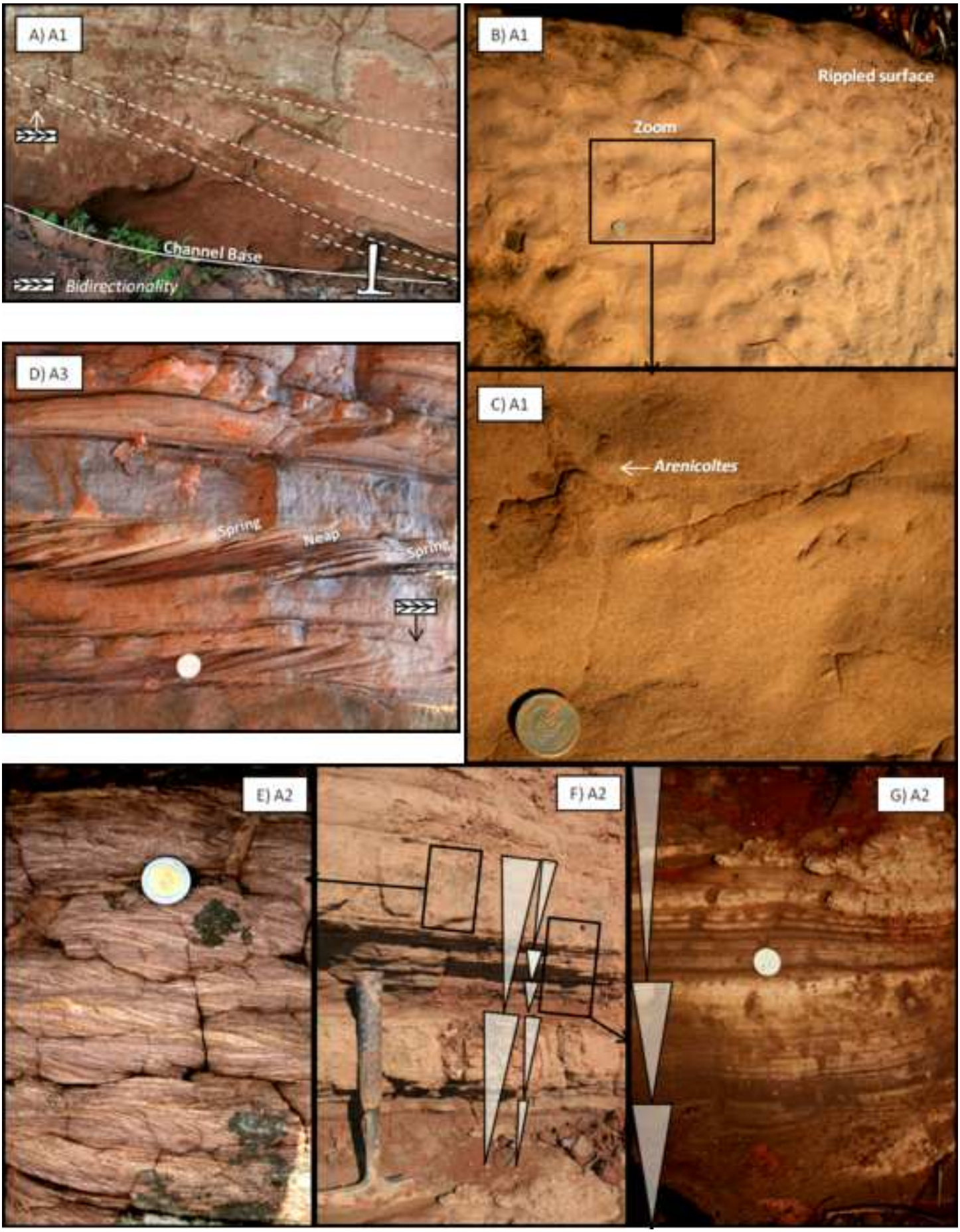

**Figure 7**

Click here to download high resolution image

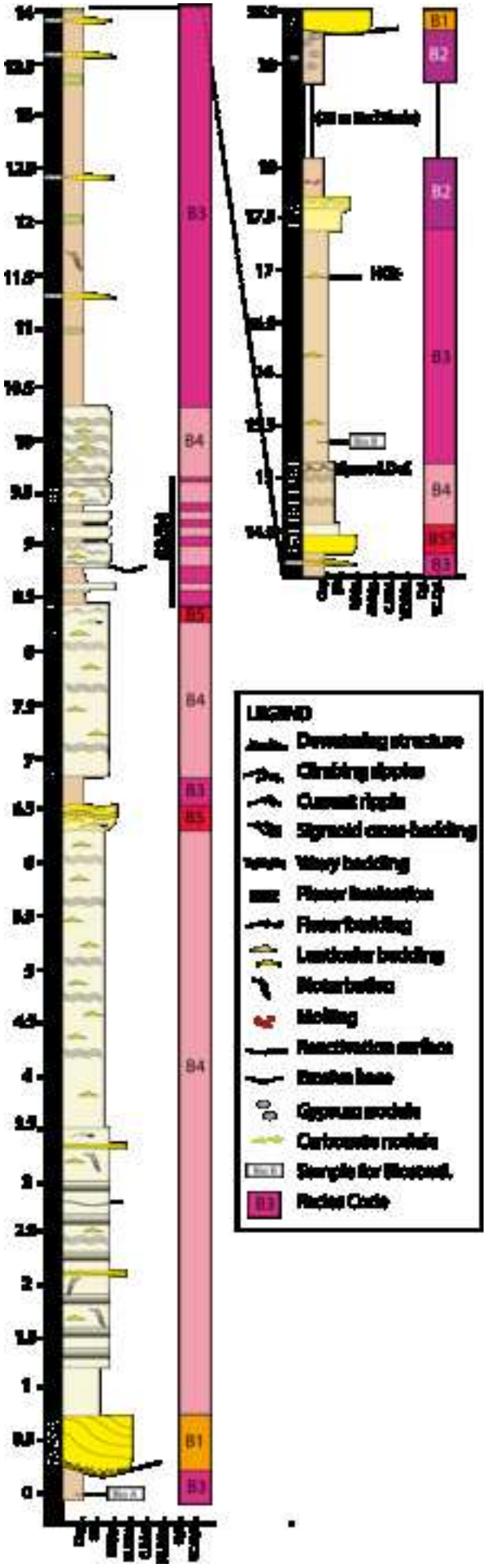

**Figure 8**

Click here to download high resolution image

**Figure 9**

Click here to download high resolution image

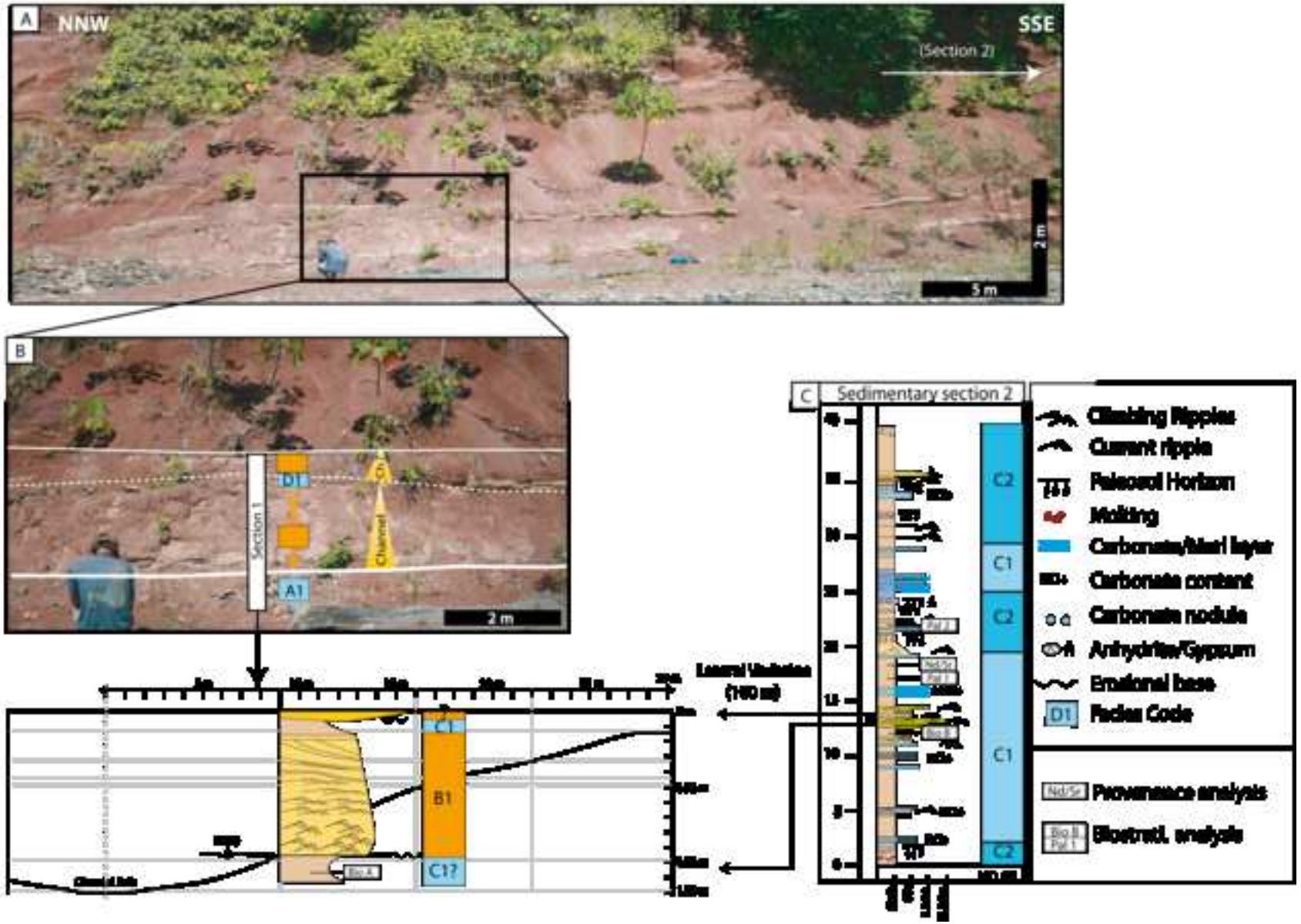

**Figure 10**

Click here to download high resolution image

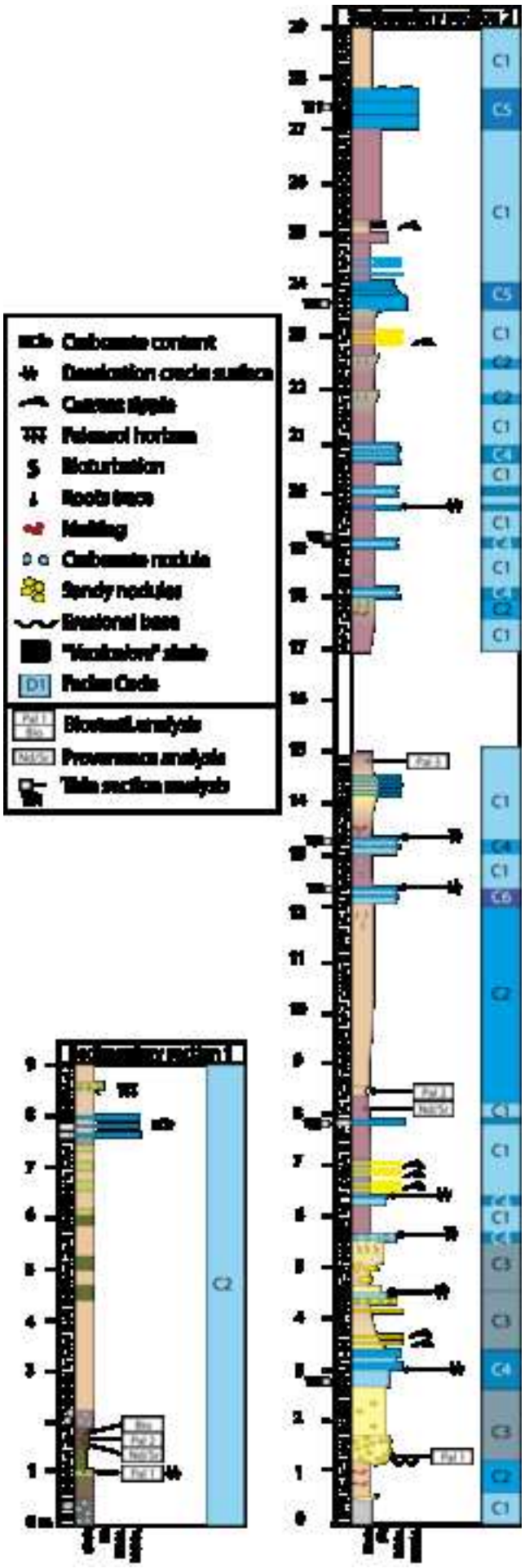

**Figure 11**
**Click here to download high resolution image**

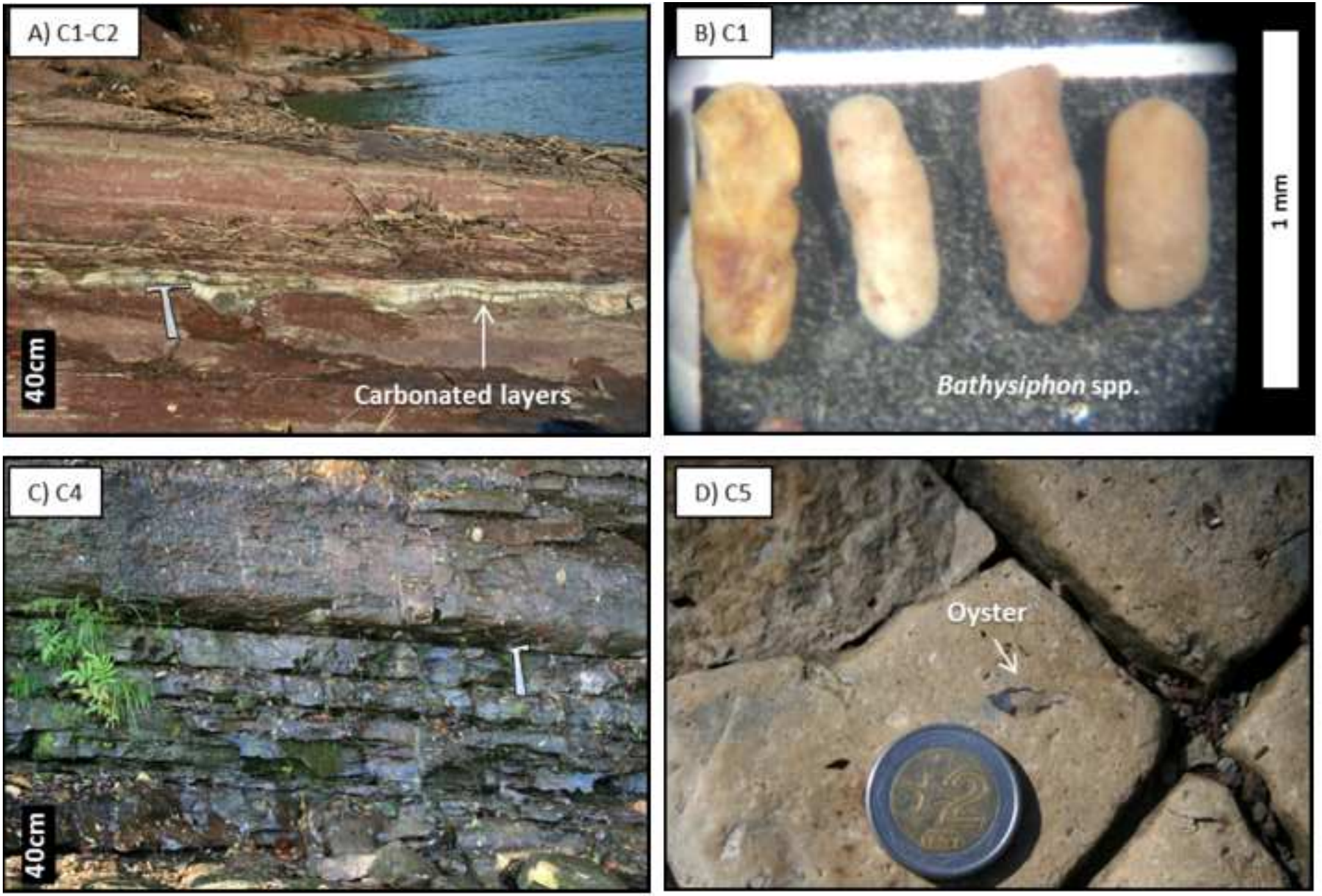

**Figure 12**

Click here to download high resolution image

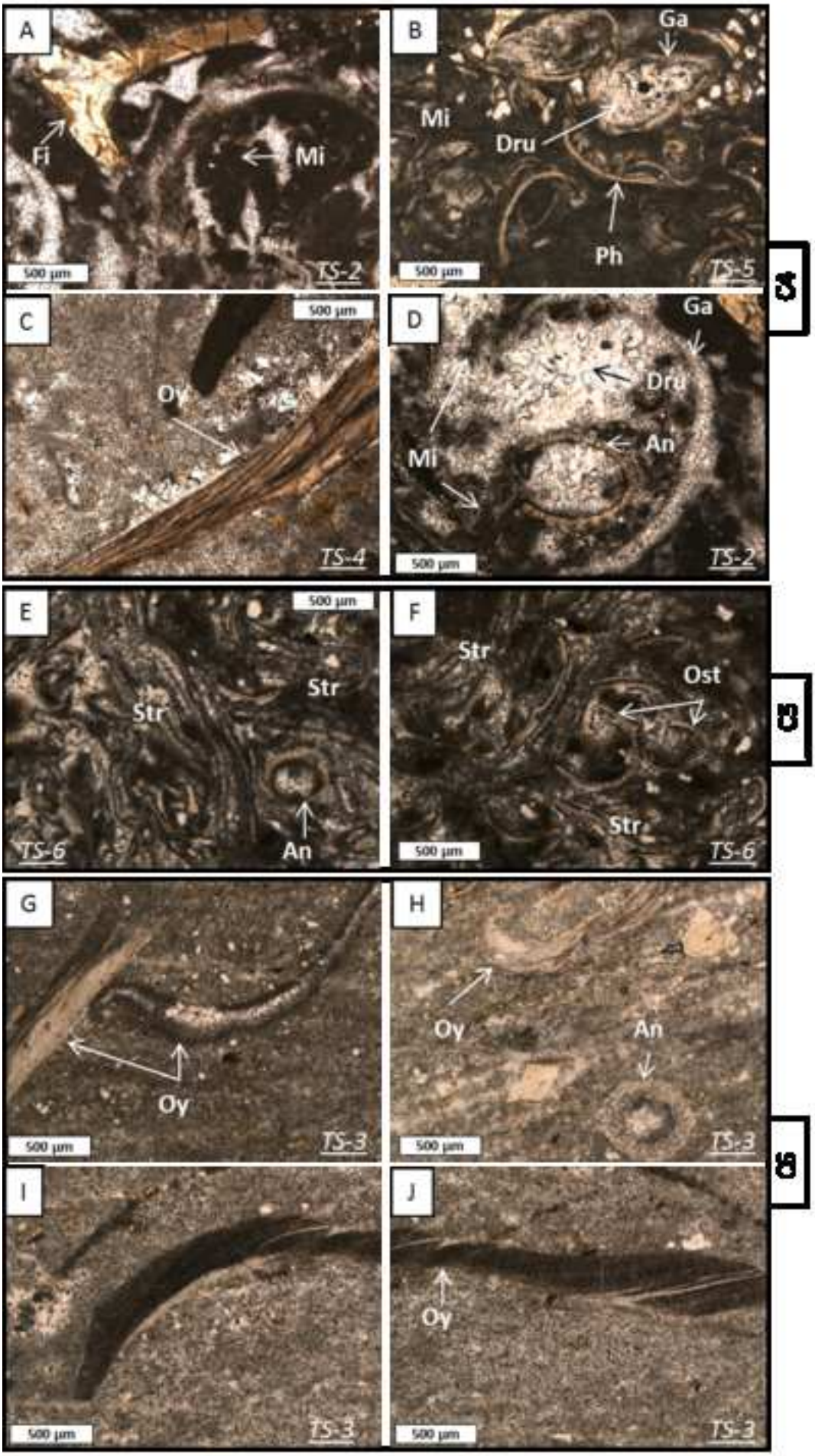

Figure 13

Click here to download high resolution image

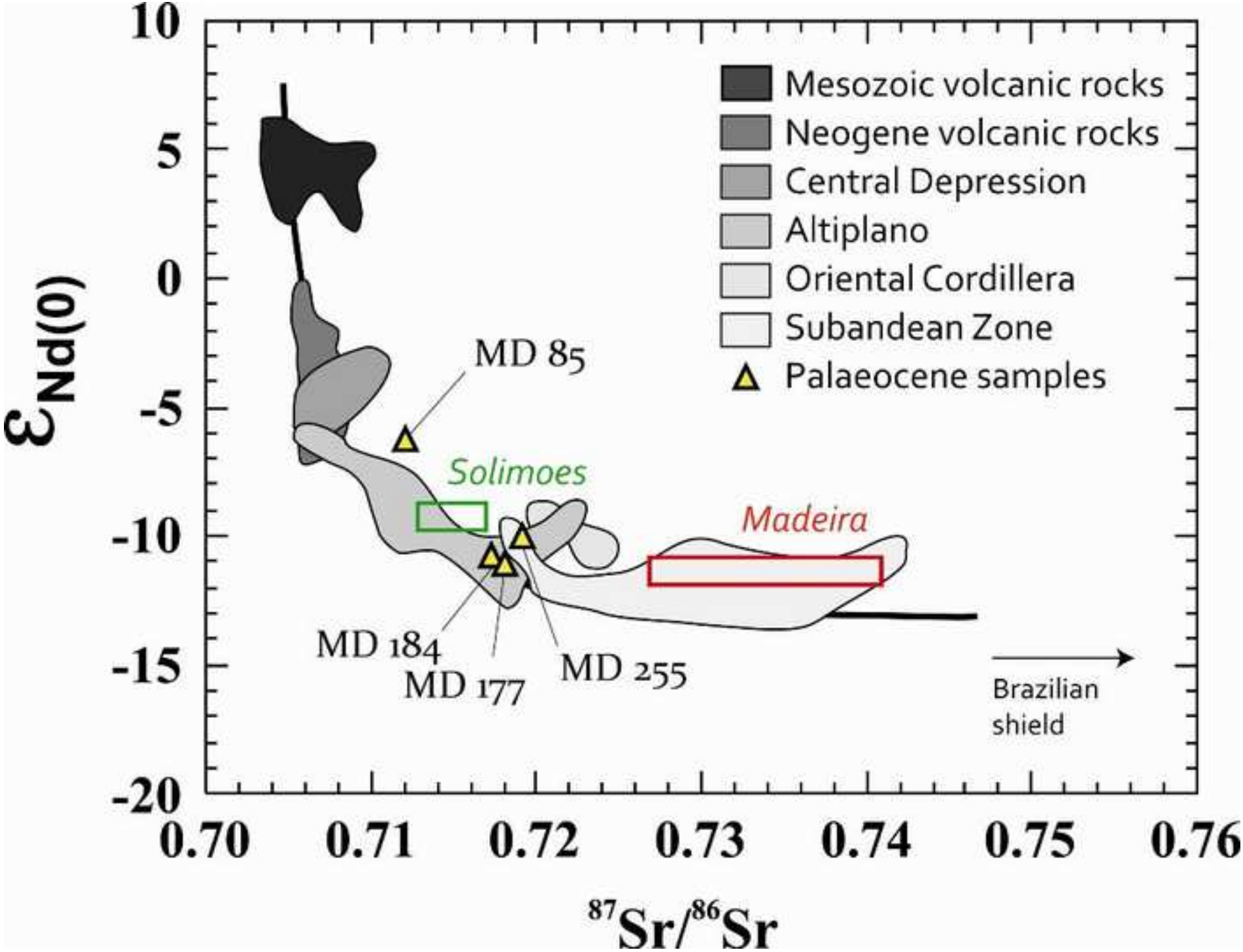

Figure 14

Click here to download high resolution image

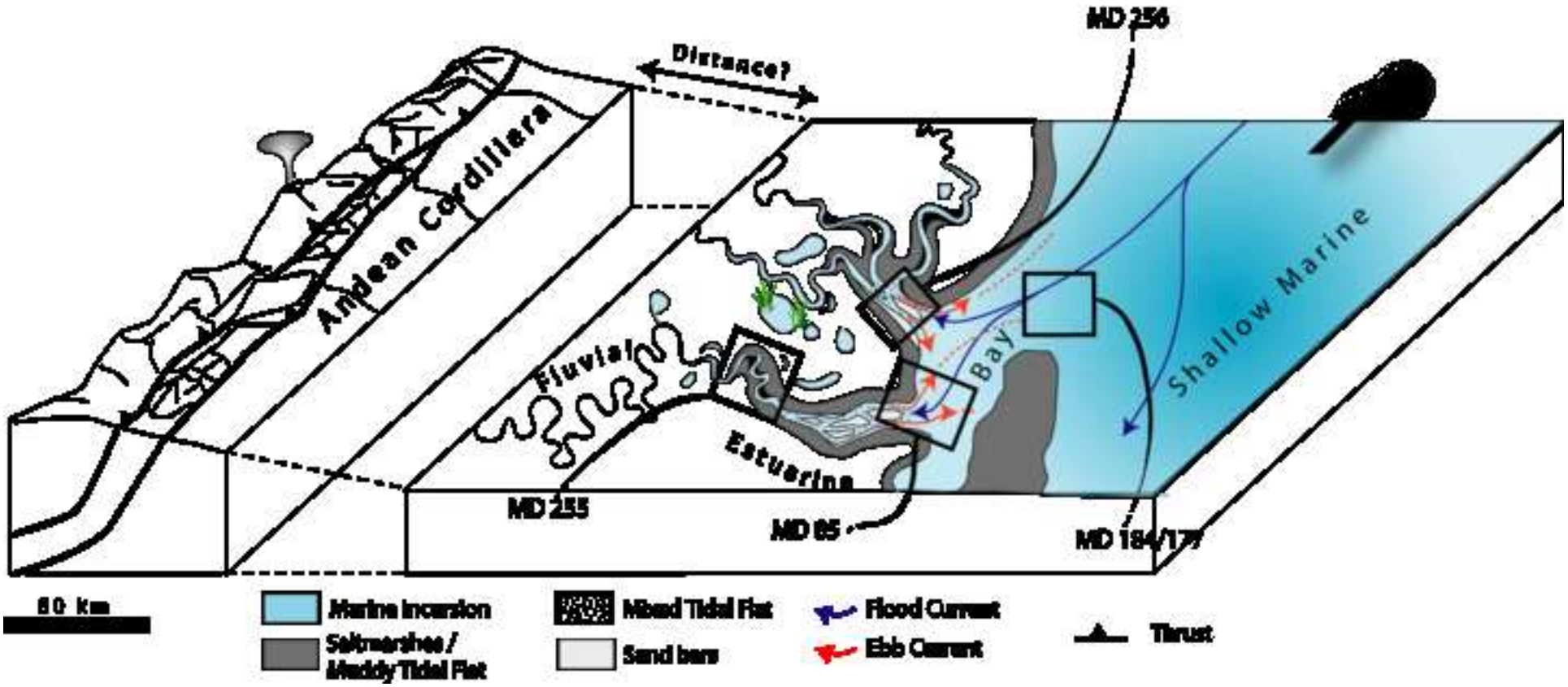

Figure 15
Click here to download high resolution image

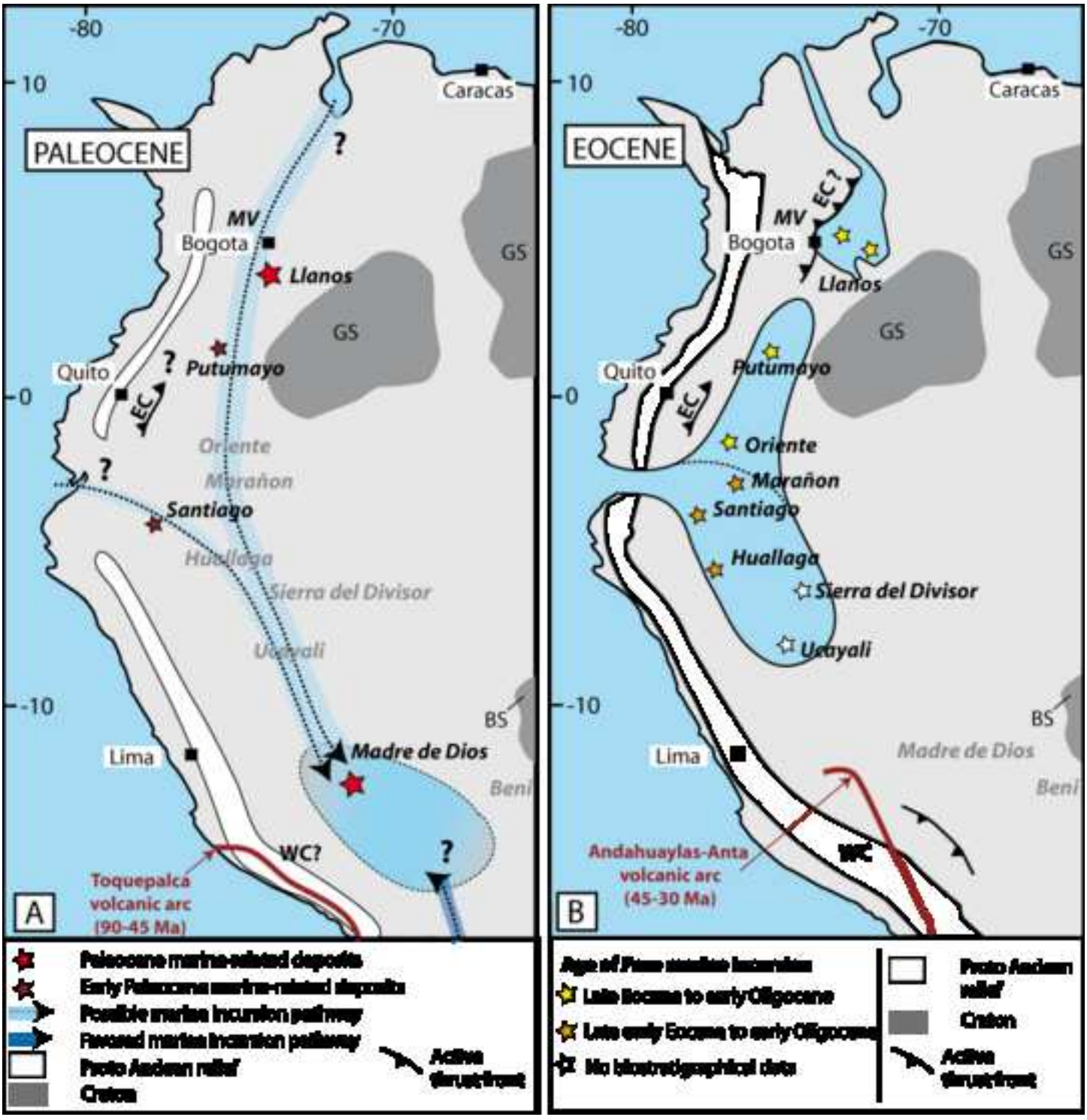

**Table 1**

**Click here to download Table: Louterbach et al_Pal3_Table1_corrected.xls**

| | Vertebrata | | | | | | | Ost. | Foraminifera | | | | Charophyta | |
|---|---|---|---|---|---|---|---|---|---|---|---|---|---|---|
| **Locality** | *Ouledia* sp. | *Potobatis* sp. | ?Dasyatidae indet. sp. 1 | ?Dasyatidae indet. sp. 2 | Pristidae indet. | Pycnodontidae indet. | Serrasalminae indet. | *Protobuntonia* sp. | *Karreriella conversa* | *Reophax* sp. | *Bathysiphon* sp. | *Rhabdammina* sp. | *Peckichara* cf. *varians meridionalis* | *Platychara perlata* ? |
| MD-85 | + | (r) | | | | | (+) | + | | + | + | + | ++ | ++ |
| MD-177 | +++ | | + | + | | +++ | ++ | | | | | | | |
| MD-184 | +++ | | (+) | | + | +++ | ++ | | | | | | | |
| MD-255 | | | | | | | | | + | | | | | |

**Table 2**

**Click here to download Table: Louterbach et al_Pal3_Table2_corrected.xls**

| Outcrops | FA | Code | Facies description | Thickness | Physical Sedimentary strucutres |
|---|---|---|---|---|---|
| *MD 255* | Facies Association A | A1 | Tangential cross-bedded fine- to medium-grained sandstone | 20 cm to 120 cm | Massive/Large scale cross-bedding with reactivation surfaces in rhythmic bundles/Ripples/Planar lamination. Lag deposit possible at the base with millimetric to centimetric mud clasts. Millimetric mud drapes. |
| *MD 255* | | A2 | Oblique Hetrolithic strata with climbing rippled cross-stratification | 1 to 1.20 m | Flaser-bedding with asymmetrical ripples+mud drapes/wavy or plana bedding . Coarsening-up patterns. |
| *MD 255* | | A3 | Oblique Hetrolithic strata with tangential cross-bedding | >60 cm | Sandy beds (20-40 cm-thick) with tangential cross-bedding and planar lamination at the base+mud drapes/ muddy to silty beds (2 to 5 cm) |
| *MD 255* | | A4 | Mudstone to siltstone, occasional rippled fine-grained sandstone | 2m, sandy layers: 10 cm | Planar stratification, ripples and climbing ripples in the silty and sandy layers |
| *MD 256/MD 85b* | Facies Association B | B1 | Fine- to medium-grained sandstone | 1 to 1.50 m | Massive, lag deposits possible at the base, sigmoid bedding (heights of set: 45 cm ). Climbing Ripples, Trough cross-bedding at the top. FU general setting |
| *MD 256* | | B2 | Red mudstone | 20 m | Gypsum nodules at the top |
| *MD 256* | | B3 | Siltstone & mudstone | 0.50 to 4 m | Scattered lenticular bedding (with carbonaceous sand) or centimetric fine-grained sandstone. |
| *MD 256* | | B4 | Highly burrowed sandstone/siltstone & heterolithic sandstone | 1 to 5m | Mud drapes,wavy and lenticular bedding. Fluid escape structures |
| *MD 256* | | B5 | Rippled fine-grained sandstone | 20 to 30 cm | Ripples |
| *MD 184/ MD 85/md 177* | Facies association C | C1 | Violet-reddish carbonaceous mudstone to siltstone with centimetric fine-grained sandy layers + thin carbonaceous layers | 50 cm to >2 m | Ripples andclimbing ripples within sandy layers |
| *MD 184/ MD 85/md 177* | | C2 | Bioturbated Facies C1 | 80 cm to 1 m | Common sandy/carbonaceous nodules, possible gypsium nodules, |
| *MD 184* | | C3 | Sand nodules breccia with muddy to silty matrix | 15 to 50 cm | Sand nodules in a muddy matrix |
| *MD 184/MD 85* | | C4 | Alternation of marl/Limestone | 10 to 25 cm | Dessiccation cracks at the top. Frequent carbonate nodules |
| *MD 184* | | C5 | Stromatholitic Limestone | 25 to 80 cm | dessiccation cracks at the top |
| *MD 184* | | C6 | *Ostrea* Limestone | 10 to 25 cm | dessiccation cracks at the top |

**Table 3**

**Click here to download Table: Louterbach et al_Pal3_Table3_corrected.xls**

| Outcrops | $\delta^{13}C_{TOC}$ (‰ VPDB) | STEDV $\delta^{13}C_{TOC}$ | TOC (wt. %) | STDEV TOC |
|---|---|---|---|---|
| MD 177 | -27.3 | 0.10 | 0.06 | 0.00 |
| MD 85 | -29.8 | 0.04 | 0.04 | 0.00 |
| MD 184 | -23.4 | 0.20 | 0.68 | 0.02 |
| MD 255 | -27.9 | 0.34 | 0.03 | 0.00 |
| MD 256 | no data | no data | no data | no data |

| Outcrops | TOC (wt. %) | S1 (mg/g) | S2 (mg/g) | S3 (mg/g) |
|---|---|---|---|---|
| MD 184 | 0.68 | 0.04 | 2.99 | 0.27 |
| | Tmax (°C) | S2/TOC (HI) | S3/TOC (OI) | Type |
| | 439.8 | 442.7 | 40.4 | II |

**Table 4**

**Click here to download Table: Louterbach et al_Pal3_Table4_corrected.xls**

| Outcrop | Sample | Lithology | Sr (ppm) | Nd (ppm) | 143Nd/144Nd | ± 2σ | eNd(0) | 87Sr/86Sr | ± 2σ1 |
|---|---|---|---|---|---|---|---|---|---|
| MD 177 | MD 177 A | Mudstone | 244.3 | 38.2 | **0.512087** | 3 | **-10.7** | 0.717287 | 10 |
| MD 85 | MD 85 Nd | Mudstone | 295.5 | 28.33 | **0.512318** | 5 | **-6.2** | 0.712024 | 8 |
| MD 184 | MD 184 A | Mudstone | 269.7 | 42.39 | **0.512117** | 6 | **-10.2** | 0.715741 | 10 |
| MD 255 | MD 255 Nd | Mudstone | NM | NM | **0.512126** | 6 | **-10.0** | 0.719026 | 10 |
| MD 256 | MD 256 | no sample | no sample | no sample | no sample | no sample | no sample | no sample | no sample |

**Supplementary Table A**

**Click here to download Table: Louterbach et al_Pal3_SupplementaryTableA.xls**

| Outcrop | Area | X | Y |
|---|---|---|---|
| MD 177 | Pongo de Coñeq | -71.360503 | -12.890300 |
| MD 85 | Pantiacolla | -71.271500 | -12.668700 |
| MD 184 | Pantiacolla | -71.265917 | -12.668783 |
| MD 255 | Pantiacolla | -71.247700 | -12.679900 |
| MD 255 | Pantiacolla | -71.244260 | -12.662260 |